# *C. elegans* gene expression in metabolic homeostasis and ageing


Doctoral thesis

for

the award of the doctoral degree

of the Faculty of Mathematics and Natural Sciences

of the University of Cologne

submitted by

Marco Giorda

2026

# Abstract

The maintenance of homeostasis requires coordination of gene expression across temporal scales, from responding to fluctuations in food availability to sustaining protein synthesis during ageing. Because of its distinct ecology and well-characterised ageing process, *C. elegans* serves as a powerful model to investigate such responses. I established two distinct research projects to explore these phenomena.

In my first project, I asked whether food-deprived worms could use an olfactory food cue to initiate transcriptional responses preparing them for the arrival of nutrients. I discovered that fasting worms exposed to volatile diacetyl rapidly induce expression of *gpdh-1* (glycerol-3-phosphate dehydrogenase) and other enzymes comprising the DHAP (dihydroxyacetone phosphate) shunt, a metabolic pathway repressed by food deprivation but induced during glucotoxicity and hyperosmotic stress. I demonstrated that this transcriptional response requires the MDT-15 (mediator subunit 15) transcription factor and drives rapid metabolic remodeling, characterised by the accumulation of glycerol and phosphatidylglycerols (PGs). If food remains absent, the metabolic activity of the DHAP shunt triggers a secondary gene expression response dominated by the dietary restriction (DR) marker *fmo-2*, promoting thermotolerance and food-seeking behaviours. These findings demonstrate that worms can indeed use an environmental food cue to preemptively rewire their gene expression and metabolic states in anticipation of nutrient arrival.

In my second project, I investigated how *C. elegans* protein synthesis changes during ageing, specifically focusing on how the translational efficiency (TE) of individual genes and broader biological processes is affected. I found that while the majority of age-related changes in protein synthesis are dictated by underlying mRNA transcript abundance, a significant number of genes are altered at the translational level. I identified GC content and codon adaptation as potential intrinsic mRNA properties underlying these translational shifts. Most notably, the TE of genes involved in the translation process itself and in protein folding is particularly downregulated with age, which may contribute to the age-related decline in protein synthesis.

Together, these projects illustrate the essential cross-talk across biological and temporal scales required to maintain homeostasis. By mapping the interplay of transcription, translation and metabolic adaptation, this thesis provides novel examples of how organisms dynamically orchestrate gene expression.

# Abbreviations

| | |
|---|---|
| **1,3BPG** | 1,3-bisphosphoglycerate |
| **4E-BPs** | eIF4E binding proteins |
| **aa-tRNA** | aminoacyl-tRNA |
| **ADP** | adenosine diphosphate |
| **AFR** | anticipatory food response |
| **AGEs** | advanced glycation end products |
| **ARD** | adult reproductive diapause |
| **ATP** | adenosine triphosphate |
| **BP** | biological processes |
| **CAI** | codon adaptation index |
| **CDS** | coding sequence |
| **cGPDH** | cytosolic glycerol-3-phosphate dehydrogenase |
| **CPIR** | cephalic phase insulin response |
| **CTP** | cytidine triphosphate |
| **DAG** | diacylglycerol |
| **DHAP** | dihydroxyacetone phosphate |
| **dORFs** | downstream open reading frames |
| **DR** | dietary restriction |
| **eEF2K** | eEF2 Kinase |
| **eIF2** | eukaryotic initiation factor 2 |
| **eIF2B** | eukaryotic initiation factor 2B |
| **ER** | endoplasmic reticulum |
| **ETC** | electron transport chain |
| **FAD** | flavin adenine dinucleotide |
| **FMO-2** | flavin-containing monooxygenase-2 |
| **G3PP** | glycerol-3-phosphate phosphatase |
| **GAP** | glyceraldehyde-3-phosphate |
| **GAPDH** | glyceraldehyde-3-phosphate dehydrogenase |
| **GCN2** | general control nonderepressible 2 |
| **GPDH** | glycerol-3-phosphate dehydrogenase |
| **Gro-3P** | glycerol-3-phosphate |
| **GSEA** | gene set enrichment analysis |
| **GSH** | glutathione (reduced) |
| **GSSG** | glutathione (oxidised) |

| | |
|---|---|
| **HLH-30** | helix-loop-helix transcription factor (TFEB ortholog) |
| **HRI** | heme-regulated inhibitor |
| **IFs** | initiation factors |
| **IGF** | insulin-like growth factor |
| **IMM** | inner mitochondrial membrane |
| **IPTG** | isopropyl β-d-1-thiogalactopyranoside |
| **ISR** | integrated stress response |
| **LAB** | lactic acid bacteria |
| **LM** | linear model |
| **MDT-15** | mediator subunit 15 |
| **MGO** | methylglyoxal |
| **mGPDH** | mitochondrial glycerol-3-phosphate dehydrogenase |
| **miRNAs** | microRNAs |
| **mRNA** | messenger RNA |
| **MS** | mass spectrometry |
| **mTORC1** | mechanistic target of rapamycin complex 1 |
| **NAD** | nicotinamide adenine dinucleotide |
| **NADP** | nicotinamide adenine dinucleotide phosphate |
| **NGM** | nematode growth medium |
| **NHR-49** | nuclear hormone receptor 49 |
| **OCM** | one carbon metabolism |
| **OGT-1** | O-GlcNAc transferase |
| **ORF** | open reading frame |
| **PA** | phosphatidic acid |
| **PABPs** | poly(A)-binding proteins |
| **PARP** | poly(ADP-ribose) polymerase |
| **PERK** | PKR-like endoplasmic reticulum kinase |
| **PFK-1** | phosphofructokinase-1 |
| **PGP** | phosphoglycolate phosphatase (same as G3PP) |
| **PGPH** | phosphoglycolate phosphatase homolog |
| **PGs** | phosphatidylglycerols |
| **PIC** | pre-initiation complex |
| **PKC** | protein kinase C |
| **PKR** | protein kinase R |
| **PPARs** | peroxisome proliferator-activated receptors |
| **RBPs** | RNA-binding proteins |
| **RPFs** | ribosome protected fragments |

| | |
|---|---|
| **rRNA** | ribosomal RNA |
| **S6Ks** | p70 S6 kinases |
| **SAM** | S-adenosylmethionine |
| **SL** | splice-leader RNA |
| **TC** | ternary complex |
| **TCA** | tricarboxylic acid |
| **TE** | translational efficiency |
| **TFEB** | transcription factor EB |
| **TOP** | terminal oligopyrimidine motif |
| **UDP-GlcNAc** | UDP-N-acetylglucosamine |
| **uORFs** | upstream open reading frames |
| **UTP** | uridine triphosphate |
| **UTRs** | untranslated regions |

# Introduction

## 1. Regulation of gene expression

### 1.1 mRNA transcription

Gene expression begins as genes encoded in DNA are transcribed into mRNAs, which are spliced and exported from the nucleus to be translated into proteins in the cytoplasm. Every step in this sequence of events can be regulated to tune gene expression responses.

In eukaryotes, transcription of DNA into precursor mRNA by RNA polymerase II is guided by a wide range of transcription factors and chromatin modifiers. As it emerges from the RNA polymerase, the 5' end is modified by the addition of a 7-methylguanosine cap, a structure essential to direct further mRNA processing, export and translation. The spliceosome complex then removes non-coding regions (introns) to establish a continuous open reading frame (ORF). When transcription ends, the 3' end is cleaved and polyadenylated. The resulting poly(A) tail is bound by PABPs, which direct the mRNA to ribosomes for protein synthesis[1].

### 1.2 mRNA and ribosome structure

The mature mRNA molecule that is exported from the nucleus contains different functional segments. At its core lies the ORF, encoding the sequence of the resulting protein. This region begins with a start codon (typically AUG) which sets the reading frame for the ribosome. Reading frames are decoded in discrete triplets known as codons. Each codon pairs with a specific cognate tRNA carrying the corresponding amino acid. Because the system relies on a degenerate genetic code, multiple synonymous codons can encode the same amino acid. The ORF concludes with a stop codon (UAA, UAG, or UGA). Flanking start and stop codons are regulatory sequences known as UTRs. The 5′ UTR is located between the cap and the start codon and regulates the recruitment of the ribosome, as well as determining the efficiency of translation initiation. The 3′ UTR, situated downstream of the stop codon, contains regulatory sequences that influence mRNA stability, localisation and translational efficiency[2].

Protein synthesis is catalysed by the ribosome, a large ribonucleoprotein particle composed of 80 proteins and four rRNA. The ribosome is divided into two subunits. The small 40S subunit binds to the

mRNA and contains the decoding centre responsible for checking codon-anticodon complementarity. The large 60S subunit houses the peptidyl transferase center, the catalytic site of the ribosome where peptide bond formation occurs, and the polypeptide exit tunnel which guides the nascent protein exit and folding. The ribosome also contains three tRNA-binding sites at the subunit interface: an A (aminoacylation) site where an aminoacylated tRNA that complements the anticodon being scanned enters the ribosome, the P (peptidyl) site where the peptide bond is formed, and the E (exit) site where the deacylated tRNA is released from the ribosome[2].

## 1.3 mRNA translation

Translation of an mRNA molecule is divided into three stages: initiation, elongation, and termination. Initiation is the rate-limiting and most highly regulated step of mRNA translation, requiring a large number of initiation factors (IFs). The ternary complex (TC), composed of active (GTP-bound) eIF2 and charged methionyl-initiator tRNA delivers the latter to the P site of the 40S ribosomal subunit. Together with eIFs 1, 1A and 3, these form the 43S pre-initiation complex (PIC). The PIC is recruited to the mRNA 5' cap via eIF4F: this  is a heterotrimeric complex composed of eIF4E, eIF4G, and eIF4A, where eIF4E directly binds the 5' cap. The PIC then scans the 5' UTR until it encounters the AUG start codon. RNA secondary structures (such as hairpins) or upstream ORFs (uORFs) located within the 5′ UTR can impede ribosomal scanning, thereby modulating the translation of the downstream main ORF. Recognition of the start codon triggers GTP hydrolysis by eIF2, release of initiation factors, and joining of the 60S subunit to form the 80S ribosome[3].

Elongation proceeds as the ribosome moves along the mRNA, decoding triplets and catalysing peptide bond formation, facilitated by elongation factors eEF1A and eEF2[4]. eEF1A delivers the correct aminoacyl-tRNA (aa-tRNA) to the ribosomal A-site based on codon-anticodon pairing. eEF2 promotes translocation of the tRNAs and mRNA on the ribosome following peptide bond formation.

Ribosomal elongation continues along the mRNA template until a stop codon (UAA, UAG, or UGA) enters the A site. These nonsense codons bind release factors, triggering the hydrolysis of the peptidyl-tRNA bond and the release of the nascent protein[5].

## 1.4 Translational regulation: intrinsic mRNA properties

Translational regulation of gene expression allows rapid adjustments in protein synthesis from transcripts already available in the cytoplasm. This can occur on two levels: specific regulation targeting single or defined subsets of mRNAs, and global regulation modulating the translational output of the entire proteome[6].

The regulation of individual transcripts is often determined by their intrinsic physical properties and sequence elements (**Fig. 1**). Translation efficiency can be enhanced by the physical circularisation of the mRNA. Interactions between PABP on the 3' poly(A) tail and the scaffold protein eIF4G at the 5' cap create a "closed-loop" structure. This arrangement facilitates re-initiation by shunting terminating ribosomes back to the 5' start site, ensuring high-efficiency recycling of the translational machinery. Shorter length increases mRNA translational efficiency, potentially by favouring a closed-loop conformation[7,8]. GC content, particularly in the 5' UTR[9], determines folding energy and thus can influence translation rates, as well as regulating mRNA stability[10].

Another important intrinsic factor is codon usage. As previously mentioned, multiple synonymous codons can encode the same amino acid. Although the genetic code is redundant, synonymous codons for the same amino acid are not used with equal frequencies in genomes, a phenomenon termed “codon usage bias”. Frequently used (optimal) codons in highly expressed genes match the most abundant tRNA isoacceptors[11]. mRNAs enriched with optimal codons, for instance those encoding the translational machinery itself, are translated more rapidly[12] than those with non-optimal codons, while mRNAs with higher levels of non-optimal codons initiate translation less efficiently and are bound by less ribosomes[13]. Variations in codon usage and elongation speed within transcripts are also important to assist with co-translational folding[14].

RNA secondary structures such as hairpins or G-quadruplexes can sterically block the scanning 43S pre-initiation complex. The inhibitory effect of these structures is often conditional, regulated by the recruitment of RNA helicases or the binding of trans-acting factors that stabilise or resolve them, like the iron-responsive elements (IREs) hairpins within the mRNAs of iron storage proteins ferritin and transferrin[15]. RNA secondary structures can also hide or expose binding sites for translational regulators[16]. More broadly, 5' and 3' UTRs are hotspots for translational regulation. uORFs are found in almost half of human transcripts and generally function to inhibit downstream translation of the

canonical ORF[17], although the extent of this effect depends on uORF numbers, length, position, sequence and cellular stress levels (discussed in more detail below). Conversely, downstream ORFs (dORFs) in the 3' UTR can promote translation of the canonical ORF[18]. Length of the 3' UTR regulates translational efficiency[19]and its sequence can act as a scaffold for binding RNA-binding proteins (RBPs) and microRNAs (miRNAs), usually to repress translation[20]. Finally, an emerging field is the chemical modification of RNA bases, which can also affect mRNA translational efficiency. Modifications such as $m^6A$ ($N^6$-Methyladenosine) or $m^1A$ ($N^1$-Methyladenosine) can alter efficiency of translation by binding initiation factors, altering 5' UTR structure or by impeding translation elongation[21].

## 1.5 Translational regulation: signalling pathways

Ribosomes are one of the most abundant cellular structures, particularly in rapidly dividing cells[22]. Unsurprisingly, protein synthesis is estimated to be one of the most ATP demanding processes in mammalian cells[22,23]. Because protein synthesis is such an energy-consuming process in the cell, global rates are tightly coupled to the organism's metabolic state and stress levels. Cells commonly respond to stress by shutting down global protein synthesis and upregulating translation of certain stress response transcripts[24]. This translational control is exerted via signalling pathways such as mTORC1, MAPK signalling and the Integrated Stress Response (ISR) (**Fig. 1**).

### 1.5.1 mTORC1

mTORC1 is a Ser/Thr kinase that serves as a master regulator of anabolic processes, integrating diverse environmental cues to promote cell growth and proliferation[25]. mTORC1 combines multiple signals to sense the cellular energetic and metabolic status. It is activated by amino acids and by glycolytic intermediates including DHAP[26,27]. It is also induced by hormones and growth factors like insulin and insulin-like growth factor (IGF). It is inhibited by AMPK detecting low ATP/ADP ratios.

Once active, mTORC1 phosphorylates a suite of substrates to modulate components of the translational machinery, including 4E-BPs (eIF4E-Binding Proteins), S6Ks (p70 S6 Kinases) and LARP1.
In their unphosphorylated state, 4E-BPs bind to the cap-binding protein eIF4E, preventing it from interacting with the scaffold eIF4G. This blocks the assembly of the eIF4F complex and translation initiation. mTORC1 phosphorylates 4E-BPs at multiple sites, triggering their dissociation from eIF4E. mTORC1 also phosphorylates and activates S6K1 and S6K2. These kinases in turn phosphorylate multiple

targets to promote translation initiation and elongation. They promote eIF4A activity, and thus initiation, via eIF4B induction and PDCD4 degradation. They phosphorylate and inhibit eEF2 Kinase (eEF2K), which would otherwise inhibit eEF2 and translation elongation. They also phosphorylate multiple residues of the ribosomal protein S6 to modulate protein synthesis[25]. S6 phosphorylation is in fact a commonly used marker of mTORC1 activity.

While mTORC1 activation promotes global protein synthesis, by the mechanisms described above and by increasing ribosome biogenesis and tRNA synthesis, it seems to particularly boost translation of mRNAs containing a 5' Terminal Oligopyrimidine (TOP) motif. This selective regulation is mediated by both 4E-BPs and LARP1[28]. 5' TOP transcripts almost exclusively encode components of the translation machinery itself (ribosomal proteins, initiation and elongation factors). This allows mTORC1 to quickly boost the cell's translational capacity[29].

### 1.5.2 The Integrated Stress Response (ISR)

Another major pathway modulating global protein synthesis rates is the ISR, sensing multiple cellular stresses and relaying their output on the phosphorylation of serine 51 on the α subunit of eIF2 (eIF2α), which forms part of the ternary complex (TC). Different kinases can phosphorylate eIF2α to activate the ISR. General control nonderepressible 2 (GCN2) is the ancestral eIF2α kinase which senses amino acid scarcity. PKR-like endoplasmic reticulum kinase (PERK) senses protein misfolding in the ER. These are the only two kinases phosphorylating eIF2α in *C. elegans*. Two additional kinases are found in mammals: the heme-regulated inhibitor (HRI), sensing heme deficiency, oxidative and mitochondrial stress; and protein kinase R (PKR), sensing viral infection[30]. Inactive (GDP-bound) eIF2 needs to be recycled to its active (GTP-bound) form after every round of translation initiation. This action is performed by the guanine nucleotide exchange factor eIF2B, which is thus essential to maintain cellular concentration of the TC and sustain initiation. ISR activation interferes with this process by changing eIF2 from a substrate to an inhibitor of eIF2B. eIF2B inhibition leads to reduced TC concentration and halts global translation[31].

Similarly to mTORC1, the ISR can regulate both global and specific protein synthesis rates. Some mRNAs, which are not translated under normal high TC levels, become de-repressed during ISR activation[32]. Lower TC concentrations facilitate skipping of small inhibitory uORFs and translation of the downstream main ORF. Despite uORFs being common (with an estimated presence in 40 to 50% of mouse and human genes[3]), their role in translational regulation during ISR activation has only been described for a handful

of transcripts, the most notable example being the ISR upregulated transcription factor ATF4. The mouse *atf-4* transcript contains two uORFs: a first 5' proximal uORF which promotes ribosome scanning a second inhibitory uORF which overlaps with the coding ORF[34]. ISR activation promotes uORF2 skipping and translationally upregulates ATF4 levels, which tunes gene expression to facilitate either pro-survival or pro-apoptotic functions[35].

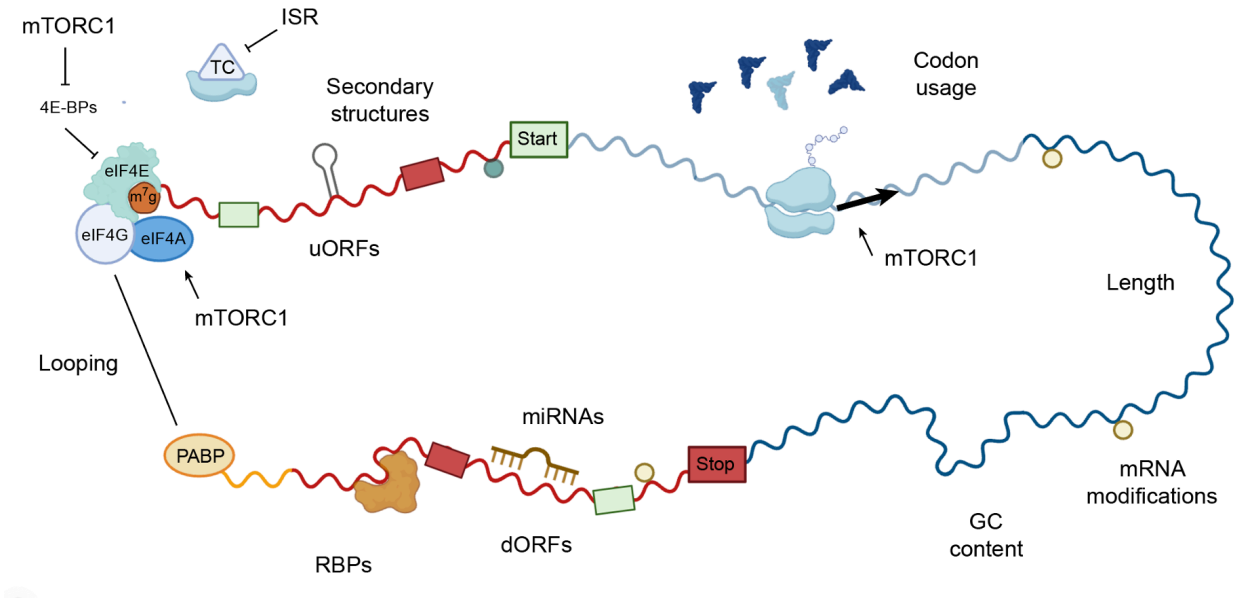


**Figure 1: Intrinsic mRNA properties and signalling pathways influencing translational efficiency.** Transcript properties that regulate translational efficiency include uORFs in the 5 'UTR, codon usage, length, mRNA modifications, GC content and secondary structures, dORFs in the 3'UTR, sequences for binding by miRNAs and RBPs. Interactions between eIF4G and PABP promote mRNA looping and translation re-initiation. ISR activation reduces TC concentration and inhibits translation initiation. Signalling by mTORC1 promotes both translation initiation and elongation. Created with BioRender.com.

## 1.6 Transcriptional versus translational regulation

Gene expression regulation involves both transcriptional and translational layers of control, offering distinct advantages regarding speed, memory, and coordination when it comes to responses to a stress.

Transcriptional Responses:

- Timescale: Transcriptional responses generally begin between minutes and hours after stress application[36]. For example, the accumulation of light stress response transcripts in plants has been detected in the timescale of seconds after stimulation[37].
- Memory and tissue specificity: Transcriptional output heavily depends on the underlying chromatin architecture. Epigenetic mechanisms can create a molecular memory of previous stress events, allowing cells to respond more strongly to recurring challenges[38]. This level of regulation is also highly tissue-specific, defined by the unique landscape of interacting transcription factors and enhancer elements[39].
- Coordination: Mechanisms such as promoter pausing (where Pol II is stalled at the transcription start site, ready for rapid release), enhancer-promoter interactions and 3D chromatin organisation allow for the precise temporal control of gene networks. Furthermore, features like operons (in prokaryotes or *C. elegans*), gene clustering, and bidirectional promoters facilitate the synchronised expression of functionally related genes[40].

Translational Responses:

- Timescale: Translational mechanisms allow for faster responses, utilising the pool of existing mRNAs already present in the cytoplasm as a starting point. This element of speed is particularly important for survival to rapid environmental changes; for instance, global repression of translation occurs within 30 seconds of glucose deprivation in yeast[41].
- Memory and tissue specificity: Translational control is closely linked to the cell's energy and stress status. The translational machinery is also differentially tuned at a tissue level[42]. For instance, specific tRNA pools in human tissues may support higher translational efficiency of tissue-specific genes[43]. There is currently little evidence for a widespread "translational memory" comparable to epigenetic memory.
- Coordination: The coordination of large numbers of genes at the translational level is achieved through shared mRNA intrinsic properties (discussed above). For example, yeast experiencing different types of stress change their tRNA pool to increase the levels of tRNAs enriched in stress response genes. This facilitates a preferential translation of these transcripts over the ones involved in growth-related functions[44].

Transcriptional and translational regulation must communicate to efficiently reshape the proteome during stress, but the intricacies of how this is achieved are still being explored. Zedan et al.[45] have recently reported how transcripts produced during glucose-deprivation stress in yeast escape the global translational shutdown through a sequence-independent mechanism.

Both layers of regulation are deeply connected to metabolism[46,47,]. For instance, a metabolic intermediate such as S-adenosylmethionine (SAM) from 1-carbon metabolism, is directly involved in both transcriptional[48] and translational[49] regulation through methylation of DNA, RNA, histones, translation and signalling factors. The dependence of gene regulatory machinery on metabolic substrates ensures that the cell's protein synthesis output is tightly linked to its nutritional status.

# 2. Nutrient homeostasis

Fluctuating nutrient and energy levels represent one of the most common homeostatic challenges for any organism. Because it serves as the primary source of cellular energy, glucose metabolism is central to managing this problem[50]. Maintenance of nutrient homeostasis requires a coordinated response, depending both on the rapid biochemical adjustment of metabolic pathways and the systemic rewiring of gene expression. Under aerobic conditions, glucose is processed through glycolysis first and then the mitochondrial TCA cycle to fuel ATP production.

## 2.1 Glycolysis and NADH shuttles

Upon entering the cell, glucose is phosphorylated by hexokinase to form glucose-6-phosphate, trapping it within the cytosol. This initiates glycolysis, a ten-step sequence of enzymatic reactions that converts one molecule of glucose into two molecules of pyruvate. The pathway can be divided into two phases[51].

The first is the preparatory phase, an energy-investment stage where ATP is consumed to prime the glucose molecule. The key regulatory step here is catalysed by phosphofructokinase-1 (PFK-1), which consumes an ATP molecule to convert fructose-6-phosphate into fructose-1,6-bisphosphate, committing this substrate to the glycolytic path. This molecule is then cleaved by aldolase into two triose phosphate isomers: glyceraldehyde-3-phosphate (GAP) and dihydroxyacetone phosphate (DHAP). DHAP is converted to GAP by triosephosphate isomerase to continue with glycolysis. DHAP can alternatively be converted to Gro-3P to feed synthesis of glycerolipids (more details discussed below).

The second glycolysis half is the "payoff phase," where energy is harvested. GAP is oxidised by the enzyme glyceraldehyde-3-phosphate dehydrogenase (GAPDH) to produce 1,3-bisphosphoglycerate (1,3BPG), while NAD+ is reduced to NADH. This is the only redox reaction in the pathway and is highly sensitive to the cellular redox state[52]. The following steps yield ATP via substrate-level phosphorylation, ending in the formation of pyruvate. Under normoxic conditions, pyruvate is then transported into the mitochondria, converted to acetyl-CoA, and fully oxidised in the Tricarboxylic Acid (TCA) cycle to generate reducing equivalents (NADH and FADH2) for the electron transport chain (ETC). Through oxidative phosphorylation, the ETC oxidises these reducing equivalents and generates ATP.

To sustain glycolysis cells must continuously replenish the pool of cytosolic NAD+ required for the GAPDH reaction. Since the mitochondrial inner membrane is impermeable to NADH, reducing equivalents must be transferred into the mitochondrial matrix via shuttle systems:

- The Malate-Aspartate Shuttle: This is the principal mechanism in most tissues. It reversibly transfers electrons from cytosolic NADH to mitochondrial oxaloacetate, forming malate which enters the matrix to regenerate mitochondrial NADH for Complex I[53].
- The Gro-3P Shuttle (**Fig. 2**): This system operates through the coordinated action of two isozymes, one cytosolic and one mitochondrial[54]. In the cytosol, cGPDH (cytosolic Glycerol-3-Phosphate Dehydrogenase, GPD1 in mammals) reduces DHAP to Glycerol-3-phosphate (Gro-3P), converting NADH to NAD+ in the process. Gro-3P then diffuses to the outer face of the inner mitochondrial membrane (IMM), where it is re-oxidised back to DHAP by the mitochondrial isozyme, mGPDH (GPD2 in mammals). mGPDH transfers the electrons to FAD, feeding them directly into the electron transport chain as $FADH_2$.

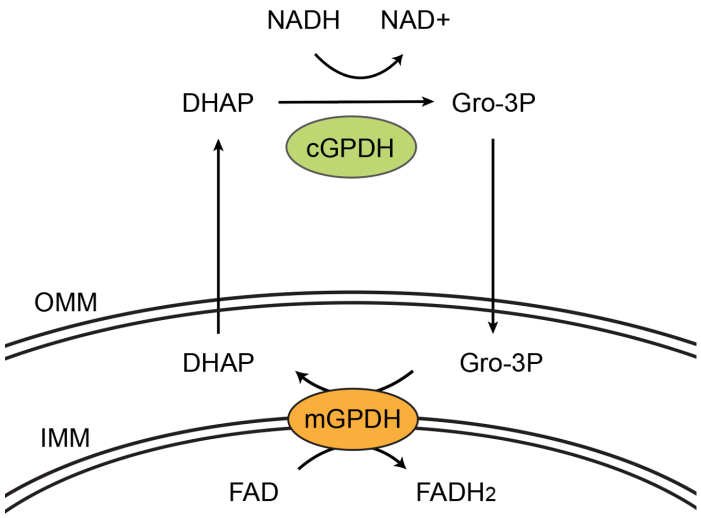


**Figure 2: Gro-3P Shuttle.** Metabolic pathway that transfers electrons from cytosolic NADH into mitochondria, reducing FAD. Operated through the coordinated action of cytosolic GPDH (cGPDH) and mitochondrial GPDH (mGPDH, on the IMM), catalysing the interconversion of DHAP and Gro-3P.

## 2.2 Mechanisms of glucotoxicity

When glucose supply exceeds the oxidative capacity of the mitochondria the normal flow of metabolites through glycolysis is disrupted. This state, termed glucotoxicity, is characterised by accumulation of reducing equivalents and glycolytic intermediates, which spill over alternative metabolic pathways and contribute to cellular stress. There are six major biochemical pathways through which excess glucose and related metabolites mediate this damage[55, 56].

### 1. Polyol Pathway

This pathway is composed of two reactions. Aldose reductase reduces glucose to sorbitol, consuming NADPH in the process. Sorbitol is then converted to fructose, with a reaction that also reduces NAD+. Under normal physiological glucose levels, the affinity of the enzyme aldose reductase for glucose is low, and the pathway is largely inactive. However, under hyperglycemic conditions, significant flux is diverted through this pathway. This results in a redox imbalance (through both NADPH and NAD+ depletion) and can also lead to osmotic stress in some tissues where sorbitol is accumulated instead of fructose[57].

### 2. Hexosamine Pathway

Excess fructose-6-phosphate can be diverted into the hexosamine biosynthetic pathway. This leads to the production of UDP-N-acetylglucosamine (UDP-GlcNAc), a substrate for the O-linked glycosylation of various proteins, including transcription factors. Modification of these transcription factors changes their activity and mediate some of the adverse effects of glucotoxicity, including insulin resistance and oxidative stress[58].

### 3. Protein Kinase C (PKC) Activation

Excess glucose increases the concentration of DHAP, which is reduced to Gro-3P for lipid synthesis. Alternatively, Gro-3P is a precursor for the formation of diacylglycerol (DAG). Elevated intracellular DAG levels allosterically activate several isoforms of Protein Kinase C (PKC). Aberrant PKC activation leads to chronic oxidative stress and diabetic-related vascular complications[59].

### 4. Advanced Glycation End-products (AGEs) and Methylglyoxal

Perhaps the most pervasive mechanism of glucotoxicity is the non-enzymatic glycation of proteins, lipids and DNA leading to formation of advanced glycation end products (AGEs). This process can occur either through direct non-enzymatic attachment of glucose molecules or through the reaction with glycolytic derivatives. A major precursor responsible for AGE formation is methylglyoxal (MGO): a highly reactive, cell permeant α-dicarbonyl compound which originates predominantly from the fragmentation of the glycolytic intermediates Gro-3P and DHAP[60]. AGE formation can cause DNA damage and impair the function and stability of proteins. Additionally, AGEs bind to and activate the Receptor for AGEs (RAGE), triggering chronic inflammation and oxidative stress[61].

The conserved glyoxalase system (Glyoxalase I and II) is considered to be the primary detoxification mechanism for MGO[62]. This glutathione-dependent pathway converts MGO into D-lactate. Despite being found ubiquitously across the domains of life, this pathway does not seem essential for viability and can be compensated by other enzymes[63].

### 5. Enediol pathway

Another mechanism of glucotoxicity arises from the autoxidation of GAP under physiological conditions, forming enediol radical anions and hydrogen peroxide and causing oxidative stress[55].

6. Mitochondrial electron transport chain

Finally, conditions of high substrate availability lead to excessive NADH that can overwhelm mitochondria, leading to excessive leakage of electrons from complexes I and III, which react with molecular oxygen to produce ROS[64].

## 2.3 Reductive stress and accumulation of glycolytic intermediates

Many of the pathways described above share a common signature of oxidative stress. This is preceded, and partially caused by, reductive stress induced by glucotoxicity[65]. Under conditions of nutrient excess, the TCA cycle generates a surplus of electron donors, specifically NADH and $FADH_2$. NADH is also produced by GAPDH in glycolysis and by the polyol pathway. When the production of these reducing equivalents exceeds the mitochondrial oxidative capacity, it triggers a state of reductive stress, characterised by a dangerously elevated NADH/NAD+ ratio (pseudohypoxia).

This surplus of reducing equivalents drives the production of mitochondrial superoxide, which acts as a "stop signal" for glycolysis. Mitochondrial superoxide overproduction leads to DNA strand breaks, which in turn activate Poly(ADP-ribose) polymerase (PARP). Activated PARP inhibits GAPDH (which also depends on NAD+ for its function) via poly-ADP-ribosylation and creates a metabolic "dam" in the glycolytic stream, forcing upstream metabolites to accumulate and spill over into some of the toxic side-pathways described above[66].

This block particularly leads to the accumulation of GAP and DHAP, the metabolites directly upstream of GAPDH (**Fig. 3**). As discussed in the previous section, elevated levels of these metabolites fuel two distinct mechanisms of toxicity: PKC activation and formation of methylglyoxal. DHAP has been shown to accumulate significantly in both *in vitro* models of glucotoxicity[26,27] and *in vivo* diabetes models[67]. DHAP has also been suggested to mediate the toxic effects of glucose in *C. elegans*[68].

## 2.4 The DHAP shunt in glucotoxicity and redox homeostasis

To counteract the accumulation of metabolic intermediates and the reductive stress caused by excess glucose, cells must deploy mechanisms that simultaneously restore redox balance and divert excess carbons. In this context, cGPDH (GPD1 in mammals, GPDH-1 and GPDH-2 in *C. elegans*) plays a critical role.

By converting accumulated DHAP into Gro-3P, and oxidising NADH to NAD+ in the process, cGPDH serves two clear homeostatic functions (**Fig. 3**):

1. Redox balance: cGPDH regenerates cytosolic NAD+, required for GAPDH activity. This allows glycolysis to proceed even when the mitochondrial oxidation of NADH is impaired.
2. Glycolytic "safety valve": cGPDH diverts glycolytic intermediates that may otherwise spillover into other metabolic pathways. It also decreases the levels of GAP that would otherwise fuel more NAD+ reduction by GAPDH.

Significantly, cGPDH activity has been identified as a conserved protective mechanism in conditions of hypoxia and ETC dysfunction in yeast, *C. elegans*, mice and human cells[69]. In Drosophila, GPDH-1 supports glycolytic flux and maintains redox balance during development[70]. GPDH-1 has also been shown to modulate the *C. elegans* response to a high-glucose diet[71]. Increased GPD1 expression and activity has been noted in obese patients[72,73], and mutations in this gene are associated with rare diseases, often involving liver steatosis and transient hypertriglyceridemia in children[74,75,76].

Excessive conversion of DHAP into Gro-3P can however cause a different set of problems. Chronic accumulation of Gro-3P drives excessive lipid synthesis and lipotoxicity, as well as PKC activation. To mitigate this secondary stress, cells utilise the glycerol shunt. In this pathway, the enzyme glycerol-3-phosphate phosphatase (G3PP), also known as phosphoglycolate phosphatase (PGP) in mammals or phosphoglycolate phosphatase homolog (PGPH) in *C. elegans,* hydrolyses the phosphate group from Gro-3P to produce glycerol. Glycerol is a less reactive solute that can be readily secreted from the cell. The induction of this shunt protects both mice[77] and *C. elegans*[78] against glucotoxicity by draining the pools of both Gro-3P and DHAP. PGP was detected in all mouse tissues examined, with notable concentrations in heart and skeletal muscle, and its expression was influenced by nutritional status in certain tissues. Further *in vivo* research has revealed that the glycerol shunt is a central regulator of metabolic stress; its activation modulates insulin secretion in pancreatic β-cells[79] and protects hepatocytes[80] from glucotoxicity under hyperglycemic conditions. Remarkably, PGP enzymes seem to have additional metabolic repair functions in glycolysis. They are also known to destroy 4-phosphoerythronate and 2-phospho-L-lactate, two toxic side-products produced by GAPDH and pyruvate kinase respectively[81]. Accordingly, pharmacological inhibition of PGP is emerging as a promising strategy to reduce the glycolytic flux[82].

Together, cGPDH and G3PP form a metabolic pathway that I describe in this thesis as DHAP shunt (**Fig. 3**).

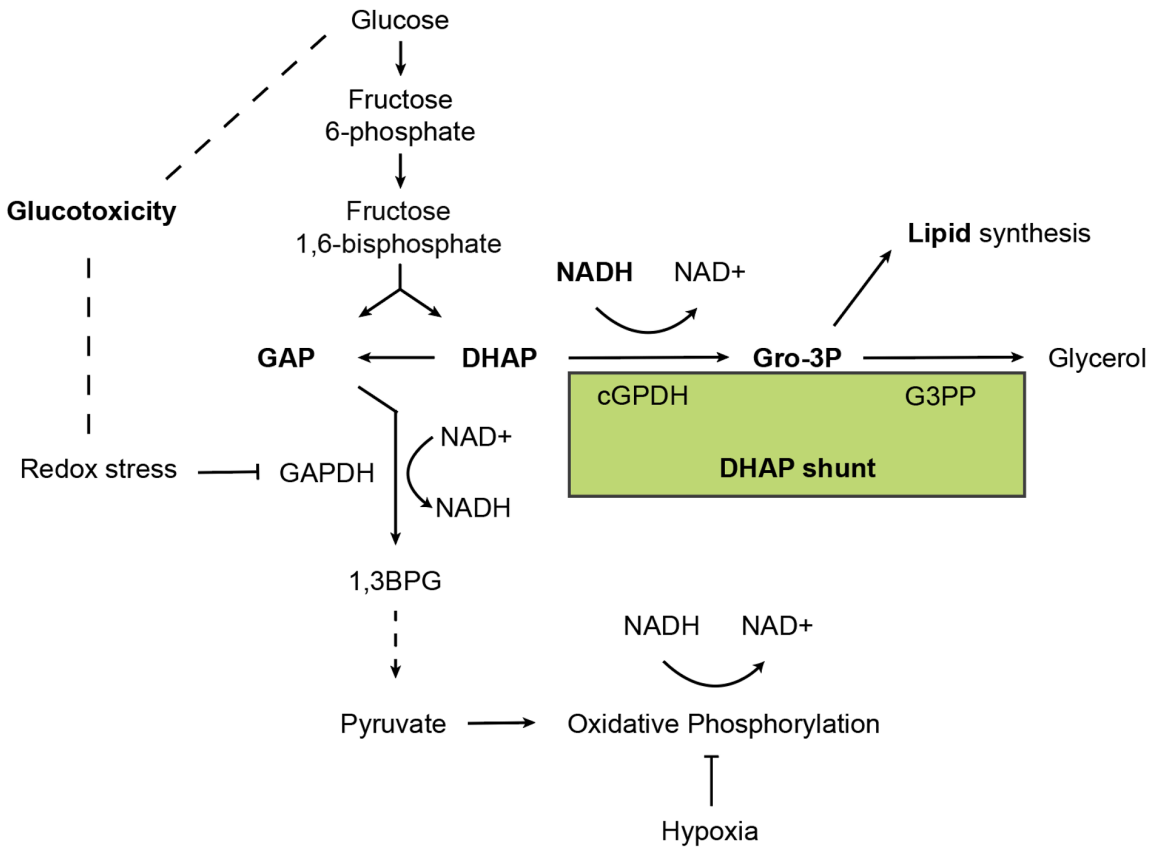


**Figure 3: The DHAP shunt in glucotoxicity and redox homeostasis.** Glucose excess can overwhelm oxidative phosphorylation and cause reductive stress (high NADH/NAD+ ratio), impairing the glycolytic flux and leading to an accumulation of reactive glycolytic intermediates upstream of GAPDH (GAP, DHAP). The DHAP shunt, composed by cGPDH and G3PP can restore redox balance and divert accumulation of glycolytic intermediates. cGPDH regenerates cytosolic NAD+ and converts DHAP into Gro-3P. G3PP redirects Gro-3P from lipid synthesis into glycerol production.

## 2.5 Gene expression responses in nutrient homeostasis

While metabolic shunts provide a rapid defence against acute nutrient stress, long-term survival requires wider rewiring of gene expression programmes. Starvation triggers a massive reorganisation of gene expression to shift metabolism from anabolism to catabolism. In yeast, limiting different individual nutrient types induces a common transcriptional response characterised by downregulation of genes involved in cellular organisation and protein synthesis[83]. In *C. elegans*, acute starvation induces

expression of genes involved in proteolysis and fatty acid degradation, while downregulating genes related to protein synthesis and processing. Many of these effects seem to be post-transcriptional[84]. In mice, both intermittent fasting and dietary restriction induce gene expression responses related to fatty acid degradation, glycolysis, gluconeogenesis and PPARα signalling[85]. PPARα is a nuclear hormone receptor highly expressed in the liver, acting as a master regulator of fasting-related gene expression responses[86]. PPARα is activated by fatty acids and other lipid derivatives to induce expression of hundreds of genes involved in lipid uptake, storage, degradation, synthesis, as well as glucose and amino acid metabolism[87]. Another transcription factor, TFEB, is induced during starvation and induces expression of genes related to autophagy[88] and lipid catabolism[89].

Organisms must also adjust gene expression to prepare their metabolism for food absorption. The effects of refeeding on gene expression are far less studied than the effects of starvation. In mice, re-feeding induces gene expression responses that can reverse some of the effects of fasting[90], and include induction of lipid synthesis and suppression of gluconeogenesis[91]. This response is driven by the acute physiological changes that occur upon eating. For instance, feeding causes a transient spike in blood glucose levels in mice[92] and humans[93]. The influx of energy substrates requires the upregulation of storage pathways (glycogen and lipid synthesis) to prevent high circulating levels of glucose and fatty acids, which can be toxic. Transcriptional regulators, including the PPAR family, continue to play a role here, inducing expression of genes involved in fatty acid storage and glucose utilisation[94,95].

## 2.6 Anticipatory Food Responses (AFR)

Organisms maintain stability by sensing and responding to environmental challenges (homeostasis). However, they can also proactively initiate responses in anticipation of environmental changes, a concept known as allostasis[96]. For instance, most organisms employ circadian clocks to predict daily fluctuations in their environment[97]. Animals can additionally rely on sensory systems to anticipate environmental conditions and coordinate complex systemic adaptation.

A primary example of this are Anticipatory Food Responses (AFR), also known as cephalic phase responses. The term "cephalic" underscores that these responses are generally driven by the brain via sensory functions (vision, olfaction, and gustation). The study of AFR dates back to the seminal work of Pavlov in the early 20th century. Pavlov’s classical conditioning experiments with dogs demonstrated that "psychic secretions" of saliva and gastric acid could be stimulated by arbitrary auditory cues that had

been associated with feeding[98]. AFR responses include secretion of hormones such as ghrelin, gastrin, glucagon and pancreatic polypeptide which regulate digestion, hunger and peripheral metabolic responses[99]. Crucially, these hormonal shifts match the direction of the physiological changes caused by feeding itself, lessening the metabolic transition from the fasted to the fed state and preventing feeding associated stress, including hyperglycemia.

The best studied AFR is the Cephalic Phase Insulin Response (CPIR). Within minutes of sensory stimulation, plasma insulin levels spike, typically peaking between 4 to 10 minutes. Although this cephalic peak is small, its functional importance is disproportionate to its size[100]. The CPIR suppresses hepatic glucose production (gluconeogenesis) and lipolysis while sensitising peripheral tissues to insulin.

## 2.7 AFR at the gene expression level: a critical gap

While hormonal and secretory aspects of the AFR are well-documented, the impact of sensory cues on gene expression is a novel avenue of exploration in this field. If the purpose of allostasis is to prioritise metabolic pathways for incoming nutrients, it follows that food cues should trigger gene expression programs to support this shift. Early evidence for an AFR at the level of gene expression arrived from an invertebrate model. Exposing food-deprived *Drosophila* to thirty minutes of vinegar odor triggered transient expression of genes encoding a glucagon-like adipokinetic hormone and insulin-like peptides[101]. More recently this concept has been validated in a mammalian model[102]. Looking specifically at the liver, Brandt et al. showed that mice exposed to caged (unaccessible) food induced gene expression responses that overlapped with those induced by refeeding. Food perception activated mTOR signalling and promoted expression of ER stress genes. Crucially, this effect on gene expression was observed as early as after 30 minutes of exposure, a similar timeline as the one observed in *Drosophila*[101].

These studies, while being fundamental in establishing the possibility of transcriptional anticipatory food responses, were focused either on specific, pre-selected pathways (digestive hormones) or on specific tissues (liver). To date, there has been no attempt to measure the whole-genome response to a food cue in a tissue-agnostic manner (e.g. in a whole organism). This is a fundamental gap in our understanding of the potential roles of gene expression in metabolic allostasis.

# 3. *C. elegans*: a model for nutrient homeostasis

## 3.1 The ecology of *Caenorhabditis elegans*

In the 1960s, Sydney Brenner championed the use of the nematode *Caenorhabditis elegans* as a simple model to dissect complex biological problems, particularly those related to the genetic basis of development and neuronal function[103]. Six decades later, Brenner's vision has been realised beyond measure: *C. elegans* stands as one of the most thoroughly understood animals on the planet in terms of genetics, development, gene expression regulation, neuronal function and ageing.

Yet, a neglected aspect of *C. elegans* biology is its ecology. In the lab, worms are maintained on predictable, abundant lawns of *Escherichia coli*. However, the natural habitat of *C. elegans* is likely much more diverse and dynamic[104]. These nematodes are mostly isolated from microbe-rich but transient niches, such as rotting fruit, decomposing vegetation, and compost heaps. These environments are defined by volatile "boom and bust" cycles[105]. A colonisation event begins when a worm encounters a rich bacterial bloom. This nutrient abundance triggers a phase of rapid feeding and exponential population growth. When the bacterial food supply is exhausted, the local environment deteriorates, leading to a "bust" phase characterised by starvation and crowding.

To survive the instability of its habitat, *C. elegans* has evolved sophisticated sensory structures to enable food foraging (discussed later) and developmental plasticity, which allows it to enter diapause life stages, most notably the stress-resistant and non-feeding diapause stage known as dauer[106]. Its ecology also makes the worm a powerful system for studying adaptations to maintain nutrient homeostasis.

## 3.2 Nutrient stress responses in *C. elegans*

### Starvation responses

Adult *C. elegans* possesses a remarkable capacity to withstand nutrient deprivation. At first, food deprivation induces foraging behaviour and increases appetite[107]. While reproducing adults often succumb to "bagging" (internal hatching of larvae) if food is removed for a prolonged period, non-reproducing animals are extremely starvation resistant. In the absence of reproductive stress, adult worms actually live longer in complete absence of food[108].

To survive acute starvation, worms undergo a rapid metabolic overhaul. Multi-omics analyses have revealed a coordinated shift from anabolism to catabolism[84]. Starvation induces the synthesis of proteins involved in proteolysis and fatty acid degradation, allowing the worm to mobilise intestinal lipid stores. Conversely, genes related to protein synthesis and processing are heavily downregulated.

These broad metabolic shifts are coordinated by several transcription factors, including:

- HLH-30: The ortholog of mammalian TFEB, which acts as a master regulator of autophagy and lysosomal function. This is induced by reduced mTOR activity and mediates dietary restriction longevity[109].
- NHR-49: The ortholog of mammalian PPARα, which regulates fatty acid β-oxidation during food deprivation[110].
- MDT-15: A subunit of the Mediator complex that interacts with NHR-49 (and other nuclear receptors) to drive the expression of lipid metabolism genes during fasting[111].

A key downstream target regulated by these factors is FMO-2 (Flavin-containing Monooxygenase-2), induced in the gut of worms exposed to hypoxia and dietary restriction. This enzyme was shown to be necessary and sufficient to extend lifespan downstream of these interventions, and required HLH-30 for its induction[112]. Its induction by food deprivation also requires NHR-49 and MDT-15[113].

While flavin-containing monooxygenases are classically known for metabolising xenobiotics, FMO-2 has emerged as a central player in endogenous metabolic regulation, particularly affecting One Carbon Metabolism (OCM) and tryptophan levels [114]. Through this metabolic rewiring, FMO-2 also modulates exploratory behaviour and satiety, effectively coupling the animal's metabolic state to its foraging decisions[115]. Both *fmo-2* overexpression and knock-out decreased chemotaxis towards diacetyl.

### Nutrient excess responses

While responses to food deprivation in *C. elegans* have been extensively studied, stress responses to refeeding are less understood. On a behavioural level, refeeding after fasting induces a satiety response with progressive decrease in foraging and feeding behaviours [107]. On a metabolic level, one hour of refeeding has been shown to reverse redox changes induced by twelve hours of fasting[116]. Refeeding after adult reproductive diapause (ARD) required a transcriptome reprogramming orchestrated by HLH-30[117].

Most research into nutrient-induced stress in worms has focused on the effects of a high-glucose diet. Similarly to other organisms, excess glucose reduces *C. elegans* lifespan by increasing levels of advanced glycation end products (AGEs) and causing oxidative stress[118,119]. At the gene expression level, high glucose has been shown to impact the expression of insulin signalling target genes[120] and metabolic genes, particularly by upregulating those involved in carbohydrate and lipid metabolism[121]. Both NHR-49 and MDT-15 have been linked to glucotoxicity responses, with MDT-15 being particularly important to promote fat conversion under excess glucose[68]. Significantly, by genetic suppression of glycolysis steps and supplementation of glycolytic intermediates, this study also concluded that DHAP may be the critical metabolite mediating the ageing effects of glucose excess.

### DHAP shunt in *C. elegans*

*C. elegans* possess two genes encoding a cGPDH (*gpdh-1* and *gpdh-2*) and three genes encoding a G3PP (*pgph-1*, *pgph-2* and *pgph-3*). The canonical function of these genes is glycerol production in the context of osmolarity regulation. Both yeast and *C. elegans* accumulate glycerol as the primary protective osmolyte against hypertonic stress[122]. The two *gpdh* genes play redundant and essential roles in hypertonic stress survival, and *gpdh-1* expression levels in particular can accurately report the degree of hyperosmotic stress experienced by the worms[123]. Expression of *pgph* genes is also induced by hyperosmotic stress. As these enzymes are required for the conversion of Gro-3P into glycerol, triple knock-out of *pgph* genes impairs worm survival under hypertonic stress. Analysis of individual mutants has shown a prominent role for *pgph-2* compared to the other two genes[78].

Beyond their role in hyperosmotic stress, and in parallel with advances in the understanding of their mammalian orthologs, these enzymes are emerging as metabolic regulators protecting worms against glucotoxicity. As mentioned in previous sections, excess glucose has been reported to induce *gpdh-1* expression[71]. High-glucose diet has been shown to reduce lifespan when started in young animals (day 1) and extend lifespan when started at day 5[124]. Mo et al. found that the lifespan extension effect depended on intestinal expression of *gpdh-1*. Significantly, the authors suggested that this could be mediated through a protective osmotic effect of glycerol accumulation[71]. However, the authors did not assess whether *gpdh-1* knockdown would also suppress the lifespan reduction from a high-glucose diet started at day 1.

Expression of *pgph* genes is also induced by glucose, and loss of these genes reduces lifespan under control conditions and in glucotoxicity. Triple knock-out of *pgph* genes increased levels of DHAP, Gro-3P and consequently lipid synthesis and accumulation. Conversely, *pgph-2* overexpression extended lifespan, decreased fat content and protected worms against glucotoxicity[78]. A follow-up study found that *pgph-2* overexpression mediated these effects through HLH-30, and that *pgph-2* could reduce oxidative stress caused by a high-glucose diet[125].

A limitation of these[71,78,125] studies on the effects of glucose excess in worms is the treatment used to achieve glucotoxicity. The standard practice is to supplement plates with 2% glucose and compare them to standard NGM plates, not considering that glucose addition to the agar also induces hyperosmotic stress, and making it challenging to distinguish between the osmotic and metabolic effects of glucose. Hyperosmotic stress by sorbitol supplementation has been shown to increase worm lifespan through a mechanism overlapping with dietary restriction, and requiring *gpdh-1* and *gpdh-2*[126].

## 3.3 The chemosensory system

Although *C. elegans* is composed of only 959 somatic cells, 302 of them are neurons and 56 more are neuronal support cells. 32 of these neurons are specifically committed to chemosensation, allowing worms to detect, integrate and locate positive and noxious chemical stimuli[127]. This reliance on chemical cues is reflected in the genome, which encodes over 1200 chemoreceptor genes, about 7% of its total gene count[128].

*C. elegans* is equipped to detect a vast array of both water-soluble and volatile compounds to navigate its environment and locate food. Volatile organic compounds, most of which are natural products of bacterial metabolism, are highly attractive to *C. elegans*. A comprehensive survey demonstrated that 50 out of 121 volatiles tested on worms were strong attractants, including alcohols, ketones, aldehydes, esters and aromatic compounds[129].

The nematode's chemosensory neurons are distributed across three organ types[127]:

1. Amphids: Two primary sensory organs located in the head, each containing 11 chemosensory neurons.
2. Phasmids: Two organs located in the tail, each containing 2 chemosensory neurons.
3. Inner Labial Organs: Six distinct organs in the head, each containing one chemosensory neuron.

These chemosensory neurons generally belong to bilaterally symmetric pairs. All sensory neurons in *C. elegans* possess specialised sensory endings called cilia. To detect environmental cues, these cilia are directly or indirectly exposed to the outside world through openings in the cuticle.

The chemosensory system is functionally divided into two modalities based on the nature of the chemical cues[130]. The detection of water-soluble chemicals typically requires closer proximity to the source. This "taste" function is mediated by neurons such as ADF, ASG, and ASI, with the bilaterally symmetric ASE amphid neurons acting as the main sensors. Volatile odors, which can be detected over longer distances, are primarily sensed by the AWA, AWB, and AWC neurons. Besides foraging, worms employ their chemosensory system to direct a wide range of other behaviours. These include avoidance of pathogens[131], predators[132] and toxins[133]. Male *C. elegans* utilise additional chemosensory circuits to find mates[134].

## 3.4 Regulation of physiology, metabolism and lifespan by food olfactory cues

Beyond guiding behaviour and chemotaxis, olfactory food cues play a profound role in regulating worm physiology. At the developmental level, the detection of food cues (or the lack thereof) is a primary determinant for the decision to enter the dauer larval stage, as well as the signal to exit dauer when conditions improve[135]. In adult animals, the perception of food odors influences organismal traits including the determination of overall body size[136] and the systemic regulation of fat storage[137]. At the cellular level, olfactory food perception can remodel homeostatic pathways by stimulating proteostatic responses[138] or modulating peripheral mitophagy and mitochondrial function[139], potentially to prepare the animal for the metabolic burden of feeding.

Because olfaction coordinates these fundamental physiological and cellular processes, it is unsurprisingly a factor influencing organismal lifespan. Early, comprehensive research on lifespan regulation by chemosensory neurons showed that ablating AWA olfactory neurons extended lifespan without affecting feeding levels, through a mechanism partially dependent on *daf-16*[140]. A later study found that exposing worms to volatiles produced by live OP50 bacteria could reduce by 50% DR-induced longevity, while having no effect on the lifespan of ad libitum fed worms. Food odours suppressed octopamine release from RIC neurons, which suppressed intestinal AMPK activation induced by DR and the resulting *daf-16* activation[141]. This food odor sensing pathway also required serotonin, dopamine and tyramine. Miller et al.[142] largely replicated these findings, by showing again that live bacteria exposure repressed DR

lifespan, and also showed that this exposure could repress *fmo-2* induction during DR. By individually testing volatiles sensed by *C. elegans*, they further found that various attractants could suppress DR-mediated induction of *fmo-2*. They showed that food odor was sensed by AWC neurons and suppressed intestinal *fmo-2* through signalling involving serotonin, dopamine and octopamine. In contrast, a smaller study found that exposure to isoamyl alcohol, a chemoattractant, could promote longevity through *daf-16*[143]. In summary, many studies seem to agree that olfactory sensing of food odors suppresses longevity, particularly lifespan extension caused by DR. This process seems to require complex neuronal signalling involving serotonin, dopamine and octopamine. There also may be a common end point in regulation of *daf-16* dependent gene expression.

The majority of studies that have looked at olfactory modulation of worm physiology and lifespan have done so by chronically suppressing olfactory functions with mutations or laser ablation, either alone[136,138,140] or in combination with chronic exposure to bacterial associated volatiles[139,141,142,143]. Consequently, while the long-term metabolic and longevity outcomes of food perception are well documented, the direct physiological responses to food cue exposure remain poorly understood. Filling this critical gap in our understanding of acute olfactory-metabolic coupling was a major objective of this thesis.

An interesting precedent in this sense is the study by Mutlu et al.[137]. These authors showed that exposing fasting worms to 2-butanone blocked the activity of $AWC^{ON}$ neurons, leading to an increase in fat storage levels within four hours of exposure. The authors speculated that this volatile, which can be produced by bacteria during fatty acid oxidation, may be acting as a signal of limited environmental lipid availability. This would make it a fascinating example of worms employing a food-associated volatile cue to inform metabolic adaptation.

## 3.5 Diacetyl food cue model

Among the volatiles sensed by *C. elegans*, diacetyl (2,3-butanedione) stands out as one of the most characterised in terms of ecological function, sensing mechanisms and effects on worm behaviour and physiology (**Fig. 4**). Diacetyl is a highly volatile, naturally occurring α-diketone produced during yeast fermentation[144] and by lactic acid bacteria (LAB) grown in the presence of citrate. Demonstrating its ecological relevance, a study found that *C. elegans* can prey on LAB growing on rotting citrus fruit by sensing their diacetyl production[145].

Bargmann et al. first showed that worms are potently attracted to diacetyl at a broad range of concentrations, from the undiluted compound to a $10^{-6}$ dilution (0.0001 %) in ethanol. The chemoattraction towards diacetyl was highest at a 1% dilution. This was found to be largely, but not completely, dependent on AWA neurons[129]. ODR-10, a transmembrane domain receptor localised to AWA sensory cilia, was later identified as the receptor specifically mediating chemotaxis towards diacetyl. *odr-10* mutants were particularly defective in sensing diacetyl over the 1 to 0.1% dilution range, but could still detect diacetyl at a 10% dilution[146].

In contrast with the early Bargmann study, a 2012 report[147] found that worms seemed to be repelled by undiluted diacetyl. This avoidance was found to be mediated by the SRI-14 receptor expressed in ASH nociceptor neurons, specifically induced by undiluted diacetyl[148]. These authors also identified four other candidate receptors for high concentrations of diacetyl, but did not validate them. More recently, another study reported diacetyl avoidance at concentrations between 10% and 100%. This effect was partially mediated by the LITE-1 photoreceptor expressed in ASH, ADL and ASK neurons[149]. These studies paint a complex picture of diacetyl sensing, which seems to involve multiple receptors active at different concentrations. Differences in the effects of diacetyl dilutions may stem from variations in individual protocols, but it seems that worms may avoid diacetyl at concentrations above 10%.

The effects of diacetyl have also been studied at the physiological level. Miller et al.[142] showed that diacetyl exposure (0.88 % dilution) slightly suppressed *fmo-2* induction in DR conditions and slightly increased it in fed conditions. Park et al.[150] found that daily exposure to 1% diacetyl reduced DR-induced lifespan extension by decreasing *daf-16* activity. Interestingly, this effect was maintained in *odr-10* and *sri-14* mutants, suggesting a different sensing mechanism. The authors also found that exposure to odors from live LAB was not sufficient to reduce DR lifespan.
In summary, existing literature indicates that volatile diacetyl is perceived as a food cue in *C. elegans*, although the direct physiological effects of diacetyl sensing have not been described.

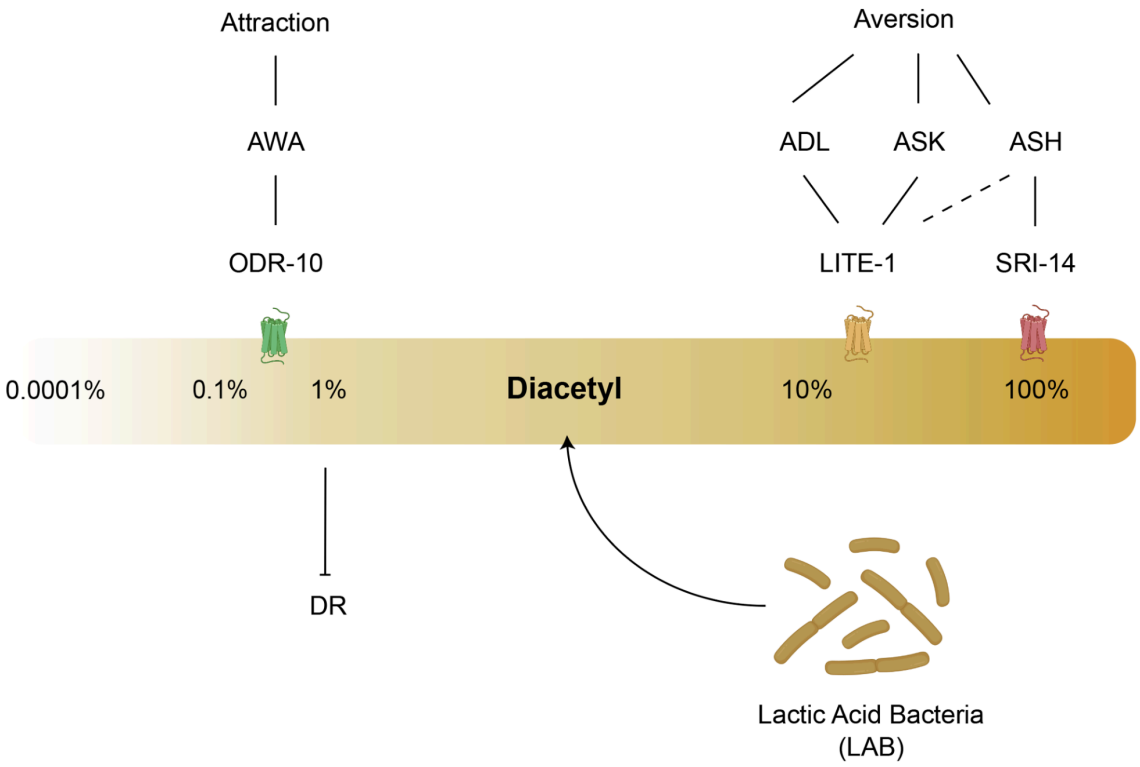


**Figure 4: Diacetyl food cue model.** Diacetyl is a metabolic byproduct of fungal and bacterial fermentation, produced by LAB predated by *C. elegans*. Diacetyl is sensed by worms across a broad range of concentrations, even at dilutions as low as 0.0001%. ODR-10, expressed in AWA neurons, has been identified as the receptor with highest diacetyl affinity, mediating chemoattraction particularly in the range of 0.1% to 1% dilutions. Chronic exposure to 1% diacetyl has been found to reduce DR longevity. At concentrations above 10%, diacetyl aversion is mediated by LITE-1,a receptor functioning mainly in ADL and ASK neurons, and also expressed in ASH neurons. Aversion to undiluted diacetyl is additionally mediated by SRI-14, activated in ASH neurons.

## 3.6 Olfactory regulation of gene expression

As previously established (section 3.4), the direct physiological responses to food cue exposure remain largely uncharted in *C. elegans*. More broadly, while physiological anticipatory food responses are well characterised in other organisms, this is just beginning to be explored at the gene expression level (section 2.7). *C. elegans* serves as an ideal model to dissect transcriptional AFR, because there are already clear precedents for olfaction driving rapid gene expression changes. These come particularly from the context of host-pathogen interactions, where the olfactory system's role in detecting environmental threats is well understood.

A 2017 study demonstrated that pre-exposure to odors from the pathogen *Pseudomonas aeruginosa* not only enhanced behavioural avoidance but actively primed the organism's cellular defences. The perception of these pathogenic cues boosted the expression of protective chaperone genes. Mechanistically, this olfactory signalling promoted the rapid localisation of HSF1 to nuclear bodies in non-neuronal tissues, arming the peripheral proteostasis network before infection ever occurred[151]. Later research identified a specific odor, 1-Undecene, produced by *P. aeruginosa* that induced behavioural avoidance and expression (after 2h exposure) of immune response genes of the *irg* family[152]. More recent work has revealed that exposure to 1-undecene also induces peripheral $UPR^{ER}$ induction[153].

These studies have set up a precedent for the role of olfaction in priming rapid, transcriptionally driven, homeostatic responses against pathogens. Building upon this framework, a major objective of this thesis was to test the hypothesis that olfactory food cues can similarly prime rapid, transcriptional homeostatic responses to defend against nutrient stress.

### 3.7 *C. elegans* as a model for memory formation

While the olfactory system allows *C. elegans* to navigate its environment and regulate its physiology, these responses are not rigid reflexes. The nematode possesses a remarkable capacity for neuroplasticity, making its olfactory system an interesting model to study learning and memory. By pairing specific volatile odors with either a positive (food) or negative (starvation or pathogenic bacteria) stimulus, researchers can train the worms and measure their chemotactic behaviour to study associative memory[154].

*C. elegans* memory formation relies on conserved molecular pathways. Like other animals, worms can form both short-term and long-term memory. Short-term memory relies on the transient changes in synaptic strength and does not require changes in gene expression. Long-term (and intermediate term) memory on the other hand, lasting longer than one hour, requires *de novo* protein synthesis[155].

## 4. Protein synthesis in ageing

### 4.1 Protein synthesis ageing decline

Loss of proteostasis is a hallmark of ageing, and protein synthesis is the first step in maintaining this balance. The evidence linking protein synthesis to the ageing process is abundant and evolutionarily

conserved across species, yet the exact nature of this relationship remains unresolved. The effects of ageing on protein synthesis have been a subject of investigation for over five decades, leading to the consensus that protein synthesis rates decline with age. Early studies utilising cell-free extracts first reported a reduction in the incorporation of radioactive amino acids into proteins in older tissues[156]. This age-related decline has been documented across models including yeast[157], *Drosophila*[158], various mouse tissues[159], and potentially even humans[160]. By 1991, a review of the literature already reported decreased global protein synthesis as a feature of organismal ageing, and pointed out to the future need to focus on changes in synthesis rates of individual proteins[161]. The molecular mechanisms driving this decline are most likely complex and interconnected, and remain a subject of investigation.

## 4.2 Mechanisms for protein synthesis decline

Decades of research have sought to identify the weak link in the protein synthesis machinery responsible for this decline. Most of the steps involved in mRNA translation have been shown to become deregulated or inefficient with ageing.

The level, and more importantly the stoichiometry, of ribosomal proteins is altered during ageing[162,163,164], potentially leading to impaired ribosome assembly and protein aggregation. A recent, comprehensive study of protein synthesis in the killifish model, found that while tRNA levels were unaltered with age, their charging state was globally decreased, potentially because of decreased abundance of tRNA synthetases[165]. Both levels and activity of translation factors are affected by ageing[166]. The levels of several translation initiation factors decrease with age [167] , as do translation initiation rates[168]. Similarly, translation elongation factors [169] and elongation rates[170] decrease with age. The decrease in the abundance of these factors has been linked to both changes in their transcription[171] and translation[172]. Interestingly, several studies have observed a loss of correlation between mRNA and protein levels with age[164,165].

Increased ribosomal pausing has recently come into the spotlight as a significant feature of ageing in organisms such as yeast, worms and killifish[173,165]. These studies have found ribosomal pausing to occur particularly on transcripts encoding stretches of positively charged amino acids (lysine and arginine), known to decrease elongation speed through interactions with the negatively charged ribosome exit channel[174]. Besides intrinsic mRNA properties, changing levels of miRNA and RNA binding proteins also contribute to modulate translation during ageing[166].

## 4.3 The protein synthesis ageing paradox

Given the essential role of protein synthesis, its decline with age has been thought to contribute to the ageing phenotype. In apparent contradiction with this, genetic or pharmacological interventions that reduce the rate of protein synthesis (and particularly mRNA translation) have been found to consistently extend lifespan[175]. Interventions such as the knockdown of specific ribosomal subunits[176], translation initiation factors[177], or inhibition of mTOR signalling[178] promote longevity across diverse species, including yeast, nematodes and mammals. This has been termed the "protein synthesis paradox"[175].

Recent findings have complicated the picture even further, by showing that certain interventions that maintain protein synthesis levels can also extend lifespan[179]. This reveals that both the inhibition and the maintenance of translation can promote longevity, potentially by acting through entirely different mechanisms or exerting effects in different tissues.

Two main types of explanations have been proposed to explain the "protein synthesis paradox":

- Hormetic Stress Responses: Inhibiting protein synthesis does not only reduce protein levels, but can also induce stress response pathways. The upregulation of these protective responses may promote longevity in an hormetic fashion. In support of this model, seminal research on *C. elegans* showed that lifespan extension from inhibition of translation initiation required *daf-16*, suggesting a stress response mechanism[180]. Later research supported this, by showing that the knock-down of translation initiation factors induced a *skn-1* dependent stress response[181]. More recently, reduction in levels of Pol III, required for tRNA synthesis, have been shown to induce the UPR and extend lifespan in worms and flies[182].
- Adaptive Decline: The natural decline in protein synthesis observed during normal ageing may not represent a "failure" of the cellular machinery, but rather an *adaptive* response. By slowing down translation, the ageing cell attempts to limit proteotoxic stress and match its protein output to its waning chaperone capacity. Supporting this, recent research in *Drosophila* has demonstrated that a transient spike of protein synthesis occurring in early adulthood drives long-term proteostatic damage and ageing. Prolonging this spike in WT flies reduced their longevity[183]. Also in support of this model, the translation-inhibiting antibiotic minocycline, extended lifespan in *C. elegans* independently of canonical stress pathways[184].

Ultimately, these complexities highlight a limitation in how we study this phenomenon. Understanding the role of protein synthesis in ageing requires a technological perspective shift: we must move away from purely quantitative approaches that measure bulk translation rates towards qualitative approaches that investigate exactly which transcripts are being preferentially translated, under what conditions, and in which tissues as the organism ages.

## 4.4 Technical developments in protein synthesis measures

Many foundational studies observing the ageing protein synthesis decline measured this in crude "cell-free" systems prepared from organ lysates, which probably did not reflect accurately *in vivo* conditions. Other studies used *in vivo* labelling with radioactive amino acids, but still lacked single protein resolution. This resolution problem was solved by methods (such as SILAC) combining metabolic pulse labeling with mass spectrometry (MS). MS based methods however suffer from bias toward abundant proteins and significant technical complexity[185].

An alternative approach which addresses these limitations is Ribo-seq (or Ribosome Profiling), developed in the Weissman lab in 2009[186]. This technique involves the deep sequencing of the mRNA fragments protected by translating ribosomes (Ribosome Protected Fragments, or RPFs), providing an indirect measure of protein synthesis. As a sequencing-based method, Ribo-seq provides the advantage of higher sensitivity and positional information of ribosomes along the transcripts. Because it requires no labelling, it offers a true snapshot of protein synthesis activity, and is easily applicable to *in vivo* systems[187].

A simple application of Ribo-seq is to pair it with mRNA sequencing to calculate Translational Efficiency (TE), also known as ribosome occupancy. TE is defined as the ratio of ribosome-protected reads (Ribo-seq) to total mRNA reads (RNA-seq) for a given gene**.** TE quantifies how efficiently ribosomes are translating the mRNAs available to them, providing a proxy for protein synthesis rates at single-transcript resolution and on a translatomic scale (**Fig. 5**).

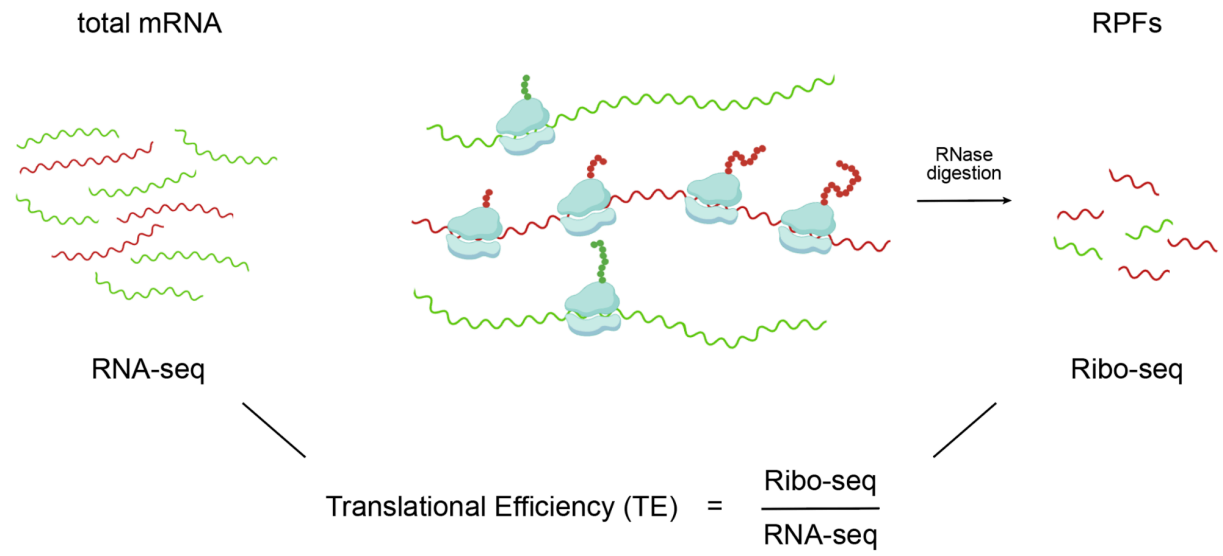


**Figure 5: Measuring Translational Efficiency (TE) by Ribo-seq and RNA-seq.** RNase digestion of ribosome bound mRNAs produces ribosome protected fragments (RPFS), which can be sequenced with Ribo-seq to provide an indirect measure of individual protein synthesis events. Ribo-seq values normalised by total mRNA levels (measured by RNA-seq) can be used to quantify TE for each transcript. Created with BioRender.com.

## 4.5 The translatome in ageing: a critical gap

Despite the proven power of combining RNA-seq and Ribo-seq, few studies have leveraged these techniques to measure changes in TE during ageing. The first study to do so looked at replicative ageing in yeast[188]. The authors observed downregulation of TE for the majority of detected transcripts, with no transcripts showing increased TE during ageing. The most severe TE declines occurred in transcripts that were highly abundant in young cells, particularly those encoding ribosomal subunits and other core components of the protein synthesis machinery. A second study looked at protein synthesis in the mouse liver and kidney[172]. These authors found no individual genes with statistically significant TE alterations with age. However, rank-based gene set analyses again revealed downregulation of translation-related transcripts. These transcripts were highly enriched for 5' TOP motifs, implying an age-related shift in mTORC1-mediated regulation. More recently, a study looking at proteostasis in the killifish brain also measured TE changes with ageing[165]. While they observed that these generally correlated with steady

state protein level changes, TE changes did not explain the age-related drop in ribosomal proteins. The study instead focused primarily on the phenomenon of translational pausing.

Overall, while Ribo-seq is beginning to penetrate ageing research, fundamental gaps remain in our understanding of how protein synthesis is rewired at the translatome level. While there is a consensus that global synthesis declines with age, the exact nature of this decline is unknown. Does this global suppression affect all genes equally, or does it follow a specific pattern? If the latter is the case, what regulatory mechanisms drive these translational shifts? It is particularly unclear which transcripts, if any, might actively increase in TE during the ageing process.

Finally, how do transcriptional and translational regulatory layers interact over time? While age-related transcriptional changes are well documented, it is unknown whether translational shifts act to buffer or exacerbate these transcriptional alterations. Answering these questions will contribute to understanding the links between protein synthesis and ageing, and may shed some light on the protein synthesis ageing paradox. This thesis aims to bridge this gap by measuring the translational landscape of ageing in *C. elegans*.

## 4.6 The ISR in ageing protein synthesis

The ISR has been proposed as a mechanism likely contributing to decreased protein synthesis and altered mRNA translation during ageing[166]. In healthy young cells, the ISR acts as a transient cellular defence mechanism. As outlined in section 1.5.2, several types of acute stress can trigger the phosphorylation of the translation initiation factor eIF2α, which halts global protein synthesis while inducing selective translation of certain stress-response transcripts. However, the accumulation of unresolved damage during ageing can lead to a state of chronic ISR activation. Accordingly, elevated levels of phosphorylated eIF2α have been observed in some ageing tissues[189]. eIF2α phosphorylation was found to increase during replicative ageing in yeast, although ATF4 translation did not[188].

Constitutive suppression of protein synthesis is particularly damaging for the nervous system. Because *de novo* protein synthesis is an absolute requirement for long-term memory consolidation, ISR activation can deprive synapses of the proteins required for this process. Mice with a heterozygous S51A mutation in eIF2α, partially blocking ISR activation, are viable and have reduced hippocampal eIF2α phosphorylation and ATF4 levels. Fascinatingly, these mice also show enhanced learning and long-term

memory across a variety of paradigms[190]. Besides its connection to memory formation, ISR hyperactivation is detected across brain diseases, including neurodegenerative disorders and traumatic injury[30]. The pathology of these diseases is also suggested to involve the activation of the ISR. Accordingly, genetic or pharmacological ISR inhibition is neuroprotective in models of Down Syndrome[191], Alzheimer's disease[192] and prion disease[193].

Beyond its role in neuroprotection, the ISR has emerged as a significant player in the ageing process. In *C. elegans*, genetic suppression of the ISR, via mutations in eIF2B or phosphorylation-defective S51A eIF2α, significantly extended lifespan and improved proteostasis[194]. This suggests that chronic ISR activation actively contributes to physiological decline, yet its specific impact on age-related translatome changes remains unknown. To address this gap, another objective of this thesis was to utilise the ISR-inhibited S51A eIF2α *C. elegans* model to map how this stress pathway contributes to the ageing translatome.

# 5. Thesis aims

This thesis covers two projects investigating gene expression responses in *C. elegans*.

**Project 1: Volatile diacetyl triggers *fmo-2* starvation response through DHAP shunt induction**

**Questions:**

1. Can a volatile food cue (diacetyl) induce an acute anticipatory food response (AFR) in *C. elegans* at the transcriptional level? Does this resemble the response to feeding or nutrient stress?
2. How would this anticipatory food response (AFR) impact metabolic adaptation and stress resistance?
3. How would this volatile-induced AFR interact with food deprivation responses?

**Impact:**

- For the first time, this work creates an unbiased, whole-body transcriptomic map of an AFR in an animal.
- I describe a model of acute and dynamic olfactory - transcriptional - metabolic coupling in *C. elegans*, where research has largely focused on chronic effects of volatile exposure.
- I uncover novel and potentially conserved mechanisms for nutrient sensing and metabolic homeostasis.

**Project 2: *C. elegans* ageing translatome**

**Questions:**

1. How does the translatome change during the normal ageing process of *C. elegans*? How is the translational efficiency (TE) of individual genes and wider biological processes affected?
2. What are potential mRNA features driving ageing translatome changes?
3. What is the integrated stress response (ISR) contribution to the ageing translatome? Is the ISR learning / memory function conserved in *C. elegans*?

**Impact:**

- For the first time, my work dissects transcriptional and translational contributions to ageing gene expression in a whole animal

# 6. Results Project 1:

# Volatile diacetyl triggers *fmo-2* starvation response through DHAP shunt induction

## 6.1 Volatile diacetyl exposure induces rapid DHAP shunt expression and phosphatidylglycerol (PG) accumulation

I chose an olfactory food cue to study how the sensory perception of food modulates gene expression in preparation for its arrival. I decided to opt for a chemical volatile instead of odour produced by live bacteria to ensure high reproducibility in Omics analyses. As a volatile odour I selected diacetyl, one of the best characterised food cue models (section 3.5). I established an experimental model for no-contact exposure to a 1% solution of diacetyl. This concentration was shown to be the most attractive to worms[129] and has been previously adopted for chronic exposure studies[150]. To identify the earliest and plausibly the most direct effects of diacetyl exposure on gene expression, I opted for a transcriptomics time course at high temporal resolution (**Fig. 6a**) with time points between 5 and 90 minutes. These time points are in line with the speed of transcriptional anticipatory food responses (AFRs) in other organisms[101,102]. Consistently with what has been done in the *Drosophila* and mouse studies, I decided to use food-deprived worms for my experiments, as well-fed animals would presumably be less responsive to a food signal.

PCA of the RNA-seq samples showed no clustering of control and diacetyl exposed groups, suggesting that diacetyl exposure did not broadly alter gene expression in my experimental model (**Fig. 6b**). In fact, differential gene expression analysis showed no significant differences between diacetyl and control groups at 5 (**Fig. 6c**) and 15 minutes of exposure (**Fig. 6d**).

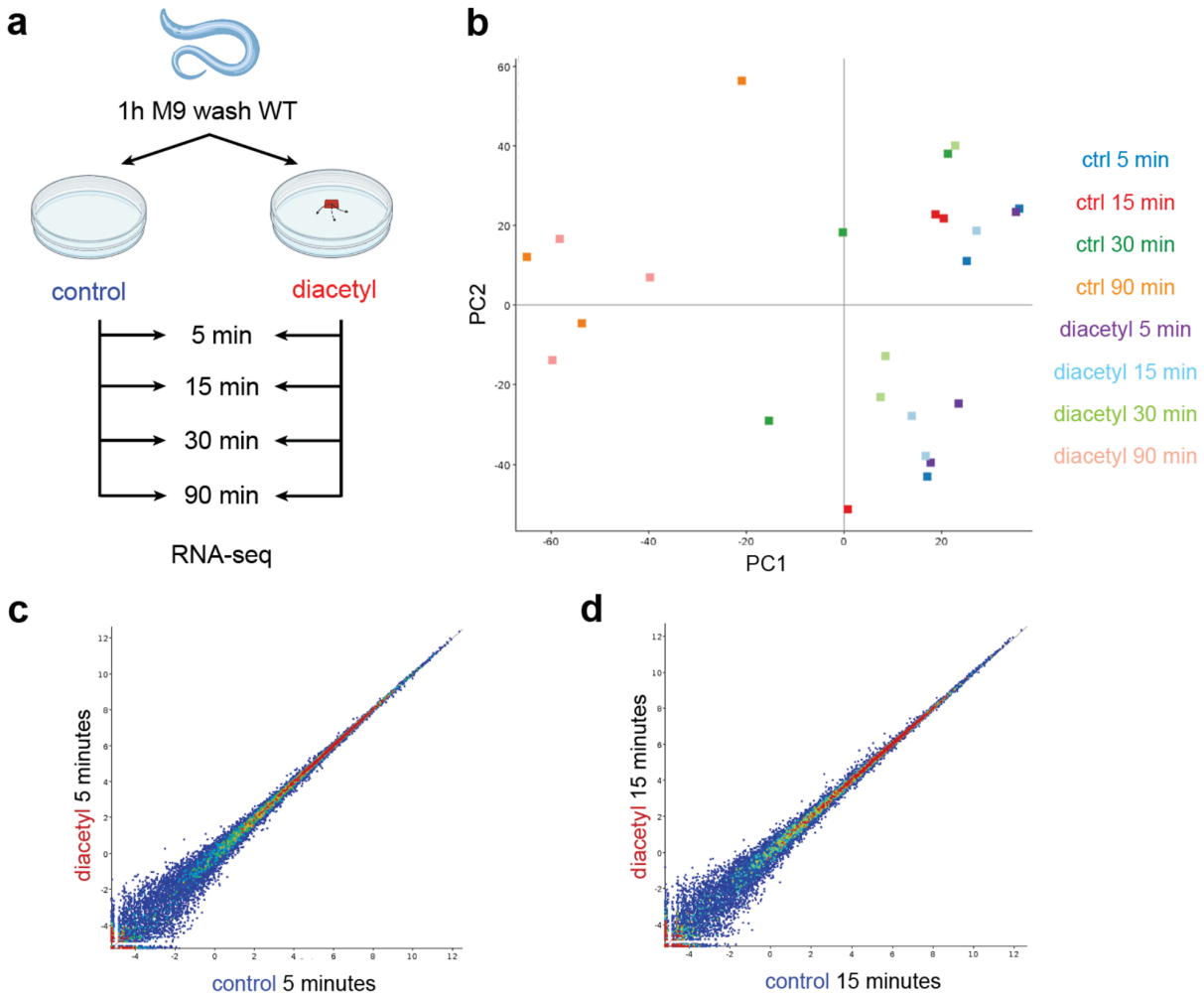


**Figure 6. Transcriptomics time course capturing acute gene expression responses to diacetyl exposure.** **a,** Experimental setup for measuring gene expression effects of diacetyl exposure in food-deprived worms, comparing control food deprivation (no volatile) to food deprivation in the presence of volatile diacetyl (1% solution in ethanol, pipetted on plate lid). Samples collected for RNA-seq over a ninety-minute time course. **b,** PCA plot of transcriptomics results from (a). **c** and **d,** Scatter plots comparing gene expression between control and diacetyl groups at 5 (**c**) and 15 (**d**) minutes of exposure.

The earliest significant effects appeared at the 30 minutes time point. Twelve genes were significantly upregulated by diacetyl exposures, while no genes were downregulated (**Fig. 7a**). The upregulated genes were *gpdh-1, pqm-1, T07E3.4, ogt-1, dpy-31, gpdh-2, pgph-2, pgph-3, F20G2.1, Y51A2D.13, Y43F8B.2* and *jmjd-3.3* (**Fig. 7b**), predicted to be expressed predominantly in the intestine and alimentary system

(**Fig. 7c**). Strikingly, five of these genes (*gpdh-1, gpdh-2, pgph-2, pgph-3* and *ogt-1*) are involved in the hyperosmotic stress response through their role in glycerol production. GPDH-1 and GPDH-2 convert DHAP into Gro-3P, which is converted by PGPH-2 and PGPH-3 into glycerol (section 3.2). Together, these two reactions form part of the DHAP shunt (section 2.4) (**Fig. 7d**). *ogt-1*, a conserved O-GlcNAc transferase, has been recently described as an essential regulator of the hyperosmotic stress response that enables *gpdh-1* upregulation[195].

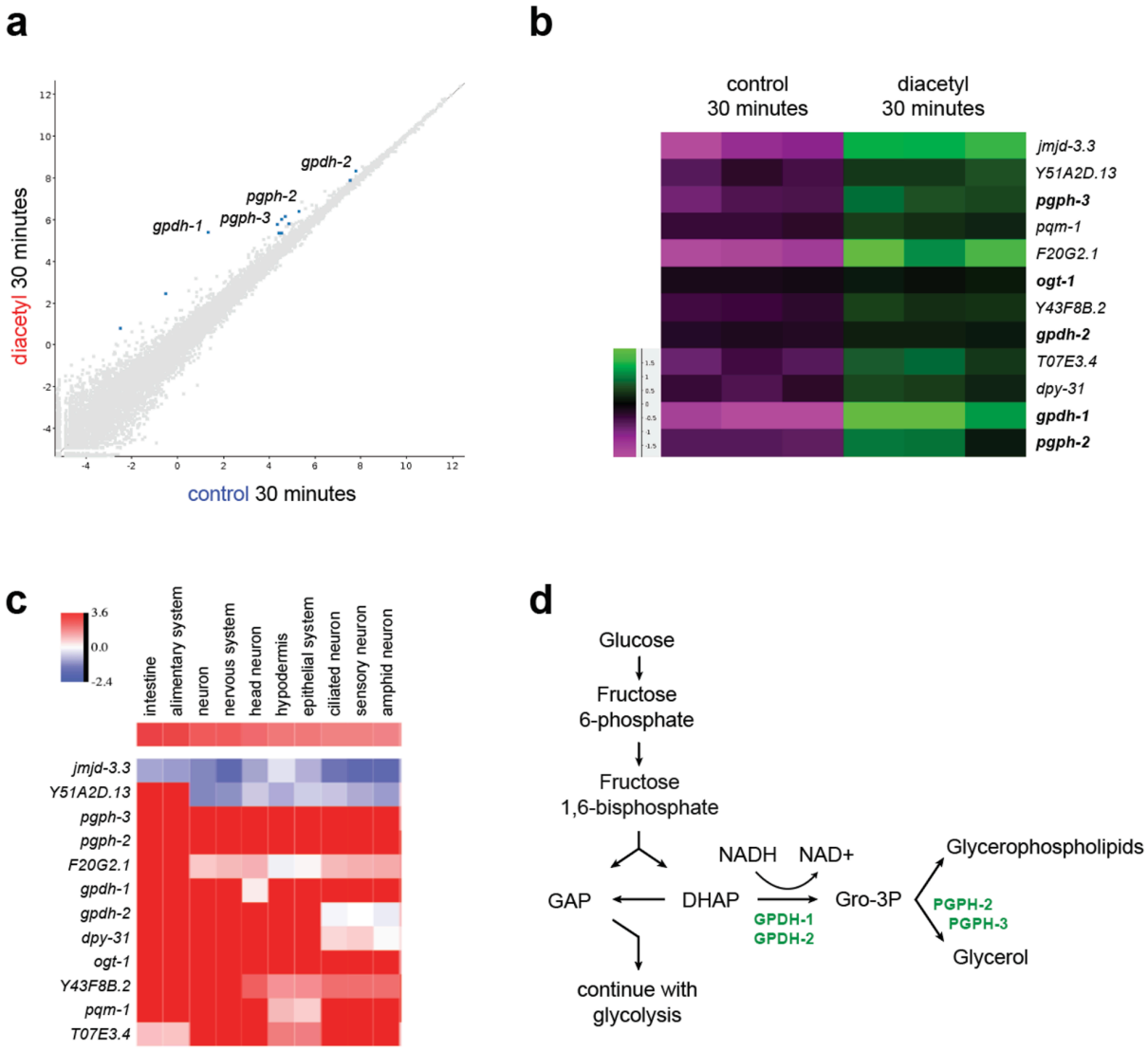


**Figure 7. Thirty minutes of diacetyl exposure induces expression of DHAP shunt enzymes.**
**a,** Scatter plot showing differential gene expression between control and diacetyl groups at 30 minutes of exposure. **b,** Heatmap showing differential gene expression between control and diacetyl groups at 30 minutes of exposure, highlighting genes involved in glycerol production. **c,** Predicted tissue expression scores for genes upregulated by diacetyl, in the top ten enriched tissues. **d,** Schematic depicting DHAP

shunt pathway, connecting glycolysis to synthesis of glycerol and glycerophospholipids. Highlighted in green are enzymes upregulated by diacetyl.

Having observed a transcriptional upregulation of enzymes in the DHAP shunt (**Fig. 8a**), I wanted to validate this response at the metabolic level. Using a colorimetric kit, I observed that diacetyl exposure led to a small (~15%) but significant increase in whole-worm glycerol levels (**Fig. 8b**). I also looked for more global diacetyl effects by employing metabolomics and lipidomics. Interestingly, I found that one hour of diacetyl exposure induced a metabolic shift primarily at the phospholipid level, and closely matching the transcriptional signature observed after 30 minutes of diacetyl exposure (**Fig. 8c**).

Diacetyl exposure altered the levels of 134 metabolites (77 increased, 57 decreased), 80 of these being glycerophospholipids. Diacetyl specifically increased the levels of 14 out of the 21 detected phosphatidylglycerols (PGs), particularly PG(16:0_20:2), PG(16:0_18:1) and PG(16:0_20:1), all containing palmitic acid (16:0). PGs are diacylglycerol (DAG) lipids with a glycerol head group, synthesised by a pathway that consumes phosphatidic acid (PA), Gro-3P and CTP (**Fig. 8d**).
Accordingly, diacetyl exposure decreased levels of 9 out of the 18 detected PA species, except PA(18:2_18:2) which was increased. Diacetyl also decreased levels of many lysophosphatidylcholines. Unexpectedly, diacetyl did not change levels of DHAP and Gro-3P, suggesting that these metabolites are being replenished after being consumed for PG synthesis.

I compared the effects of diacetyl exposure to the effects of hyperosmotic stress, which also induces the DHAP shunt (section 3.2). I exposed worms (in the presence of food) to 200 mM NaCl for three hours. As expected, this stress induced broader metabolic changes (132 metabolites increased, 121 decreased) compared to food cue exposure, but the nature and direction of the changes strongly overlapped to the diacetyl effects (**Fig. 8e**). Of the 77 metabolites increased by diacetyl, 31 were also induced by hyperosmotic stress. Of the 57 decreased by diacetyl, 30 were also decreased by 200 mM NaCl. 134 out of the 253 metabolites altered by hyperosmotic stress were glycerophospholipids. In detail, this stress increased the levels of 13 out of the 21 detected PGs (including the three species most induced by diacetyl), decreased levels of 10 out of the 18 detected PAs (except PA(18:2_18:2)) and most lysophosphatidylcholines. Unlike diacetyl, hyperosmotic stress reduced levels of both DHAP and Gro-3P, the latter being the metabolite most downregulated by this stress.

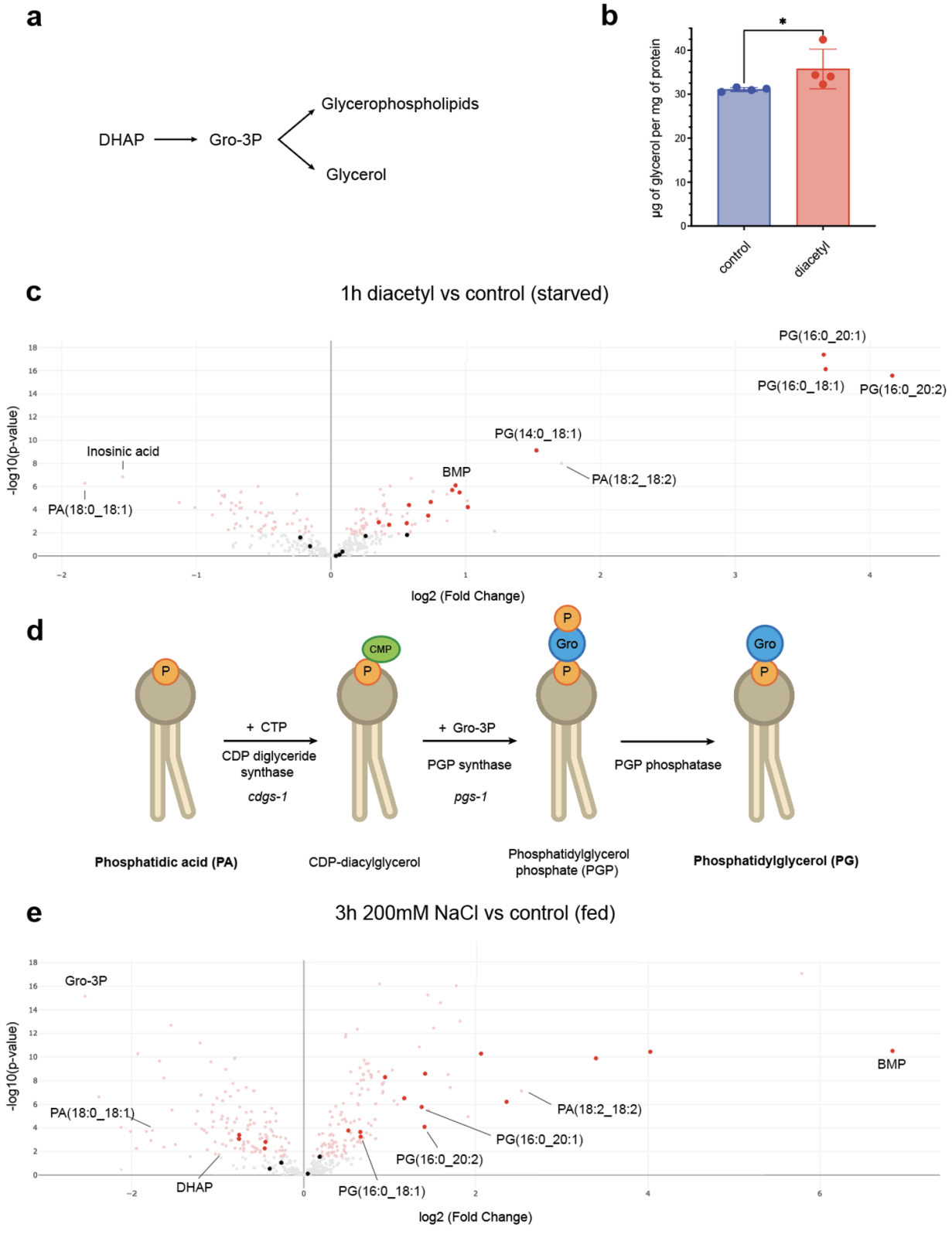
a
DHAP
Gro-3P
Glycerophospholipids
Glycerol
b
µg of glycerol per mg of protein
control
diacetyl
*
c
1h diacetyl vs control (starved)
-log10(p-value)
log2 (Fold Change)
Inosinic acid
PA(18:0_18:1)
BMP
PG(14:0_18:1)
PA(18:2_18:2)
PG(16:0_20:1)
PG(16:0_18:1)
PG(16:0_20:2)
d
P
CMP
Gro
+ CTP
CDP diglyceride synthase
cdgs-1
+ Gro-3P
PGP synthase
pgs-1
PGP phosphatase
Phosphatidic acid (PA)
CDP-diacylglycerol
Phosphatidylglycerol phosphate (PGP)
Phosphatidylglycerol (PG)
e
3h 200mM NaCl vs control (fed)
-log10(p-value)
log2 (Fold Change)
Gro-3P
PA(18:0_18:1)
DHAP
PG(16:0_18:1)
PG(16:0_20:2)
PG(16:0_20:1)
PA(18:2_18:2)
BMP

**Figure 8. Diacetyl exposure induces accumulation of glycerol and phosphatidylglycerols (PGs), resembling metabolic response to hyperosmotic stress. a,** Schematic depicting DHAP shunt pathway. **b,** Worm glycerol levels following two hours of diacetyl exposure, normalised by protein content (error bars represent means ± SD, Mann-Whitney test with *P = 0.0286). **c,** Volcano plot comparing metabolomic effects of diacetyl exposure (one hour) to control food deprivation. Metabolites significantly altered in red (FDR <0.05, Welch's t-test). Highlighted are metabolites classified as PGs. **d,** Schematic depicting synthesis of PGs from PA precursor lipids and Gro-3P. **e,** Volcano plot comparing metabolomic effects of hyperosmotic stress (three hours, 200 mM NaCl plates with food) to control NGM plates. Metabolites significantly altered in red (FDR <0.05, Welch's t-test). Highlighted are metabolites classified as PGs.

I decided to test whether the DHAP shunt and subsequent metabolic remodelling I observed could protect worms against hyperosmotic stress (**Fig. 9a**). Indeed, I found that one hour pre-exposure to diacetyl strongly protected worms from an acute hyperosmotic stress (M9 drop placed on a 500 mM NaCl plate) (**Fig. 9b**), suggesting an overlap in diacetyl and hyperosmotic responses not only at the transcriptional and metabolic levels, but also in stress adaptation.

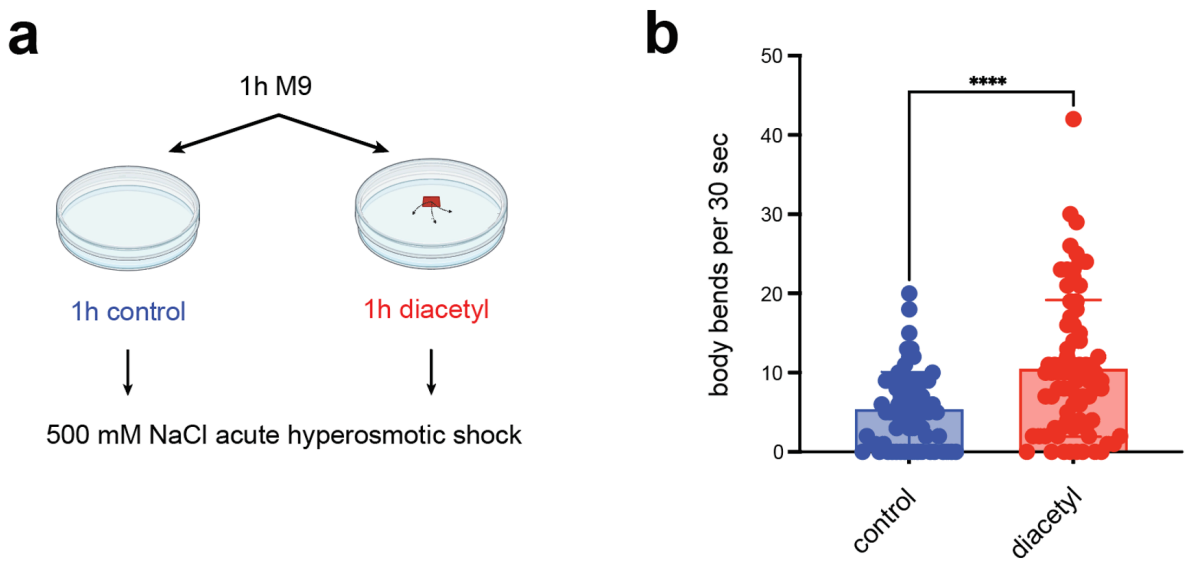


**Figure 9. Diacetyl exposure protects from acute hyperosmotic stress. a,** Experimental setup for measuring the effects of diacetyl exposure on acute hyperosmotic stress resistance. Worms were exposed to diacetyl for one (in the absence of food), before being transferred to an M9 droplet placed on 500 mM NaCl plates, where thrashing was recorded. **b,** Body bends of worms pre-exposed to diacetyl and measured in hyperosmotic stress conditions (error bars represent means ± SD, Mann-Whitney test with ****P < 0.0001).

These results identify the earliest transcriptional response to diacetyl as upregulation of the DHAP shunt, a metabolic pathway that funnels the DHAP glycolytic intermediate into production of glycerol and glycerophospholipids. Both the gene expression and metabolic responses to diacetyl resemble a hyperosmotic stress response, and consistently diacetyl exposure protects worms from acute hyperosmotic stress.

## 6.2 *gpdh-1* expression is modulated by nutrient availability and hyperosmotic stress

In addition to their canonical role in the *C. elegans* hyperosmotic stress response, enzymes in the DHAP shunt have recently emerged as metabolic regulators involved in glucotoxicity protection across organisms, as well as modulators of glycolytic flux (sections 2.4 and 3.2). I hypothesised that exposure to diacetyl leads worms to anticipate imminent feeding, causing an upregulation of the DHAP shunt to prepare for the nutritional demands associated with food ingestion.

I decided to focus on *gpdh-1* expression as a DHAP shunt proxy for the following experiments, being this the key enzyme supplying Gro-3P for PG synthesis, as well as the gene most upregulated by diacetyl. While a previous study[124] observed *gpdh-1* upregulation in worms raised on a high glucose diet (NGM supplemented with 2% glucose), the authors did not investigate whether this occurred through the metabolic or osmotic effects of glucose supplementation. Using plates supplemented with sorbitol as a control for the osmotic effect of glucose (2% glucose is equivalent to 111 mM), I showed that excess glucose induced the DHAP shunt through both osmotic and metabolic effects (**Fig. 10a** and **b**).

I then reasoned that if DHAP induction by diacetyl was an anticipatory food response, expression of these genes should also be regulated by food availability. I measured expression of the four DHAP shunt genes during four hours of food deprivation and after one hour of refeeding (**Fig. 10c**). *gpdh-1* was the gene most responsive to food deprivation and refeeding. During food deprivation, the expression of *gpdh-1* was rapidly repressed, and then upregulated upon refeeding. Of the other three genes measured, only *pgph-2* responded similarly to *gpdh-1*, although to a lesser extent (**Fig. 10c**). *gpdh-2* expression in particular was completely unaffected by starvation / refeeding. Whole-body *gpdh-1* expression remained at low levels throughout 24 hours of starvation (**Fig. 10d**). This is consistent with GPDH-1 playing a particularly important role in energy homeostasis during glucotoxicity, feeding and diacetyl exposure.

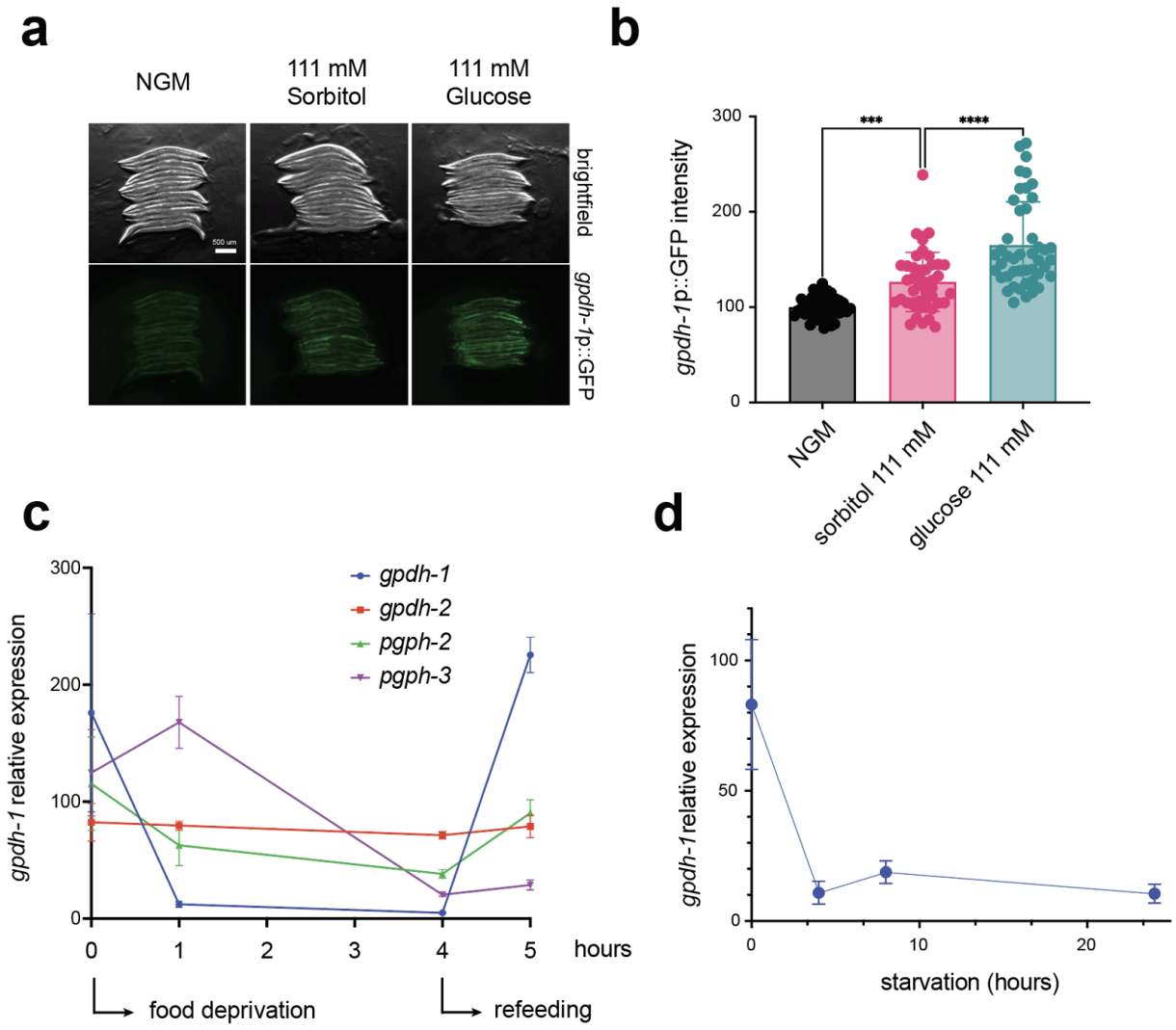


**Figure 10. *gpdh-1* expression is induced by glucotoxicity and repressed by food deprivation. a,** Induction of *gpdh-1* transcriptional reporter in worms raised on control, sorbitol or glucose supplemented plates. **b,** Quantification of reporter induction in experiment from (a). Error bars represent means ± SD, one-way ANOVA Tukey's post hoc test with ***P = 0.0005 NGM vs. sorbitol, ****P < 0.0001 sorbitol vs. glucose. **c,** Expression levels of DHAP shunt genes over four hours of food deprivation followed by one hour of refeeding, measured by qPCR. **d,** *gpdh-1* expression levels over twenty-four hours of food deprivation, measured by qPCR.

Knowing that *gpdh-1* expression is induced by hyperosmotic stress and repressed by food deprivation, I wanted to investigate how these opposing signals would interact when combined. As expected, exposure to 200 mM NaCl in the presence of food strongly induced a *gpdh-1* transcriptional reporter. Surprisingly, I

found that the repressive signal from food deprivation completely overrode the inductive signal from hyperosmotic stress, suggesting that nutrient availability is the dominant input governing the induction of this gene (**Fig. 11a**).

Having established this, I wanted to test whether diacetyl exposure may be acting as a hyperosmotic stressor or as a food signal. Similarly to above, I sought to dissect the overlap of food deprivation and diacetyl signals by exposing worms to diacetyl in the presence and absence of food. I found that unlike hyperosmotic stress, diacetyl upregulated *gpdh-1* expression more strongly during food deprivation: a 5.8 fold in the absence of food against a 2.4 fold increase in the presence of food. This result supports the hypothesis that diacetyl acts as a preemptive food signal that partially overlaps with, and anticipates, the response to food itself (**Fig. 11b**).

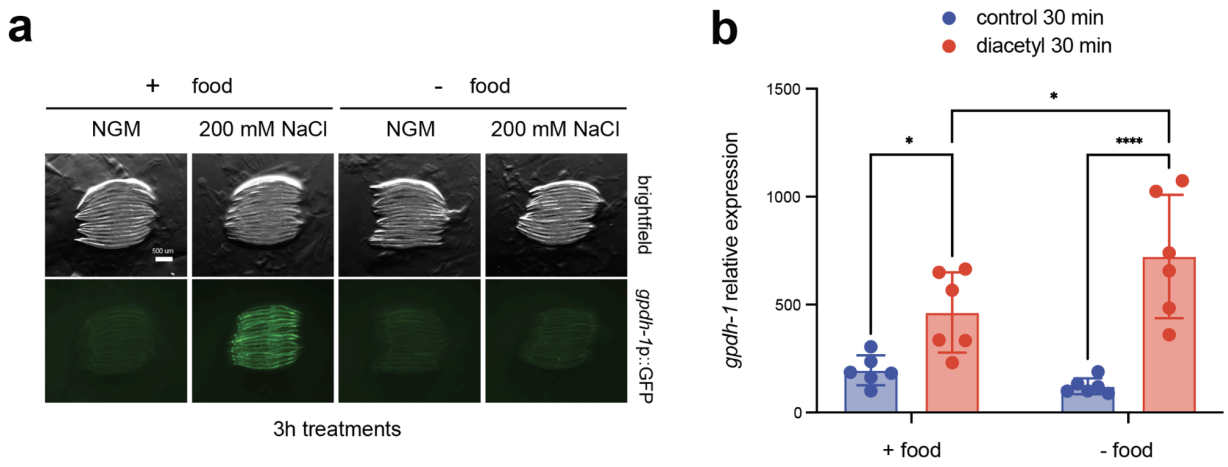


**Figure 11. Food deprivation differentially regulates *gpdh-1* induction by hyperosmotic stress and diacetyl. a,** Induction of *gpdh-1* transcriptional reporter in worms exposed to hyperosmotic stress (200 mM NaCl), in the presence or absence of food. **b,** *gpdh-1* expression levels following 30 minutes of diacetyl exposure, in the presence or absence of food. Measured by qPCR, normalised to control treatment for each food condition. Error bars represent means ± SD, two-way ANOVA Sidak's post hoc test; *P = 0.0447 control vs diacetyl (+food), ****P < 0.0001 control vs diacetyl (-food), *P = 0.0447 +food vs -food (diacetyl).

Together, these results show that *gpdh-1* expression, induced by diacetyl and hyperosmotic stress, is also more broadly induced by nutrient availability in the form of excess glucose or food. I hypothesise that the DHAP shunt may be shut down in the absence of food to maintain efficient energy metabolism, by promoting glycolysis over synthesis of glycerophospholipids and glycerol.

## 6.3 Continued diacetyl exposure during food deprivation accelerates induction of *fmo-2* dependent starvation response

While DHAP shunt genes were no longer differentially expressed by 90 minutes, my transcriptomic analysis revealed a second, distinct wave of gene expression changes. Nine genes were significantly upregulated by diacetyl exposures, while no genes were downregulated (**Fig. 12a**). The upregulated genes were *C45E5.1, C06E4.3, F56D5.3, fmo-2, D1054.8, F20G2.1, cth-1, argk-1* and *eef-1A.2* (**Fig. 12b**). This wave was dominated by a strong upregulation of *fmo-2*, a flavin-containing monooxygenase that is a well-established marker of the dietary restriction (DR) response, as well as being required for longevity effects of DR [112]. This was particularly surprising and seemed to contradict previous literature on diacetyl and its interaction with DR (section 3.5).

Using a transcriptional *fmo-2* reporter I confirmed this effect and began to characterise this phenomenon by tinkering with the details of the protocol. I first showed that diacetyl exposure dramatically accelerated the induction of *fmo-2* during food deprivation (**Fig. 12c**), beginning from 90 minutes of exposure , consistent with the RNA-seq results. This effect peaked between 3 and 6 hours of exposure, resulting in a 6-fold induction of *fmo-2* compared to control starvation (**Fig. 12d**). Diacetyl exposure during a longer starvation period (15h) did not further increase the level of *fmo-2* induction, which remained around 5-fold (**Fig. 12e**). I decided to focus on three hour diacetyl treatments for most following experiments, as this point consistently induced strong *fmo-2* upregulation compared to control starvation. I tested whether increasing the pre-exposure starvation period could suppress or even reverse the effects of diacetyl. Instead, I observed that even worms that had been starved for 24 hours would induce *fmo-2* further when exposed to diacetyl (**Fig. 12f**). I also tested that diacetyl could induce *fmo-2* in older worms, specifically at day 5 (**Fig. 12g**), excluding the possibility that the effect was limited to young adults.

Most importantly, I found that diacetyl induction of *fmo-2* was dependent on food deprivation. Exposing worms to diacetyl in the presence of bacterial food (OP50) suppressed *fmo-2* induction (**Fig. 12h**). By using the drug ivermectin to block pharyngeal pumping and thus food ingestion, I reversed this suppressive effect of food, confirming that the act of ingestion, rather than an opposing olfactory signal from the food, is the mechanism by which food suppresses the *fmo-2* diacetyl response. I also confirmed that ivermectin treatment by itself would not induce *fmo-2* (**Fig. 12h**).

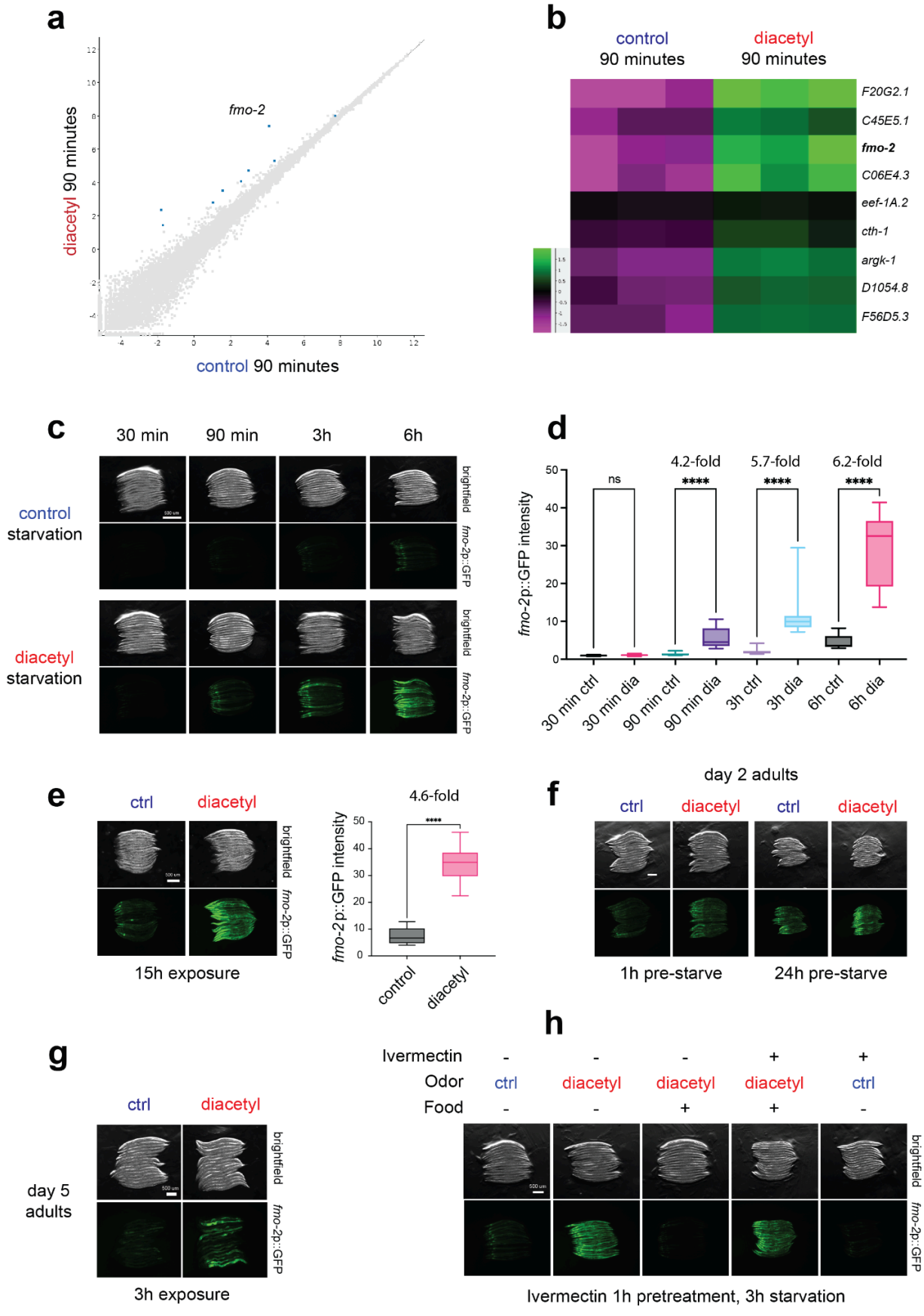
a
fmo-2
diacetyl 90 minutes
control 90 minutes
b
control
90 minutes
diacetyl
90 minutes
F20G2.1
C45E5.1
fmo-2
C06E4.3
eef-1A.2
cth-1
argk-1
D1054.8
F56D5.3
c
30 min
90 min
3h
6h
control
starvation
diacetyl
starvation
brightfield
fmo-2p::GFP
d
fmo-2p::GFP intensity
ns
4.2-fold
5.7-fold
6.2-fold
****
30 min ctrl
30 min dia
90 min ctrl
90 min dia
3h ctrl
3h dia
6h ctrl
6h dia
e
ctrl
diacetyl
15h exposure
4.6-fold
control
diacetyl
f
day 2 adults
1h pre-starve
24h pre-starve
g
day 5
adults
3h exposure
h
Ivermectin
Odor
Food
Ivermectin 1h pretreatment, 3h starvation

**Figure 12. Continued diacetyl exposure in the absence of food induces *fmo-2* expression. a,** Scatter plot showing differential gene expression between control and diacetyl groups at 90 minutes of exposure. **b,** Heatmap showing differential gene expression between control and diacetyl groups at 90 minutes of exposure, highlighting *fmo-2*. **c,** Induction of *fmo-2* transcriptional reporter in food deprived worms over six hours of food deprivation, in the presence or absence of diacetyl. **d,** Quantification from experiment in (c), Brown-Forsythe and Welch ANOVA test, ****P < 0.0001. **e,** Induction of *fmo-2* transcriptional reporter by diacetyl over 15 hours of starvation. Welch's t test, ****P < 0.0001. **f,** Induction of *fmo-2* transcriptional reporter by diacetyl over three hours of food deprivation, after a pre-starvation of either one or twenty-four hours. **g,** Induction of *fmo-2* transcriptional reporter by diacetyl over three hours of food deprivation, in day 5 old worms. **h,** *fmo-2* reporter worms treated with ivermectin for one hour, followed by diacetyl exposure in the presence or absence of food for three hours.

On a metabolic level, the effects of diacetyl remained largely consistent between one and three hours of exposure. PGs, particularly PG(16:0_20:2), PG(16:0_18:1) and PG(16:0_20:1), were still increased after three hours in diacetyl exposed worms compared to controls (**Fig. 13a**). At three hours of exposure, diacetyl additionally depleted the cellular nucleoside triphosphate (NTP) pool, specifically decreasing levels of ATP, CTP, and UTP (**Fig. 13b** - **d**). This depletion of high-energy phosphate donors may indicate a state of decreased energy availability in diacetyl exposed worms, consistent with increased *fmo-2* expression. Supporting the hypothesis that diacetyl exposure may be diverting metabolites away from glycolysis and mitochondrial respiration, diacetyl exposure also decreased levels of pyruvic acid starting from one hour of exposure (**Fig. 13e**).

I also looked for known metabolic signatures of *fmo-2*. Increasing the expression of this gene has been shown to increase levels of methionine and decrease levels of tryptophan, a direct substrate of FMO-2[114]. The metabolic effects of diacetyl exposure are consistent with an increased FMO-2 activity: diacetyl exposure consistently increased methionine levels at 1 and 3 hours (**Fig. 13f**) and decreased tryptophan at the one hour timepoint (**Fig. 13g**).

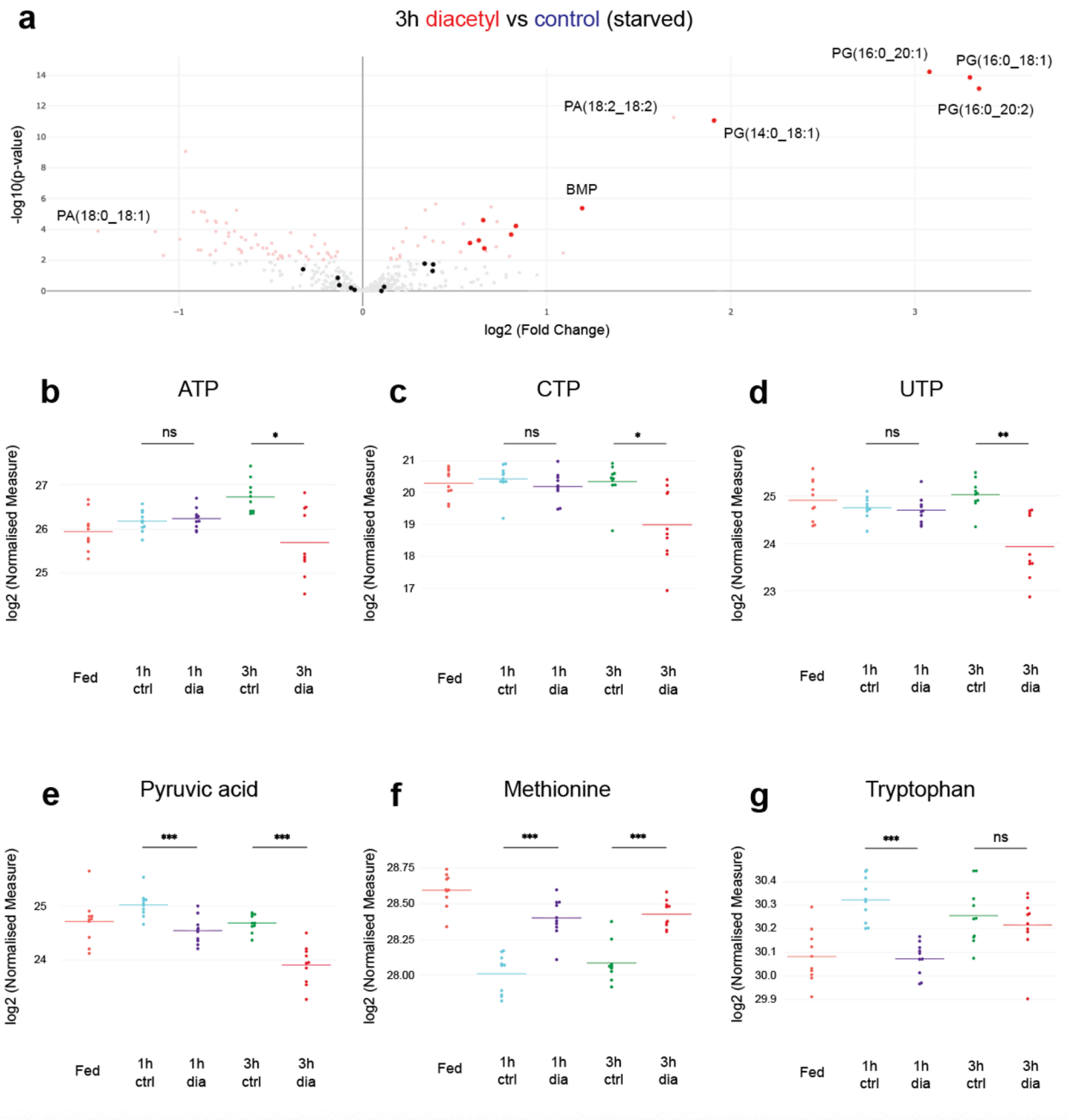


**Figure 13. Metabolic effects of prolonged diacetyl exposure. a,** Volcano plot comparing metabolomic effects of diacetyl exposure (three hours) to control food deprivation. Metabolites significantly altered in red (FDR <0.05, Welch's t-test). Highlighted are metabolites classified as PGs. **b** - **g**, Individual metabolite levels in fed and food deprived worms, starved either in control (ctrl) conditions or with diacetyl (dia) exposure. One hour and three hour time points. Log2 normalised levels on vertical axes. **b,** ATP levels, Welch's t-test with *P = 0.02. **c,** CTP levels, Welch's t-test with *P = 0.03. **d,** UTP levels, Welch's t-test with **P = 0.006. **e,** Pyruvic acid levels, Welch's t-test with ***P = 0.0003 (1h) and ***P = 0.0009 (3h). **f,**

Methionine levels, Welch's t-test with ***P = 0.0001 (1h) and ***P = 0.0003 (3h). **g,** Tryptophan levels, Welch's t-test with ***P = 0.0001 (1h).

To test if diacetyl might affect other known starvation-related phenotypes, I looked at feeding rates, measured by ingestion of fluorescent bacteria. Food deprivation has been shown to increase feeding rates (appetite) in *C. elegans*[107]. Diacetyl exposure in the absence of food increased appetite upon refeeding, while exposure to diacetyl on food did not have any effect (**Fig. 14a** and **b**). This suggests that diacetyl boosts the starvation-related appetite behaviour.

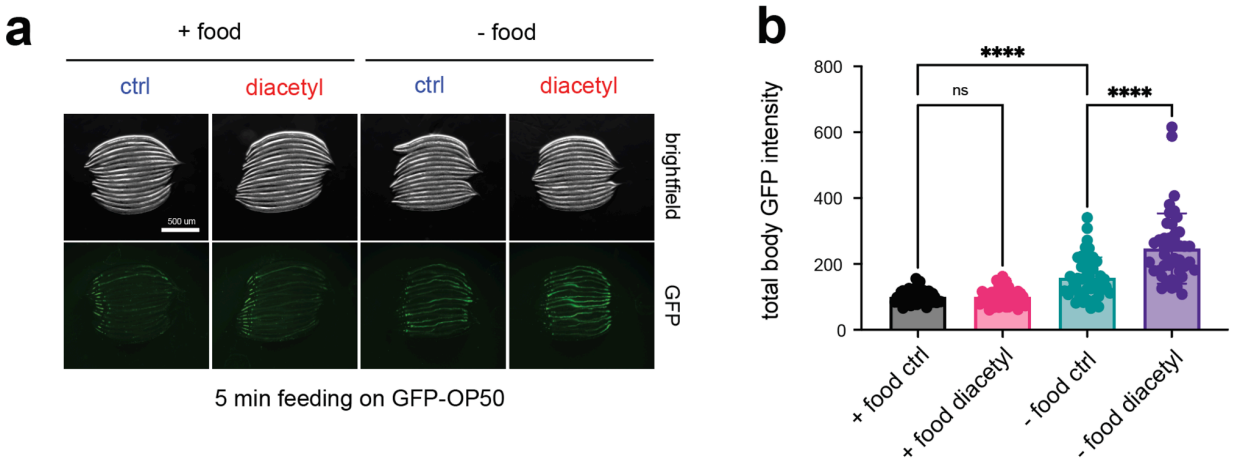


**Figure 14. Diacetyl exposure in the absence of food increases feeding rates. a,** Worms fed with GFP expressing bacteria following a three-hour exposure to diacetyl in the presence or absence of food. **b,** Quantification of GFP intensity from experiment in (a). Brown-Forsythe and Welch ANOVA test, ****P < 0.0001.

Fasting is known to produce beneficial effects in worms[196] . Similarly, *fmo-2* overexpression extends worm lifespan and increases stress resistance[112]. Given the effect of diacetyl in boosting *fmo-2* expression during food deprivation, I decided to test if diacetyl could also improve beneficial effects of starvation. I found that a three-hour starvation period on day 1 greatly improved thermotolerance on day 2, as assessed by thermorecovery on day 3. Diacetyl exposure combined with this starvation treatment further protected the worms, while diacetyl exposure on food had no effect (**Fig. 15a**). Additionally, I showed that this effect was *fmo-2* dependent (**Fig. 15b**). Together, these results indicate that continued diacetyl exposure during food deprivation accelerates the induction of *fmo-2* expression,

depletes high-energy phosphate donors and boosts starvation-related appetite and thermotolerance phenotypes.

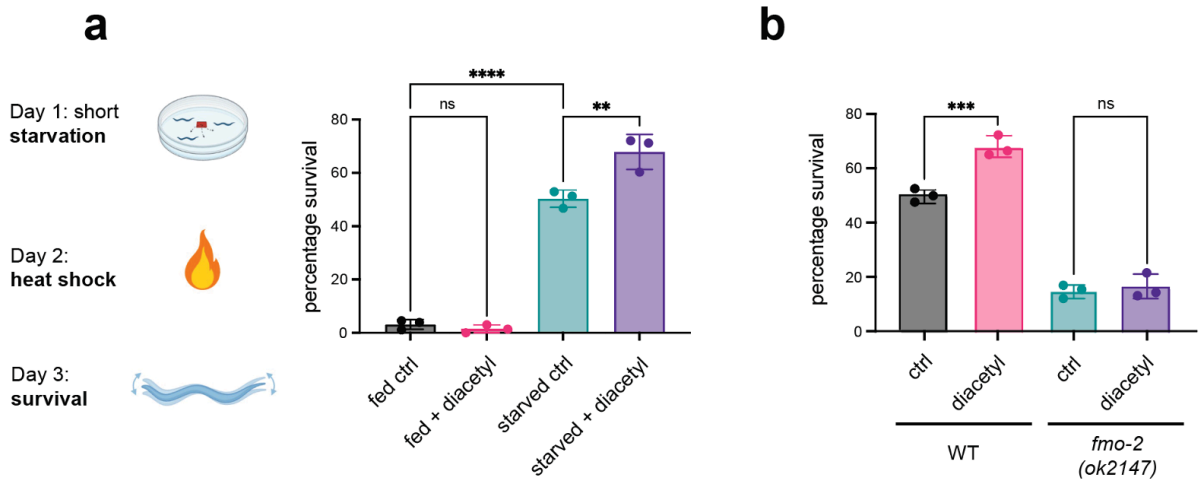


**Figure 15. Diacetyl exposure in the absence of food increases thermotolerance. a,** Day three survival of worms exposed for three hours to diacetyl in the presence or absence of food and heat-shocked on day two. Error bars represent means ± SD, one-way ANOVA Sidak's post hoc test with ****P < 0.0001 fed vs starved (ctrl), **P = 0.0015 ctrl vs diacetyl (starved). **b,** Day three survival of WT and *fmo-2* KO worms exposed for three hours to diacetyl in the absence of food and heat-shocked on day two. Error bars represent means ± SD, one-way ANOVA Sidak's post hoc test with ***P = 0.004 ctrl vs diacetyl (WT).

## 6.4 *fmo-2* induction does not depend on canonical diacetyl sensing mechanisms

Diacetyl has been shown to be chemoattractive to worms at dilutions ranging from 0.0001% to 10-100% and aversive above these concentrations, depending on the specific study (section 3.5). I thus wanted to test the relationship between diacetyl concentration and *fmo-2* activation. I exposed worms to ten-fold dilutions of diacetyl and found that it induced *fmo-2* more than the ethanol control in the 0.1% to 1% dilution range. Interestingly, the ethanol control itself induced *fmo-2* when compared to the worms exposed to no volatiles (**Fig. 16a** and **b**), opening the possibility that the effect might not be specific to diacetyl alone. For this reason, I tested two other attractive volatiles, 2-butanone and isoamyl alcohol,

previously found to affect worm lifespan and physiology as food cues (section 3.4). However I found that neither could induce *fmo-2* above the ethanol level (**Fig. 16c**), indicating that this is not a general property of volatile food cues. I also wanted to test whether methylglyoxal (MGO), an α-dicarbonyl compound chemically similar to diacetyl, could induce *fmo-2*. Given that MGO is primarily a breakdown product of GAP and DHAP, I reasoned that diacetyl may be mistaken for MGO and induce the DHAP shunt as a specific detox response. However, I did not observe any effect of MGO on reporter induction (**Fig. 16d**).

Diacetyl sensing has been previously linked to three receptors: ODR-10, SRI-14 and LITE-1 (section 3.5). ODR-10, the canonical receptor, particularly affects chemotaxis over the 1 to 0.1% dilution range[146]. SRI-14 mediates avoidance to undiluted diacetyl[148]. More recently, LITE-1 was shown to also modulate avoidance to 10-100% diacetyl[149]. I tested *odr-10* and *sri-14* mutants defective in diacetyl chemotaxis through an *fmo-2* qPCR. Either mutant induced *fmo-2* expression equally to WT worms, when exposed to my standard 1% diacetyl treatment (**Fig. 16e**). Chronic exposure to volatile food cues has been found to affect worm lifespan, depending particularly on serotonin and dopamine signalling (section 3.4). Accordingly, I decided to investigate if these signalling pathways would also mediate *fmo-2* induction in my model. I tested *tph-1* mutants, defective in serotonin production, and *cat-2* mutants, defective in dopamine production[142]. Again, I found that both mutants remained competent in *fmo-2* induction, with *tph-1* mutants even showing slightly higher response to diacetyl exposure (**Fig. 16f**).

Insulin signalling is another master regulator of feeding and food deprivation responses in *C. elegans*[107,197]. I observed that *daf-2* insulin receptor mutants also showed stronger *fmo-2* upregulation in response to the volatile treatment (**Fig. 16g**). Having found no individual signalling mutants that could suppress the effect of diacetyl, I shifted to blocking more fundamental mechanisms of neuronal transmission. UNC-13 is an essential protein required for neurotransmitter release from synaptic vesicles[198]. UNC-31 is required for neuropeptide release from dense-core vesicles[199]. I found that *unc-13* mutants behaved like WT in diacetyl induced *fmo-2* expression, while *unc-31* mutants had an even stronger diacetyl response (**Fig. 16h**). All together, these findings show that diacetyl induces *fmo-2* at a range of chemoattractive concentrations. However, diacetyl induction of *fmo-2* does not depend on canonical diacetyl receptors and neuronal signalling mechanisms.

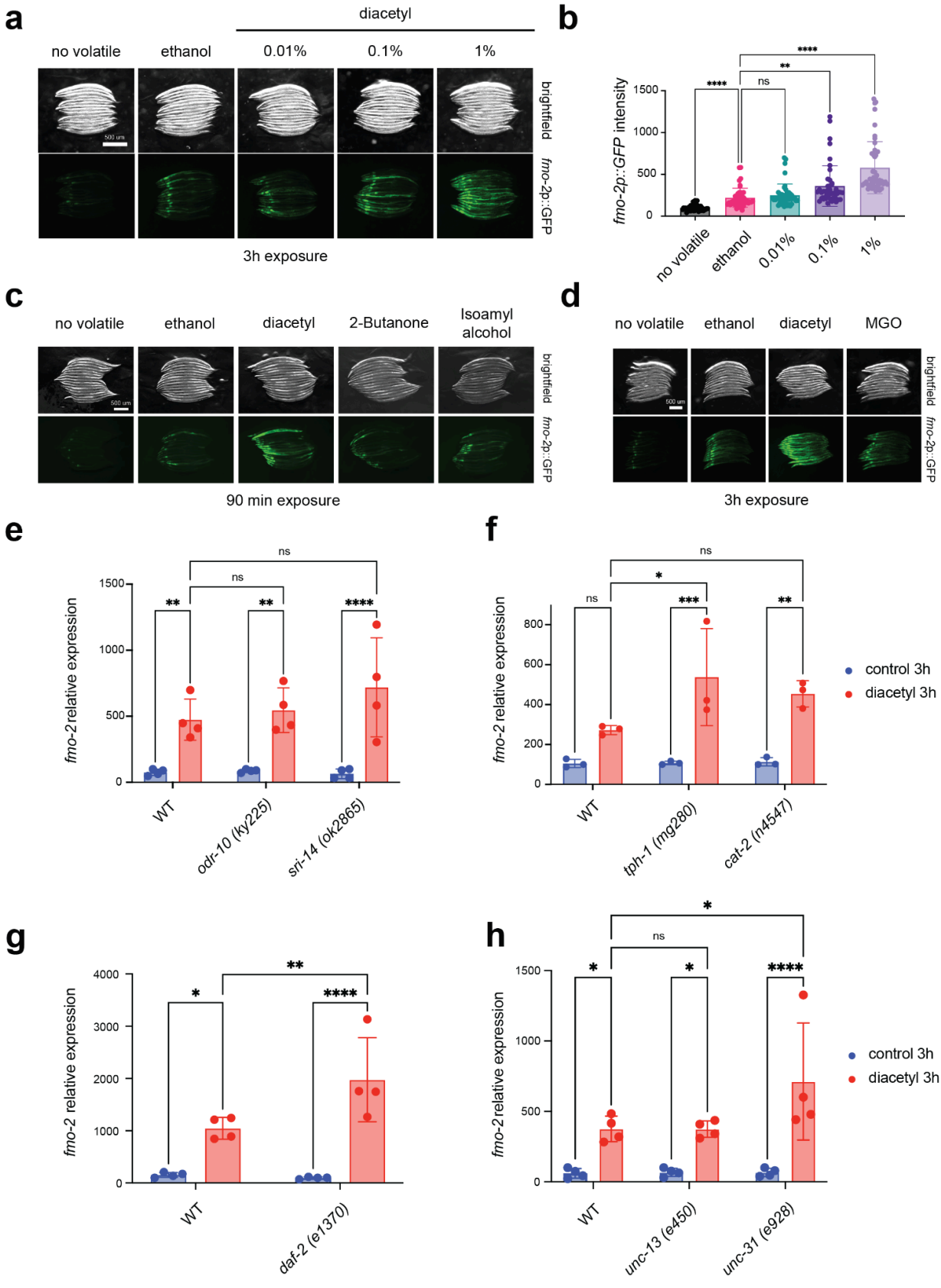
a
diacetyl
no volatile
ethanol
0.01%
0.1%
1%
brightfield
fmo-2p::GFP
3h exposure
b
fmo-2p::GFP intensity
no volatile
ethanol
0.01%
0.1%
1%
c
no volatile
ethanol
diacetyl
2-Butanone
Isoamyl alcohol
90 min exposure
d
no volatile
ethanol
diacetyl
MGO
3h exposure
e
fmo-2 relative expression
WT
odr-10 (ky225)
sri-14 (ok2865)
f
fmo-2 relative expression
WT
tph-1 (mg280)
cat-2 (n4547)
control 3h
diacetyl 3h
g
fmo-2 relative expression
WT
daf-2 (e1370)
h
fmo-2 relative expression
WT
unc-13 (e450)
unc-31 (e928)
control 3h
diacetyl 3h

**Figure 16. *fmo-2* induction by diacetyl does not depend on canonical sensing mechanisms. a,** *fmo-2* reporter worms exposed to no volatile (control), ethanol or diacetyl dilutions in ethanol, over three hours of food deprivation. **b,** Quantification from experiment in (a). Error bars represent means ± SD, Brown-Forsythe and Welch ANOVA test with ****P < 0.0001 vs no volatile, **P = 0.0035 vs 0.1% diacetyl, ****P < 0.0001 vs 1% diacetyl. **c,** *fmo-2* reporter worms exposed to no volatile, pure ethanol, 1% ethanol dilutions of diacetyl, 2-butanone and isoamyl alcohol, over 90 minutes of food deprivation. **d,** *fmo-2* reporter worms exposed to no volatile, pure ethanol, 1% ethanol dilutions of diacetyl and methylglyoxal (MGO), over three hours of food deprivation. **e** - **h**, *fmo-2* expression levels in worms starved either in control conditions or in the presence of diacetyl for three hours. Detected by qPCR. Normalised to control for each genotype. **e,** *fmo-2* expression levels in WT, odr-10 (ky225) and sri-14 (ok2865). Error bars represent means ± SD, two-way ANOVA Tukey's post hoc test with **P = 0.0059 ctrl vs diacetyl (WT), **P = 0.0021 ctrl vs diacetyl (odr-10), ****P < 0.0001 ctrl vs diacetyl (sri-14). **f,** *fmo-2* expression levels in WT, tph-1 (mg280) and cat-2 (n4547). Error bars represent means ± SD, two-way ANOVA Tukey's post hoc test with ***P = 0.0003 ctrl vs diacetyl (tph-1), **P = 0.0017 ctrl vs diacetyl (cat-2), *P = 0.0223 WT vs tph-1 (diacetyl). **g,** *fmo-2* expression levels in WT and daf-2 (e1370). Error bars represent means ± SD, two-way ANOVA Fisher's LSD test with *P = 0.01 ctrl vs diacetyl (WT), ****P < 0.0001 ctrl vs diacetyl (daf-2), **P = 0.008 WT vs daf-2 (diacetyl). **h,** *fmo-2* expression levels in WT, unc-13 (e450) and unc-31 (e928). Error bars represent means ± SD, two-way ANOVA Tukey's post hoc test with *P = 0.0211 ctrl vs diacetyl (WT), *P = 0.0244 ctrl vs diacetyl (unc-13), ****P < 0.0001 ctrl vs diacetyl (unc-31), *P = 0.0375 WT vs unc-31 (diacetyl).

## 6.5 DHAP shunt induction in the absence of food drives *fmo-2* expression

The distinct temporal sequence from my transcriptomic and metabolomics analyses, where DHAP shunt activation after 30 minutes is followed by PG accumulation at one hour of exposure, followed by *fmo-2* upregulation at 90 minutes, suggested a causal relationship between the shunt metabolic remodelling and *fmo-2* induction. I initially tested this hypothesis using genetic epistasis experiments. I found that combining RNAi knockdown of the DHAP shunt components *pgph-2* and *pgph-3* significantly reduced the induction of *fmo-2* by diacetyl, supporting a causal link between these (**Fig. 17a** and **b**).

Next, to test if shunt activation would be sufficient to induce *fmo-2* in the absence of a food cue, I leveraged its induction by hyperosmotic stress. Hyperosmotic stress in the presence of food slightly induced (29% increase) *fmo-2* expression. In comparison, three hours of starvation doubled *fmo-2* expression (**Fig. 17 c** and **d**). Pairing hyperosmotic stress and starvation did not increase FMO-2

induction. Having previously shown that food deprivation strongly suppresses shunt induction (**Fig. 11a**), I decided to pretreat worms with 200 mM NaCl while on food, before starting starvation at regular osmolarity. I found this pretreatment induced *fmo-2* by 8-fold (**Fig. 17c** and **d**), mimicking the effects of diacetyl. The effect could be suppressed by combined RNAi targeting either *gpdh-1* and *gpdh-2* or *pgph-2* and *pgph-3* (**Fig. 17e** and **f**), demonstrating that this metabolic pathway is the critical factor inducing *fmo-2* regardless of the upstream trigger.

I also tested if this effect on *fmo-2* expression would be coupled with a boost in starvation-related benefits. Indeed, I found that pairing the 200 mM NaCl pretreatment with food deprivation increased the beneficial effects on heat shock recovery (**Fig. 17g**), an effect not seen with hyperosmotic treatment on its own, mimicking the effects of diacetyl on thermotolerance.

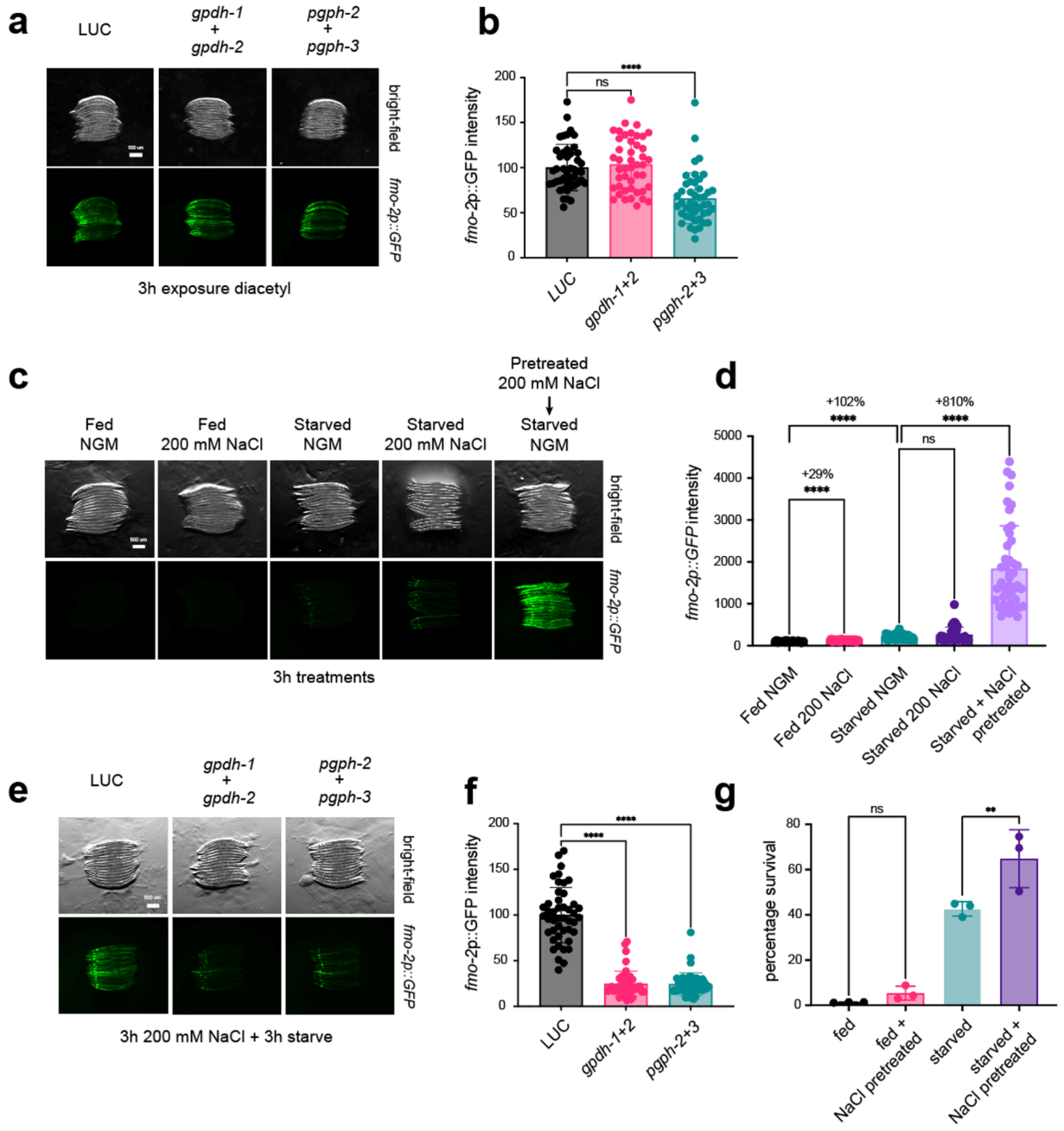


**Figure 17. Diacetyl and hyperosmotic stress induce *fmo-2* expression through DHAP shunt enzymes. a,** Three hour diacetyl induction of *fmo-2* reporter in worms raised on non-targeting Luciferase (LUC), combined RNAi targeting DHAP shunt components *gpdh-1* and *gpdh-2* or *pgph-2* and *pgph-3*. **b,** Quantification from experiment in (a). One-way ANOVA Tukey's post hoc test with ****P < 0.0001. **c,** Induction of *fmo-2* reporter by three hours of hyperosmotic stress (Fed, 200 mM NaCl), food deprivation (Starved, NGM), hyperosmotic stress combined with food deprivation (Starved, 200 mM NaCl) and hyperosmotic stress pretreatment in the presence of food followed by food deprivation at control osmolarity (Pretreated 200 mM NaCl + Starved NGM). **d,** Quantification from experiment in (c).

Brown-Forsythe and Welch ANOVA test with ****P < 0.0001 NGM vs 200 mM NACl (fed), ****P < 0.0001 fed vs starved (NGM), ****P < 0.0001 starved NGM vs NaCl pretreated. Percentage increase between conditions indicated above significance levels. **e,** Induction of *fmo-2* reporter by hyperosmotic stress pretreatment in the presence of food followed by food deprivation at control osmolarity, in worms raised on non-targeting Luciferase (LUC), combined RNAi targeting DHAP shunt components *gpdh-1* and *gpdh-2* or *pgph-2* and *pgph-3*. **f,** Quantification from experiment in (e). One-way ANOVA Tukey's post hoc test with ****P < 0.0001. **g,** Day three survival of worms exposed for three hours to 200 mM NaCl in the presence of food, followed by three hours at control osmolarity in the presence (fed + NaCl pretreated) or absence of food (starved + NaCl pretreated). Worms heat-shocked on day two. Error bars represent means ± SD, one-way ANOVA Sidak's post hoc test with **P = 0.0077.

The results so far suggested that induction of the DHAP shunt (by diacetyl or hyperosmotic stress) in the absence of food could drive *fmo-2* expression. I compared the metabolic effects of control starvation, starvation in the presence of diacetyl and hyperosmotic stress (on fed worms), looking for shared metabolic signatures (**Fig. 18a**). 14 metabolites were induced in common by these treatments, including 8 PGs and the three species most induced by diacetyl: PG(16:0_20:2), PG(16:0_18:1) and PG(16:0_20:1). 7 metabolites were reduced by all three treatments, including four PA species and reduced glutathione (GSH).

When reducing DHAP into Gro-3P, GPDH-1 also oxidises NADH into NAD+. I hypothesised that, by inducing *gpdh-1*, diacetyl and hyperosmotic stress may also be driving a shift towards an oxidative cell state. To test this, I calculated the ratio of reduced to oxidised glutathione (GSSG) measured across conditions. I found that prolonged diacetyl exposure (3h), but not hyperosmotic stress on fed worms, could strongly reduce this ratio, supporting the hypothesis of an oxidative shift in the worm redox state (**Fig. 18b**). Three hours of diacetyl exposure also decreased the levels of ATP and other high-energy phosphate donors (**Fig. 13b** - **d**). I calculated the ratio of ATP to ADP across conditions and again found that this decreased particularly after three hours of diacetyl exposure, indicating a low energy status (**Fig. 18c**). These results suggest that after three hours of exposure, diacetyl induces a metabolic shift not recapitulated by hyperosmotic stress in fed worms. This shift is characterised by an oxidised redox state and bioenergetic deficit, matching the *fmo-2* upregulation observed with this treatment.

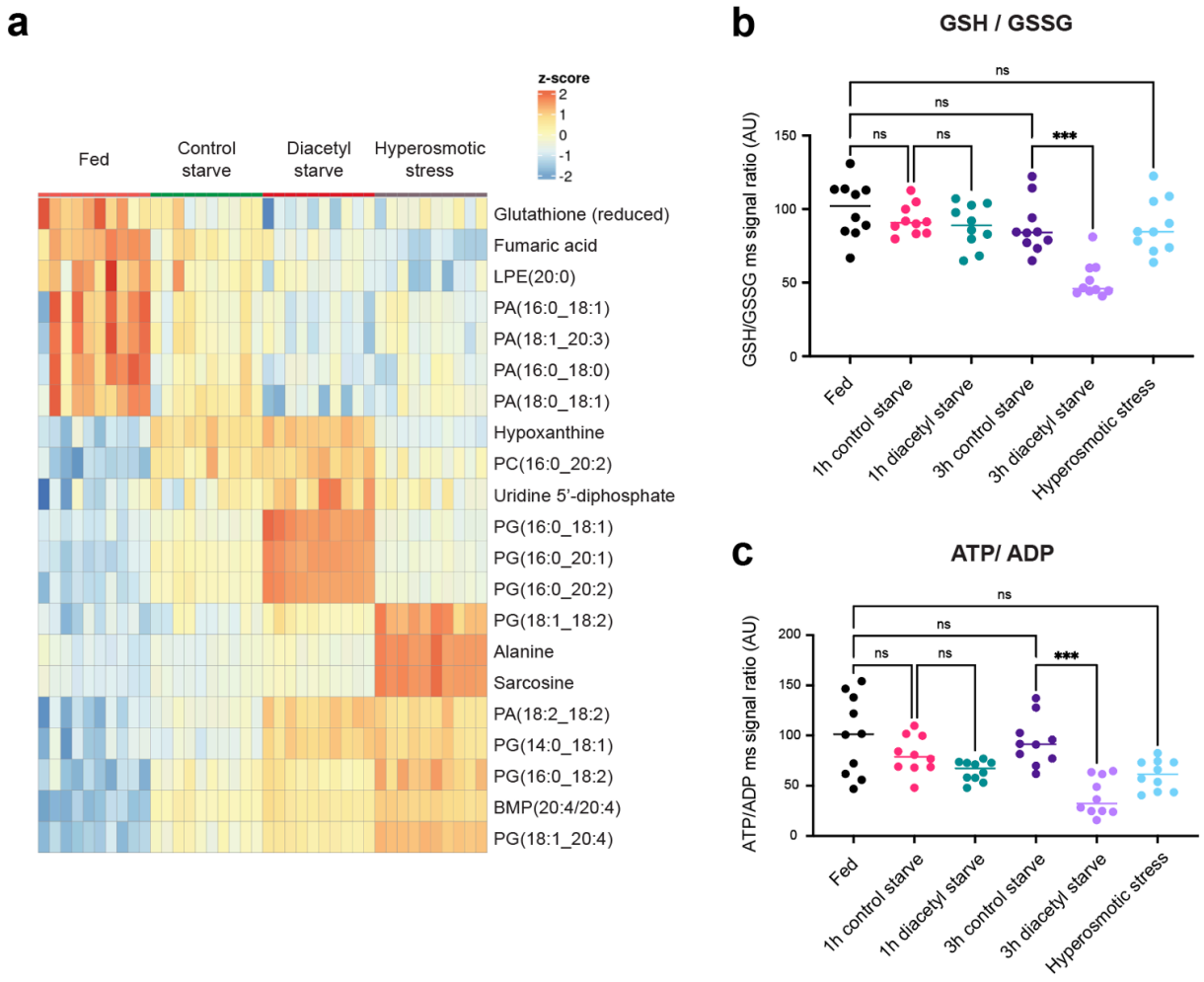


**Figure 18. Three hours of diacetyl exposure decrease GSH/GSSG and ATP/ADP ratios. a,** Heatmap of metabolites significantly altered (FDR <0.05, Welch's t-test) with the same directionality by four hours of food deprivation, diacetyl exposure (compared to control food deprivation at the three hour timepoint) and hyperosmotic stress. Positive z-score in red for upregulated metabolites, negative z-score in red for downregulated metabolites. **b** - **c**, Ratios of LC-MS peak area measurements (Arbitrary Units) for metabolites detected across samples in fed worms, starved worms in control conditions, starved worms exposed to diacetyl (1 and 3 hour timepoints), worms on hyperosmotic stress (fed). **b,** Reduced glutathione (GSH) to oxidised glutathione (GSSG). Brown-Forsythe and Welch ANOVA tests with ***P = 0.0004. **c,** ATP to ADP. Brown-Forsythe and Welch tests with ***P = 0.0001

I then investigated transcription factors potentially linking DHAP shunt induction and metabolic remodelling to *fmo-2* expression. Low ATP levels during starvation activate AMPK to induce TFEB-dependent transcriptional programs[200]. *pgph-2* overexpression has also been shown to activate the

worm TFEB homolog HLH-30[125]. I observed that knocking down *hlh-30* by RNAi suppressed *fmo-2* induction by diacetyl (**Fig. 19a**). *hlh-30* did not however block *gpdh-1* induction at 30 minutes of diacetyl exposure (**Fig. 19b**), nor did it block the diacetyl mediated hyperosmotic stress protection (**Fig. 19c**), reinforcing the hypothesis that it acts downstream or in parallel to shunt induction.

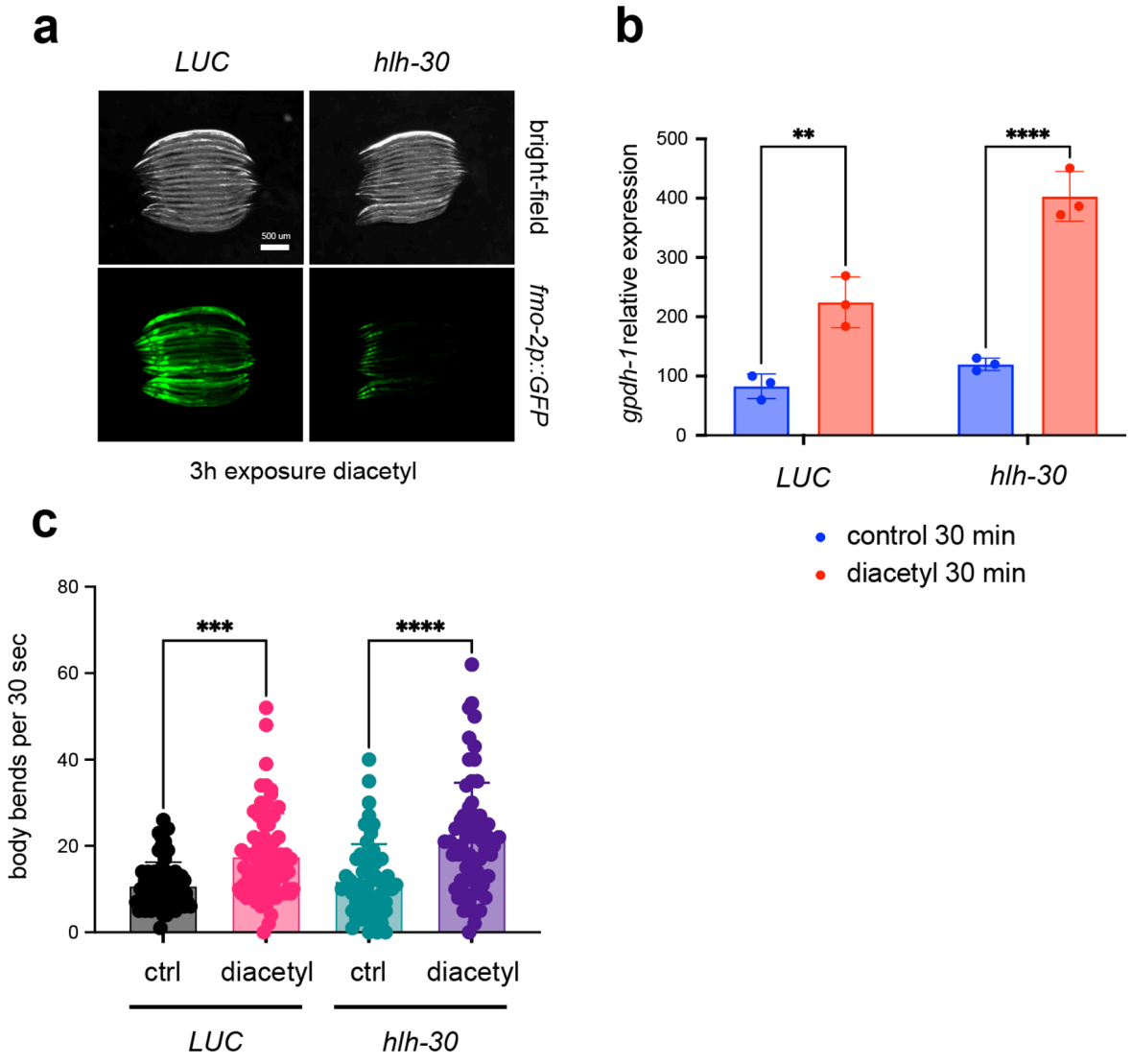


**Figure 19. HLH-30 knock-down suppresses *fmo-2* but not DHAP induction by diacetyl. a,** Three hour diacetyl induction of *fmo-2* reporter in worms raised on Luciferase (LUC) or RNAi targeting *hlh-30*. **b,** *gpdh-1* expression levels following 30 minutes of diacetyl exposure (in the absence of food) of worms raised on Luciferase (LUC) or RNAi targeting hlh-30. Detected by qPCR, error bars represent means ± SD, two-way ANOVA Sidak's post hoc test; **P = 0.0013 (LUC), ****P < 0.0001 (hlh-30). **c,** Acute hyperosmotic stress resistance of worms raised on Luciferase (LUC) or RNAi targeting hlh-30, following one hour of diacetyl exposure in the absence of food. Measured by counting body bends on 500 mM

NaCl plates. Error bars represent means ± SD, two-way ANOVA Sidak's post hoc test; ***P = 0.0001 (LUC), ****P < 0.0001 (hlh-30).

These findings collectively indicate that the induction of the DHAP shunt precedes, and is likely sufficient for, the induction of *fmo-2* in the absence of food. This effect is observed regardless of whether the specific trigger is diacetyl or hyperosmotic stress. Induction of *fmo-2*, but not the DHAP shunt, depends on HLH-30. Diacetyl exposure, hyperosmotic stress and food deprivation share some common metabolic effects, including changes in the levels of specific PGs and PAs. Additionally, prolonged diacetyl exposure during starvation decreases the levels of reduced glutathione and ATP.

## DHAP shunt induction *in vitro* reduces S6 phosphorylation

In parallel to the work in *C. elegans*, I decided to validate some of the effects of the DHAP shunt in a system where I could conditionally induce it. I designed a construct to express the mouse ortholog of the GPDH and PGPH worm enzymes: GPD1 (cGPDH) and PGP (G3PP) (**Fig. 20a**). I put both genes under the control of a doxycycline inducible promoter and expressed the DHAP shunt construct in C2C12 immortalised mouse myoblasts.

I validated my DHAP shunt construct by showing that a 24 hour induction of expression of my construct could increase by over 5 fold the concentration of glycerol that cells secreted in their media (**Fig. 20b**). At the same time, I showed that inducing the DHAP shunt reduced the levels of S6 phosphorylation under replete, high glucose, culturing conditions (**Fig. 20c** and **d**). These results suggest that DHAP shunt induction may be sufficient to inhibit mTORC1 signalling in mouse cells.

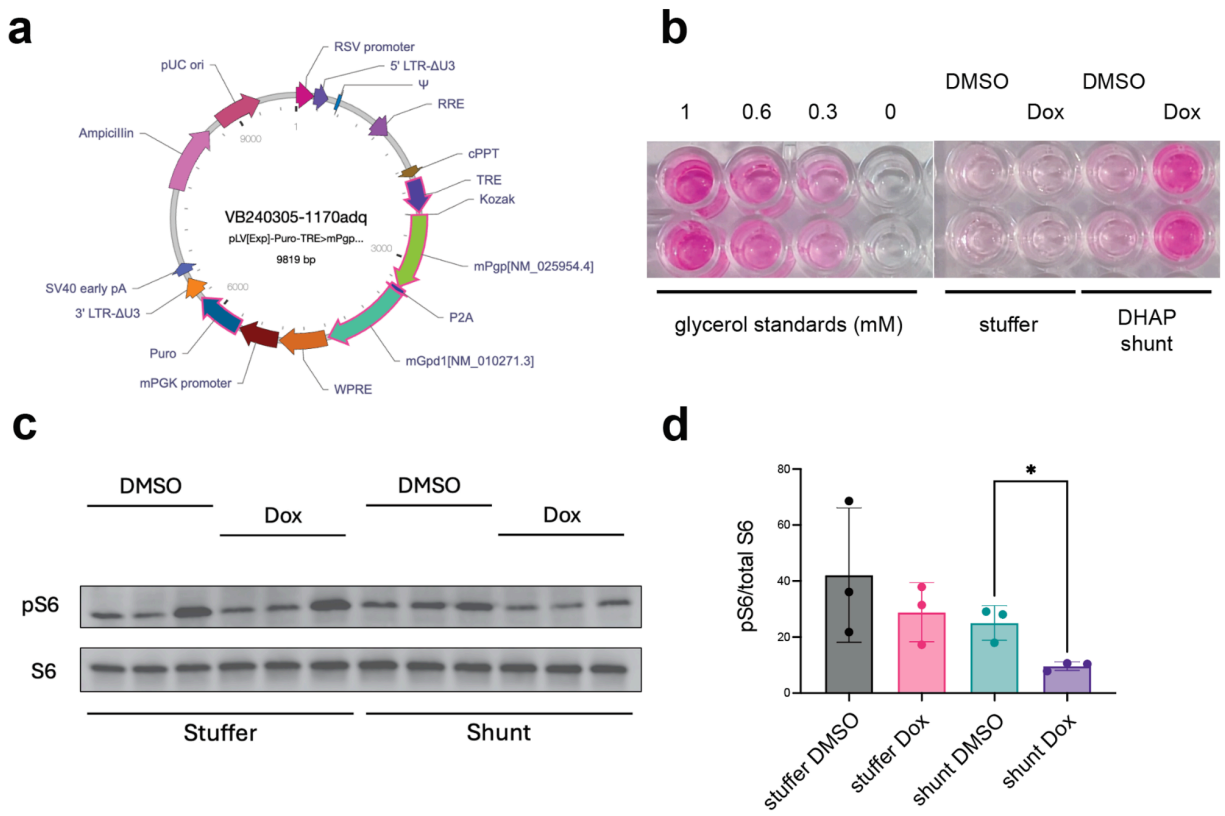


**Figure 20. Expression of DHAP shunt enzymes *in vitro* increases glycerol production and decreases S6 phosphorylation. a,** Vector for doxycycline inducible expression of mouse GPD1 and PGP shunt genes, connected by P2A linker. **b,** Colorimetric assay of glycerol secretion from C2C12 cells expressing either control (stuffer) or DHAP shunt vector, cultured for 24 hours in the presence or absence of doxycycline. Compared to glycerol standard dilution. **c,** Detection of phosphorylated (pS6) and total S6 by western blot, from C2C12 cells expressing either control (stuffer) or DHAP shunt vector, cultured for 24 hours in the presence or absence of doxycycline. **d,** Quantification from western blot in (d). pS6 and S6 band intensity was normalised to actin bands cut from the same gel, then pS6/S6 ratio was calculated for each sample. Paired t-test with *P = 0.02.

## 6.6 *gpdh-1* induction and phosphatidylglycerol (PG) synthesis depend on MDT-15

Having established that diacetyl exposure induces a transcriptional response related to nutrient stress, I wondered whether regulators of glucotoxicity could also be involved in the response to diacetyl in the worm. I screened a panel of 31 RNAi clones previously shown to suppress a glucose-responsive reporter reporter, *far-3p::GFP* [68]. I hypothesised that some of these may also suppress *fmo-2* induction by

diacetyl. Interestingly, I found that *mdt-15* and *nhr-49* knockdown largely suppressed *fmo-2* induction (**Fig. 21a** and **b**). In line with this result, knockdown of either gene also suppressed the boost in thermotolerance provided by diacetyl exposure during starvation (**Fig. 21c**).

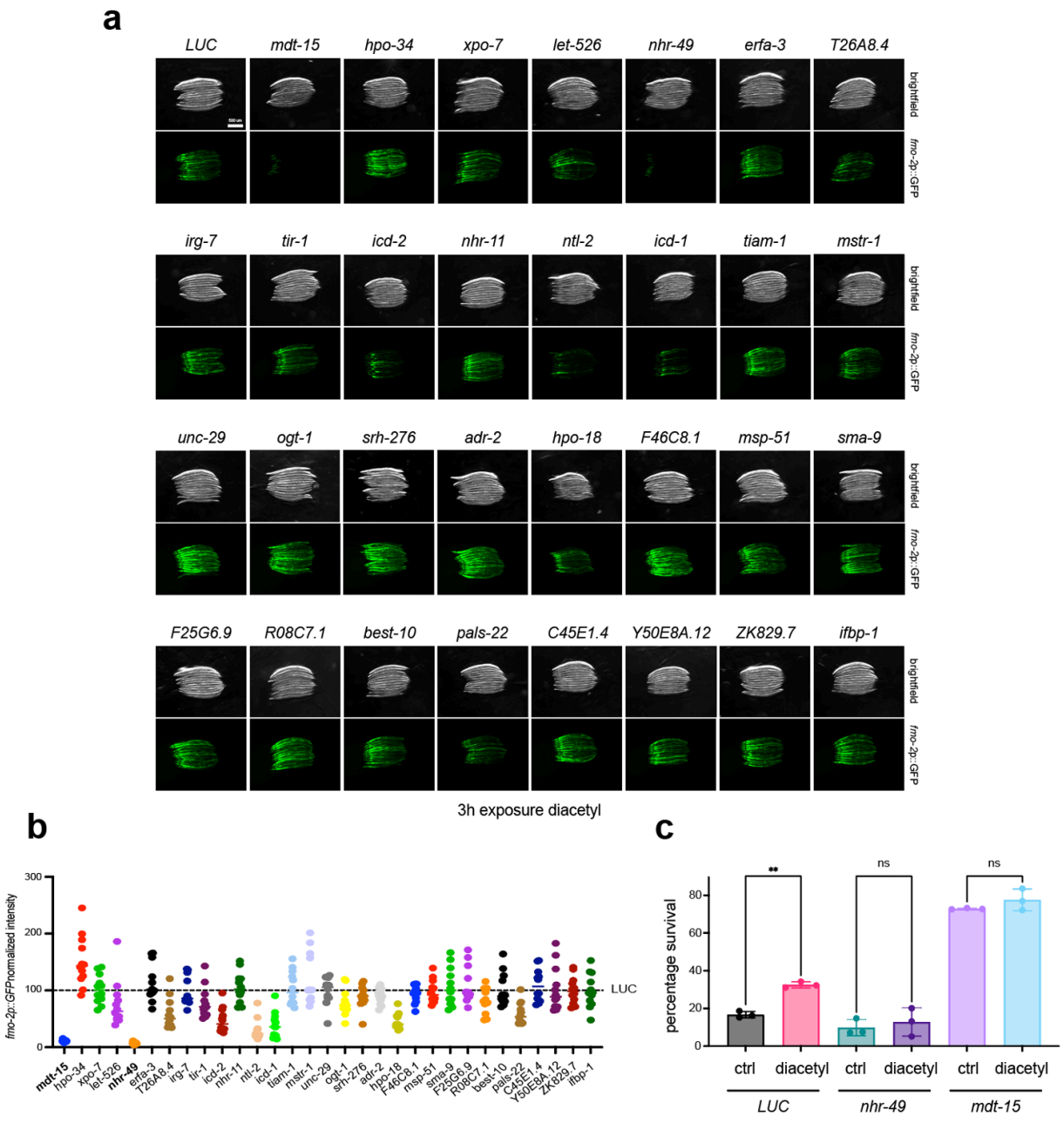


**Figure 21. Diacetyl *fmo-2* induction depends on MDT-15 and NHR-49 . a,** Three hour diacetyl induction of *fmo-2* transcriptional reporter in worms raised on 31 RNAi clones targeting suppressors of *far-3p*::GFP glucose induction[68] or non-targeting Luciferase (LUC). **b,** Quantification from screen in (a), normalised to

LUC controls. **c,** Day three survival of worms raised on Luciferase, *nhr-49* and *mdt-15* targeting RNAi, exposed for three hours to diacetyl in the absence of food and heat-shocked on day two. Error bars represent means ± SD, one-way ANOVA Sidak's post hoc test with **P=0.0023.

MDT-15, a subunit of the Mediator complex, was identified in the previously mentioned glucose RNAi screen[68] as the key transcription factor protecting against glucose toxicity by modulating fatty acid metabolism. NHR-49, a functional homolog of PPARα, is another transcription factor regulating lipid metabolism and a cofactor of MDT-15[111] (section 3.2). Both genes have also been previously linked to the starvation response[111], but I wondered if they could also directly control DHAP shunt expression. I observed that both *nhr-49* and *mdt-15* RNAi significantly suppressed *gpdh-1* induction by diacetyl, suggesting they act upstream of this pathway (**Fig. 22a**). Accordingly, *mdt-15* and *nhr-49* RNAi blocked the protective effects of diacetyl exposure on acute hyperosmotic stress resistance (**Fig. 22b**).

I focused on *mdt-15* RNAi, which showed the strongest effect on *gpdh-1* suppression, to confirm that blocking the shunt induction by diacetyl would also reverse the metabolic effects of diacetyl exposure. To do this, I compared the metabolic profiles of worms grown either on Luciferase (LUC) non-targeting RNAi or *mdt-15* RNAi. In LUC worms, one hour of diacetyl exposure largely recapitulated the effects measured on WT worms (**Fig. 22c**): it increased the levels of PGs, particularly PG(16:0_20:2), PG(16:0_18:1) and PG(16:0_20:1), while decreasing levels of PAs, except PA(18:2_18:2). *mdt-15* RNAi completely abolished these effects (**Fig. 22d**). In these worms, diacetyl exposure changed the abundance of only 7 metabolites, compared to the 70 in LUC controls. No PGs were increased by diacetyl. PG(14:0_18:1), one of the metabolites most induced by diacetyl in WT and LUC ctrl worms, was in fact decreased by diacetyl in *mdt-15* RNAi. Likewise PA(18:2_18:2), induced by diacetyl in WT and LUC ctrl worms, was significantly decreased in *mdt-15* RNAi. These results demonstrate that MDT-15 is required for diacetyl to induce the DHAP shunt, as well as the following metabolic remodelling and hyperosmotic stress resistance.

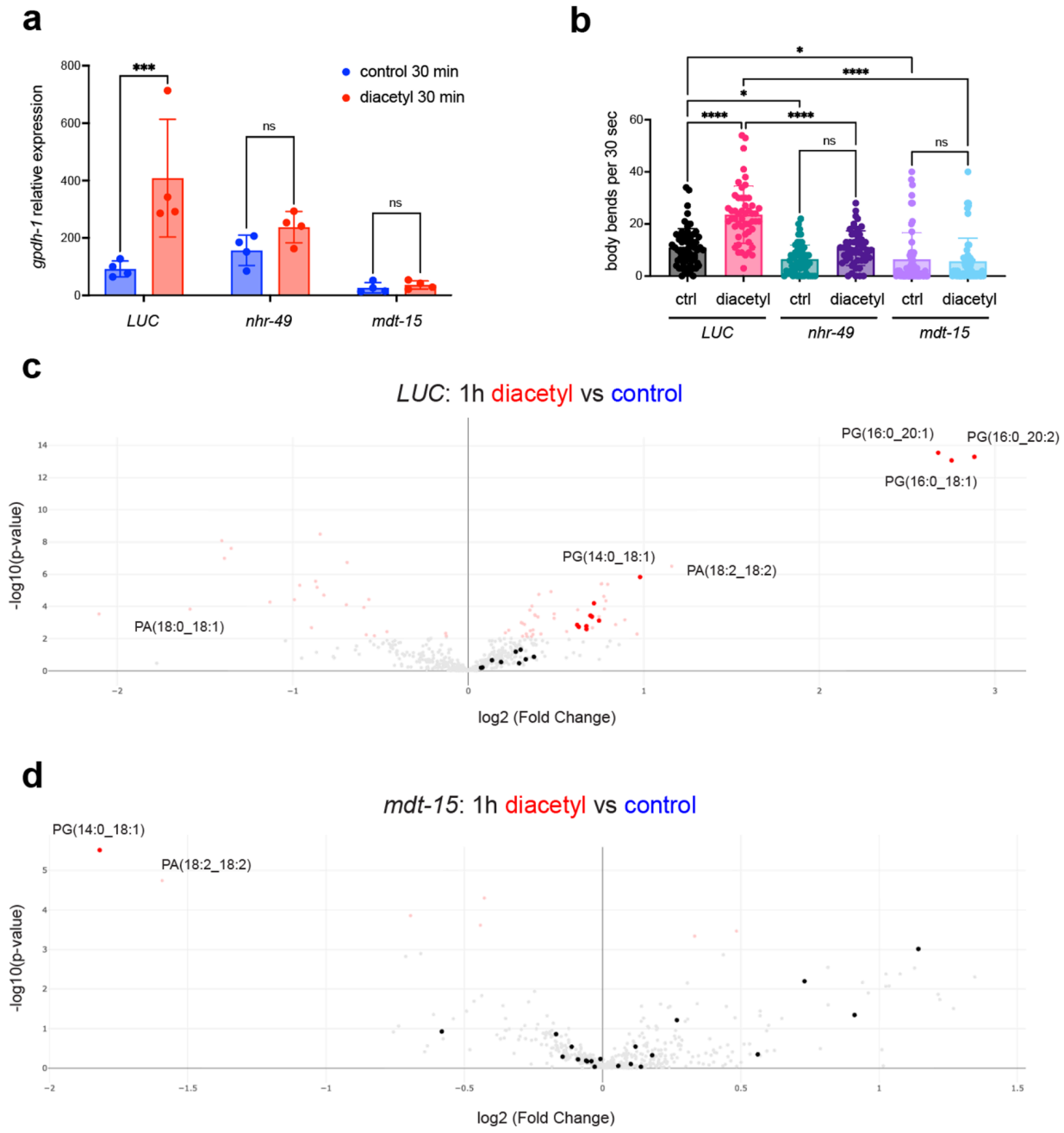


**Figure 22. Diacetyl dependent *gpdh-1* induction and PG accumulation require MDT-15. a,** *gpdh-1* expression levels following 30 minutes of diacetyl exposure (in the absence of food), in worms raised on Luciferase, *nhr-49* and *mdt-15* targeting RNAi. Detected by qPCR, error bars represent means ± SD, two-way ANOVA Sidak's post hoc test with ***P = 0.0003. **b,** Acute hyperosmotic stress resistance of worms raised on Luciferase, *nhr-49* and *mdt-15* targeting RNAi, following one hour of diacetyl exposure in the absence of food. Measured by counting body bends on 500 mM NaCl plates. Error bars represent means ± SD, one-way ANOVA Sidak's post hoc test with ****P < 0.0001 ctrl vs diacetyl (LUC), ****P < 0.0001 LUC vs *nhr*-49 (diacetyl), ****P < 0.0001 LUC vs *mdt-15* (diacetyl), *P = 0.02 LUC vs *nhr*-49

(control), *P = 0.02 LUC vs *mdt-15* (control). **c** - **d,** Volcano plots comparing metabolomic effects of diacetyl exposure (one hour) to control food deprivation, for worms raised on Luciferase (LUC) RNAi (**c**) or *mdt-15* RNAi (**d**). Metabolites significantly altered in red (FDR <0.05, Welch's t-test). Highlighted are metabolites classified as PGs.

I next asked if NHR-49 and MDT-15 could regulate shunt induction independently of nutritional stressors. Surprisingly, I found that *nhr-49* RNAi reduced *gpdh-1* induction by hyperosmotic stress (200 mM NaCl), and *mdt-15* RNAi completely suppressed it (**Fig. 23a** and **b**). Accordingly, I tested if *mdt-15* and *nhr-49* would also be required for responses to hyperosmotic stress. I found that knockdown of *mdt-15* caused developmental arrest on 200 mM NaCl (**Fig. 23c** and **d**). Knockdown of *mdt-15* also reduced survival over 4 days of hyperosmotic stress treatment with 400 mM NaCl (**Fig. 23e**), without affecting survival over this time-window in control conditions.

In sum, via an RNAi suppressor screen I identified *mdt-15* and *nhr-49* as regulators of diacetyl responses. I positioned these genes upstream of *gpdh-1* induction, both in the context of diacetyl exposure and hyperosmotic stress. *mdt-15* in particular was found to be essential for the metabolic remodelling induced by diacetyl, as well as for hyperosmotic stress resistance (**Fig. 23f**).

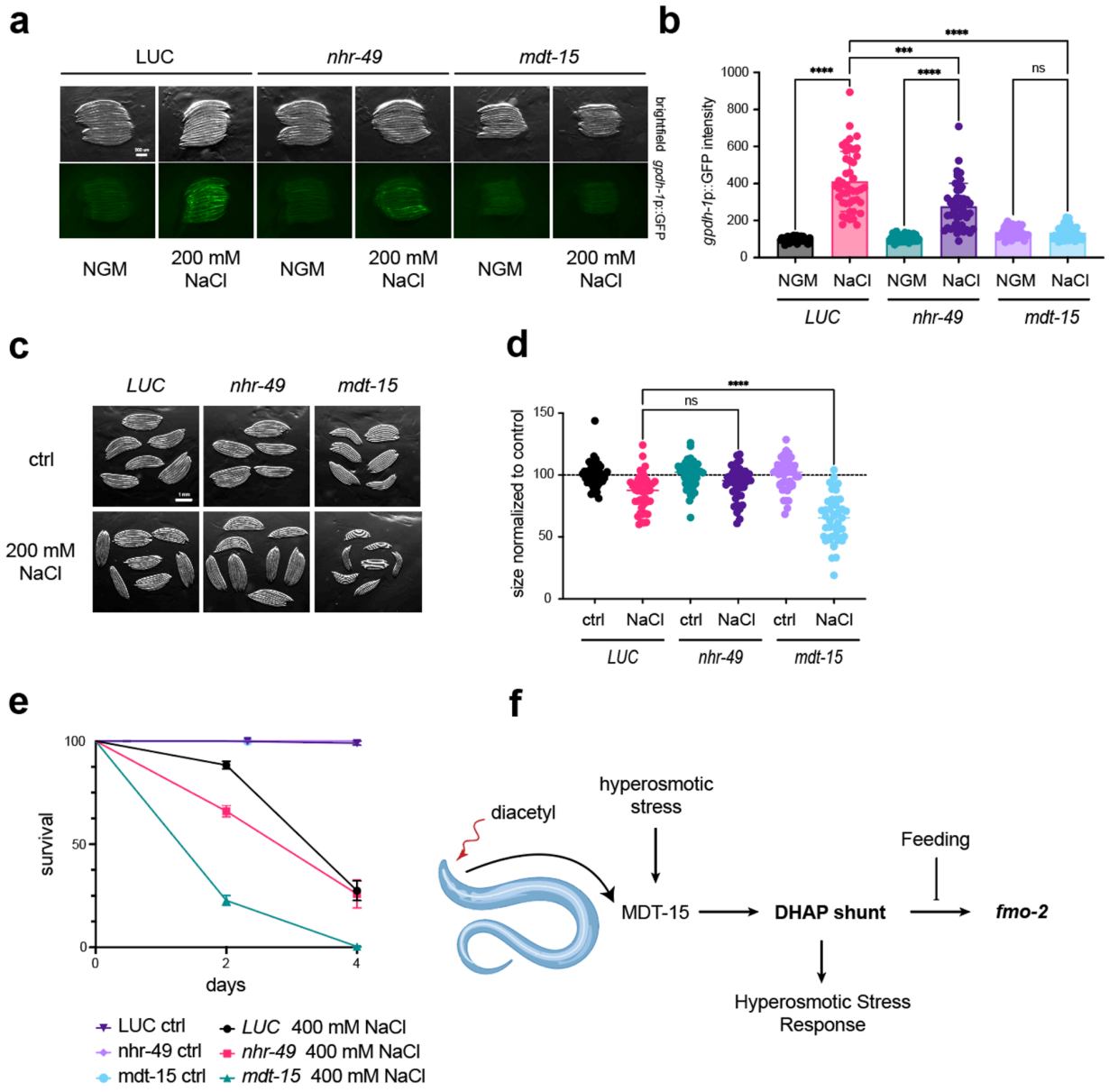


**Figure 23. MDT-15 is required for DHAP shunt induction in hyperosmotic stress response. a,** Induction of *gpdh-1* transcriptional reporter in worms raised on Luciferase (LUC), *nhr-49* and *mdt-15* targeting RNAi and exposed to 200 mM NaCl for three hours. **b,** Quantification from experiment in (a). Error bars represent means ± SD, Brown-Forsythe and Welch tests with ****P < 0.0001 NGM vs NaCl (LUC), ****P < 0.0001 NGM vs NaCl (*nhr*-49), ***P = 0.0002 LUC vs *nhr*-49 (NaCl), ****P < 0.0001 LUC vs hlh-30 (NaCl). **c,** Development of worms raised on Luciferase (LUC), *nhr-49* and *mdt-15* targeting RNAi, either at control osmolarity or in the presence of 200 mM NaCl. **d,** Quantification worm size from (c),normalised to size of worms in control osmolarity for each RNAi condition. One-way ANOVA Dunnett's post hoc test with ****P < 0.0001. **e,** Survival of worms on Luciferase (LUC), *nhr-49* and *mdt-15* targeting RNAi, either

at control osmolarity or in the presence of 400 mM NaCl. **f,** Model for DHAP induction by diacetyl or hyperosmotic stress requiring MDT-15, and resulting in *fmo-2* upregulation during food deprivation.

# 7. Results Project 2:

# *C. elegans* ageing translatome

## 7.1 Ageing effects on gene expression and Translational Efficiency (TE)

In this project, I aimed to determine the relative contributions of transcription and translation to ageing gene expression. I characterised the ageing translatome by calculating genome-wide changes in TE using a combination of RNA-seq and Ribo-seq (**Fig. 24a**). To assess how the ISR contributes to these changes (section 4.6), I performed this analysis on both WT and long-lived S51A eIF2α mutants (**Fig. 24b**). Worms were aged on FUDR-treated plates to prevent larval contamination. Samples were collected at three distinct stages: day 1 (young), day 6 (middle-age), and day 12 (old). Due to the high material requirements of Ribo-seq, day 12 was the latest practical timepoint for collection. From each sample, I extracted both total mRNA and ribosome-protected fragments (RPFs) generated via RNase digestion. I confirmed that the Ribo-seq results were consistent with digestion of ribosome protected fragments. As expected, read length was distributed around 30 nt (**Fig. 24c**), RPFs mapped predominantly to coding sequences (CDS) (**Fig. 24d**) and in the translating frame 0 (**Fig. 24e**). Principal component analysis (PCA) of FPKM values for all samples clearly showed clustering (**Fig. 24f**) that separated samples across a linear age component (PC2).

To characterise general ageing effects, I initially focused only on the data from WT worms. Before looking at translational effects, I wanted to confirm that the transcriptional ageing effects in my dataset would match an independent *C. elegans* transcriptomic ageing clock[201]. I compared the transcripts transcriptionally downregulated from day 1 to day 12 to young age predictor genes, and found a very significant overlap ($p = 1.36e{-}5$). Vice versa, I compared the transcripts significantly upregulated from day 1 to day 12 to old age predictor genes, and found again a significant overlap ($p = 0.0069$) (**Fig. 24g**). These results confirm that the transcriptional ageing signatures in this dataset are consistent with published ageing models.

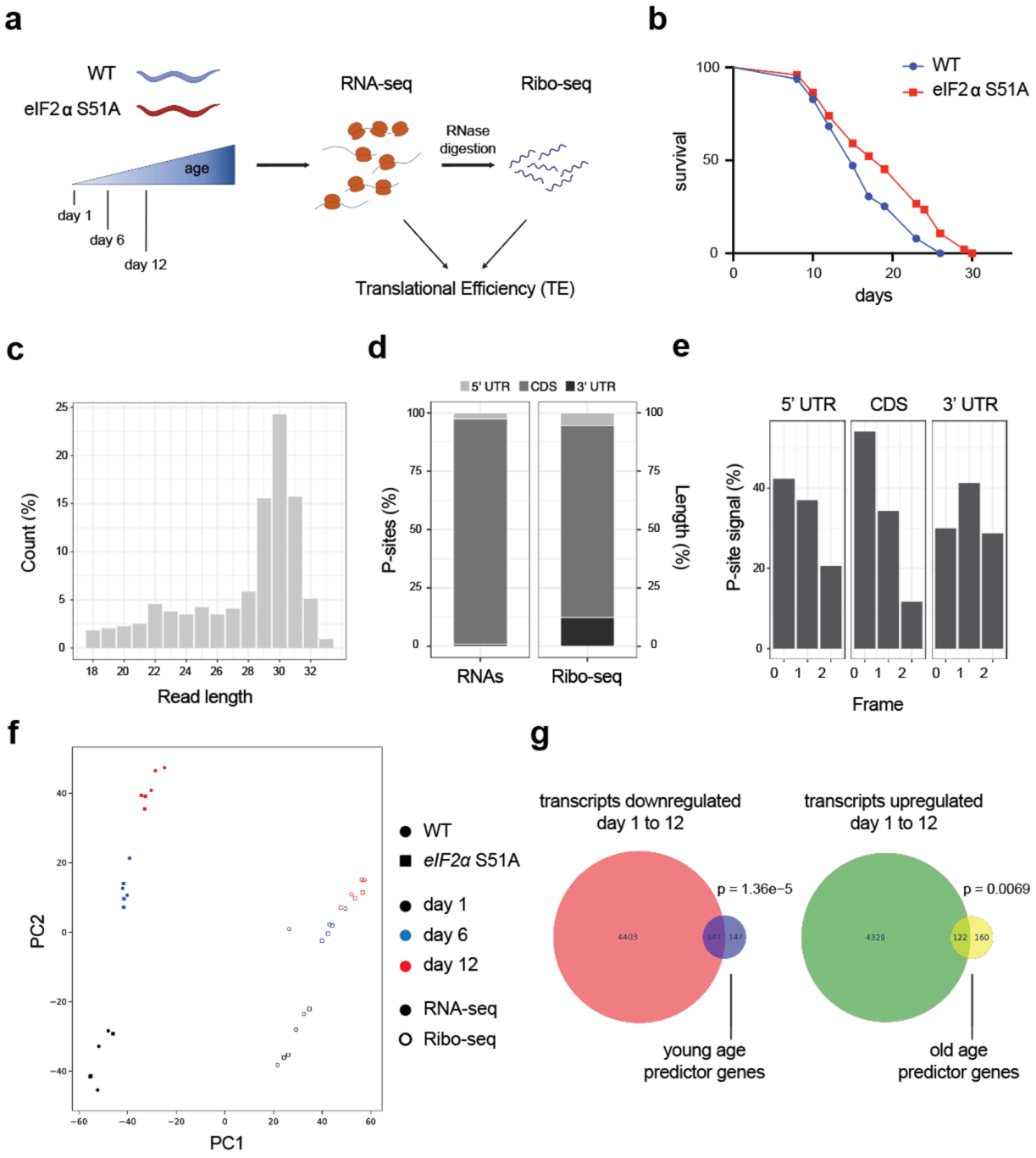


**Figure 24. RNA-seq and Ribo-seq analyses of *C. elegans* ageing. a,** Experimental setup for collection of WT and S51A eIF2α mutant samples across three ages (day 1, 6 and 12). RNA collected from each sample was used for RNA-seq (total mRNA) and Ribo-seq (ribosome protected fragments produced by RNase digestion) analysis. **b,** Survival of WT and S51A mutants. **c** - **e,** Representative results from the first Ribo-seq replicate of day 1 WT worms. **c**, Read length distribution. **d**, Percentage of reads mapping to

UTRs and coding sequence (CDS), compared to the distribution expected from a random fragmentation of RNA ("RNAs" column). **e**, Percentage of reads mapping to each reading frame. **f**, PCA plot of RNA-seq (full shapes) and Ribo-seq (empty shapes) results, calculated from FPKM values of 10% most variable genes. WT (circles) and S51A mutants (squares) at day 1 (black), 6 (blue) and 12 (red).
**g**, Comparison between RNA-seq age changes in my data and transcriptomic ageing clock[201]. Overlap between transcripts downregulated from day 1 to 12 and young age predictor genes ($p = 1.36e{-}5$) and between transcripts upregulated from day 1 to 12 and old age predictor genes ($p = 0.0069$), tested by hypergeometric test.

As a proxy of individual protein synthesis events, Ribo-seq values depend on the combined contributions of mRNA availability and TE. I matched Ribo-seq and RNA-seq FPKM values to dissect these effects in ageing. I compared the relative changes from day 1 to day 12 in gene reads at the levels of total RNA (RNA-seq) and translated RNA (Ribo-seq) (**Fig. 25a**). Ribo-seq changes correlated strongly with RNA-seq changes ($r = 0.77$, p value < 2.2 e-16), supporting the principle that age-related changes in protein synthesis are largely dependent on the underlying levels of available mRNAs.

However, many genes still changed on a translational level. Specifically, 551 transcripts significantly decreased in TE from day 1 to day 12, while 748 transcripts increased in TE from young to old (**Fig. 25b**). A first question I wanted to address with this data was whether age-related changes in TE would be matching underlying changes at the transcriptional level, or whether the two levels of regulation would be disconnected. I compared transcriptional and TE age changes for all the transcripts significantly changing in age related translation (**Fig. 25c**). Interestingly, I found a moderate but significant anticorrelation ($r = -0.26$, $p < 0.0001$) between these values, showing that as age-related transcription increases, age-related TE decreases, and vice versa. This potentially indicates a form of buffering between transcriptional and translational age effects.

As a parallel approach to quantify age-related TE effects that would include all three collected time points (not just day 1 and 12), linear models were fitted to the TE values of individual transcripts as a function of age. Transcripts exhibiting a statistically significant linear trend (FDR < 0.05) were then divided according to the direction of their regression coefficient (**Fig. 25d**). 392 transcripts were found to increase linearly with age in TE (positive coefficient), and 76 were found to decrease linearly with age in TE (negative coefficient). Both methods used to assess ageing related TE changes (**Fig. 25b** and **c**) found more transcripts increasing rather than decreasing in TE with age.

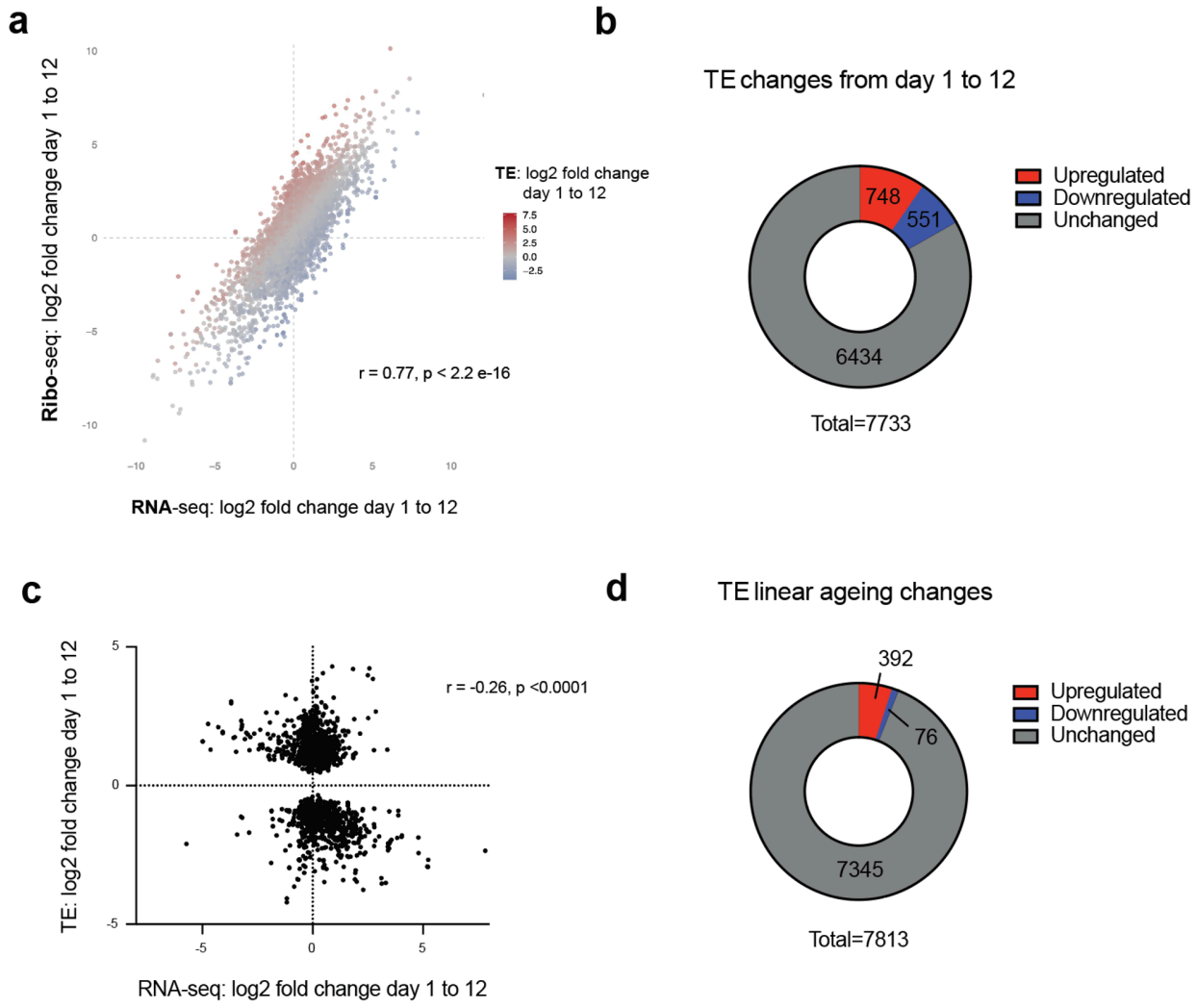


**Figure 25. Ageing affects Translational Efficiency (TE) of hundreds of transcripts. a,** Scatter plot comparing log2 fold changes in individual gene expression at the RNA-seq and Ribo-seq level. On the horizontal axis is log2 fold change in RNA-seq from day 1 to 12, with positive values indicating increase with age. On the vertical is the equivalent measured by Ribo-seq. Colour coding represents log2 fold changes in TE, with positive values in red (increasing with age) and negative values in blue. Pearson's correlation with $p < 2.2\ e^{-16}$ and r = 0.77. **b,** Pie chart dividing transcripts with TE increasing (red), decreasing (blue) or unchanged (grey) from day 1 to 12. Significance calculated by Riborex, with $p < 0.05$. **c**, Scatter plot comparing log2 fold changes in individual gene expression at the RNA-seq (horizontal axis) and TE (vertical axis) level, plotting only genes with significant TE changes with age. Spearman correlation with $p < 0.0001$ and r = -0.26. **d**, Pie chart dividing transcripts according to a linear model of age-dependent TE changes. Red indicates transcripts with a significant positive coefficient (increasing TE with age). Blue indicates transcripts with a significant negative coefficient (decreasing TE with age). Grey indicates transcripts with no significant age-dependent trend. The significance of linear trends was

determined using Student's t-tests on the regression coefficients, with p-values adjusted for multiple testing (FDR < 0.05).

## 7.2 Translation and protein folding related transcripts are translationally downregulated with age

Having found that ageing affected the TE of a significant number of  transcripts, I wanted to test whether these transcripts shared common biological processes (BP). Comparing day 1 to day 12 (**Fig. 25b**) I found that transcripts translationally upregulated with age were enriched with terms related to chromatin organisation, DNA repair and transcription (**Fig. 26a**). On the other hand, transcripts translationally downregulated with age were very significantly enriched in terms related to translation and protein folding (**Fig. 26b**). Using a gene set enrichment analysis (GSEA) I found a disproportional loss of TE on transcripts related to translation ($p < 0.0001$), protein folding ($p < 0.0001$) and metabolic processes ($p = 0.007$) (**Fig. 26c**).

To test if these were true ageing effects and not an observation limited to the comparison of day 1 and 12, I also applied a GO-term analysis to transcripts linearly changing in TE during ageing (**Fig. 25d**). With these parameters, I did not find significant enrichment of biological processes in transcripts increasing in TE. On the other hand, transcripts with TE linearly decreasing with age were still enriched in terms related to mRNA translation, protein folding and ribosome biogenesis (**Fig. 26d**). From these two approaches, translational elongation particularly emerged as a process strongly downregulated with age. In particular, 6 out of the 76 transcripts with a linear ageing decline were tRNA synthetases (**Fig. 26e**). As a final approach to visualise the ageing effect on TE, I clustered my samples according to their TE values in a PCA (**Fig. 26f**). This showed that TE itself divided samples along an ageing component (PC1). The biggest negative contributor to this component was *hsp-90*, a chaperone closely linked with ageing[202] (**Fig. 26g**).

Overall these results demonstrate that ageing-related increase or decrease in TE affects particular classes of transcripts. While there are proportionately more transcripts translationally upregulated with age (**Fig. 25b** and **c**), transcripts downregulated with age are more significantly enriched in particular biological functions, namely those related to protein synthesis itself.

**a** TE upregulated day 1 to 12

| Biological process | Enrichment | p-value |
|---|---|---|
| chromatin organization | 3.11 | 0.0002 |
| DNA repair | 2.67 | 0.0002 |
| negative regulation transcription | 3.97 | 0.0011 |
| mitotic sister chromatid segregation | 4.21 | 0.0020 |
| meiotic chromosome segregation | 4.09 | 0.0023 |
| ncRNA-mediated gene silencing | 3.39 | 0.0189 |

**b** TE downregulated day 1 to 12

| Biological process | Enrichment | p-value |
|---|---|---|
| translation | 2.64 | 2.3e−6 |
| protein folding | 3.47 | 8.0e−6 |
| ribosomal large subunit biogenesis | 5.00 | 0.0462 |
| translational elongation | 5.74 | 0.0462 |

**c**

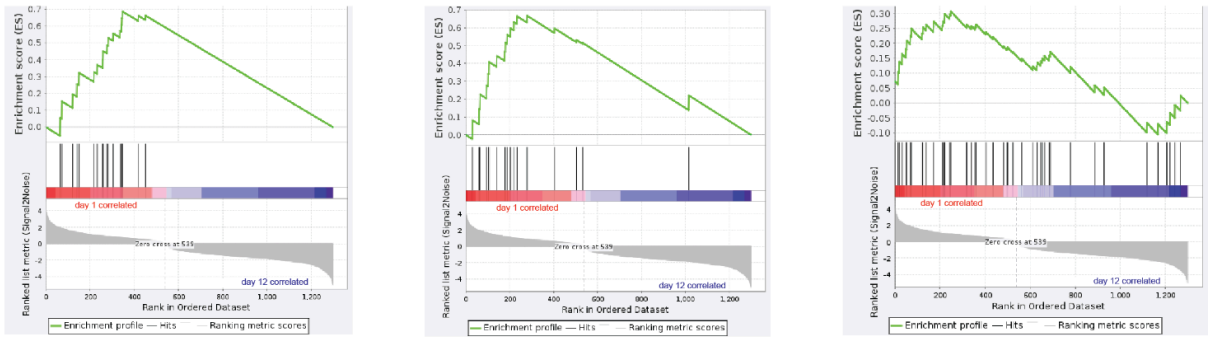


**d** TE linearly downregulated with age

| Biological process | Enrichment | p-value |
|---|---|---|
| translatioal elongation | 32.47 | 0.0001 |
| translation | 5.86 | 0.0001 |
| protein folding | 8.81 | 0.0004 |
| ribosomal large subunit biogenesis | 20.91 | 0.0035 |
| ER unfolded protein response | 12.43 | 0.0226 |

**e** tRNA synthetases TE

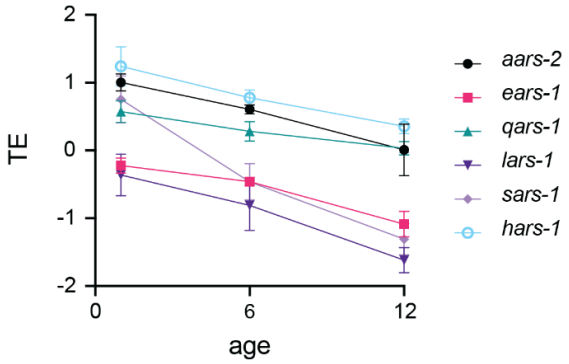


**f**

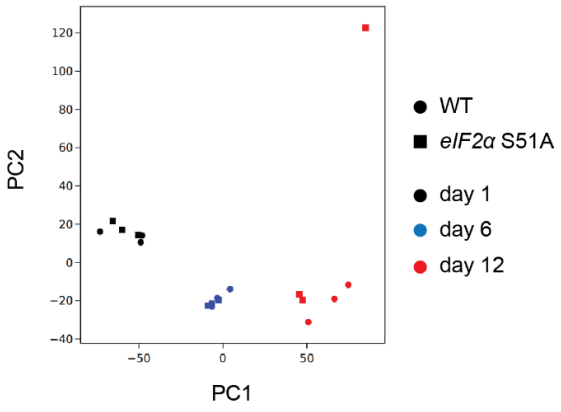


**g** *hsp-90* TE

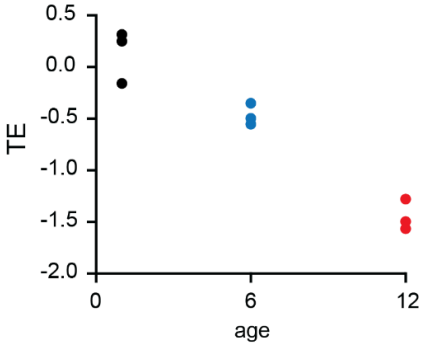

**Figure 26. Translation and protein folding related transcripts are translationally downregulated with age. a,** Biological Processes (BPs) enriched in transcripts with TE increasing from day 1 to day 12. **b,** BPs enriched in transcripts with TE decreasing from day 1 to day 12. **c**, Gene set enrichment analysis (GSEA) showing gene sets enriched at day 1 compared to day 12, $p < 0.01$. **d**, BPs enriched in transcripts with TE linearly decreasing with age. Error bars represent means ± SD. **e**, Six tRNA synthetases with linear ageing decrease in TE, plotted across the three ages analysed (WT). **f**, PCA plot of TE values from my entire dataset. WT (circles) and S51A mutants (squares) at day 1 (black), 6 (blue) and 12 (red). **g**, *hsp-90* TE plotted across the three ages analysed (WT). **a**, **b**, **d**, Significantly enriched terms were determined using a Benjamini-Hochberg adjusted p-value < 0.05.

## 7.3 mRNA features underlying ageing translational changes

Having found that transcripts changing in TE with age have common biological functions, I looked for intrinsic mRNA properties (section 1.4) that might suggest mechanisms for common translational regulation. De novo motif enrichment analyses on the ORF and UTRs did not identify any motifs enriched in transcripts translationally affected by age. Next, I decided to investigate whether mRNA properties apart from sequence could explain the ageing trends observed. Using the lists of downregulated, upregulated, and unchanged TE from day 1 to 12 (**Fig. 25b**), I tested a number of properties including length of CDS and UTRs, GC content, codon and amino acid usage. Two mRNA properties stood out as correlating with age related changes in TE.

GC content was lower in transcripts translationally upregulated with age ($p = 4.26e{-10}$), and higher in transcripts translationally downregulated with age ($p = 1.12e{-29}$) (**Fig. 27a**). Additionally, metrics of codon adaptation significantly correlated with age-related translational changes. For instance, the Codon Adaptation Index (CAI) of transcripts upregulated with age was lower than the unchanged background ($p = 1.22e\text{-}13$), while CAI of transcripts downregulated with age was higher ($p = 1.28e\text{-}45$) (**Fig. 27b**).

Measures of codon adaptation, such as CAI, are highly predictive of expression levels. Because the transcripts regulated by age in my dataset have different baseline expression levels, I wanted to ensure that the observed CAI effects were not simply a byproduct of these underlying transcriptional differences. To test this, I compared the upregulated and downregulated transcript lists against expression-matched subsets of the background list. Although correcting for either day 1 or day 12 expression levels slightly reduced the magnitude of the effects, the differences in CAI remained highly significant (day 1 correction: $p = 8.22e\text{-}06$ for upregulated, $p = 9.63e{-14}$ for downregulated; day 12 correction: $p = 2.81e\text{-}09$ for upregulated, $p = 1.36e{-13}$ for downregulated).

These results hint at the possibility that either GC content or codon usage may influence the efficiency to which mRNAs are translated during ageing, independently of the underlying transcriptional levels or expression changes.

**Figure 27. GC content and codon adaptation correlate with ageing changes in TE. a** - **b,** Density plots

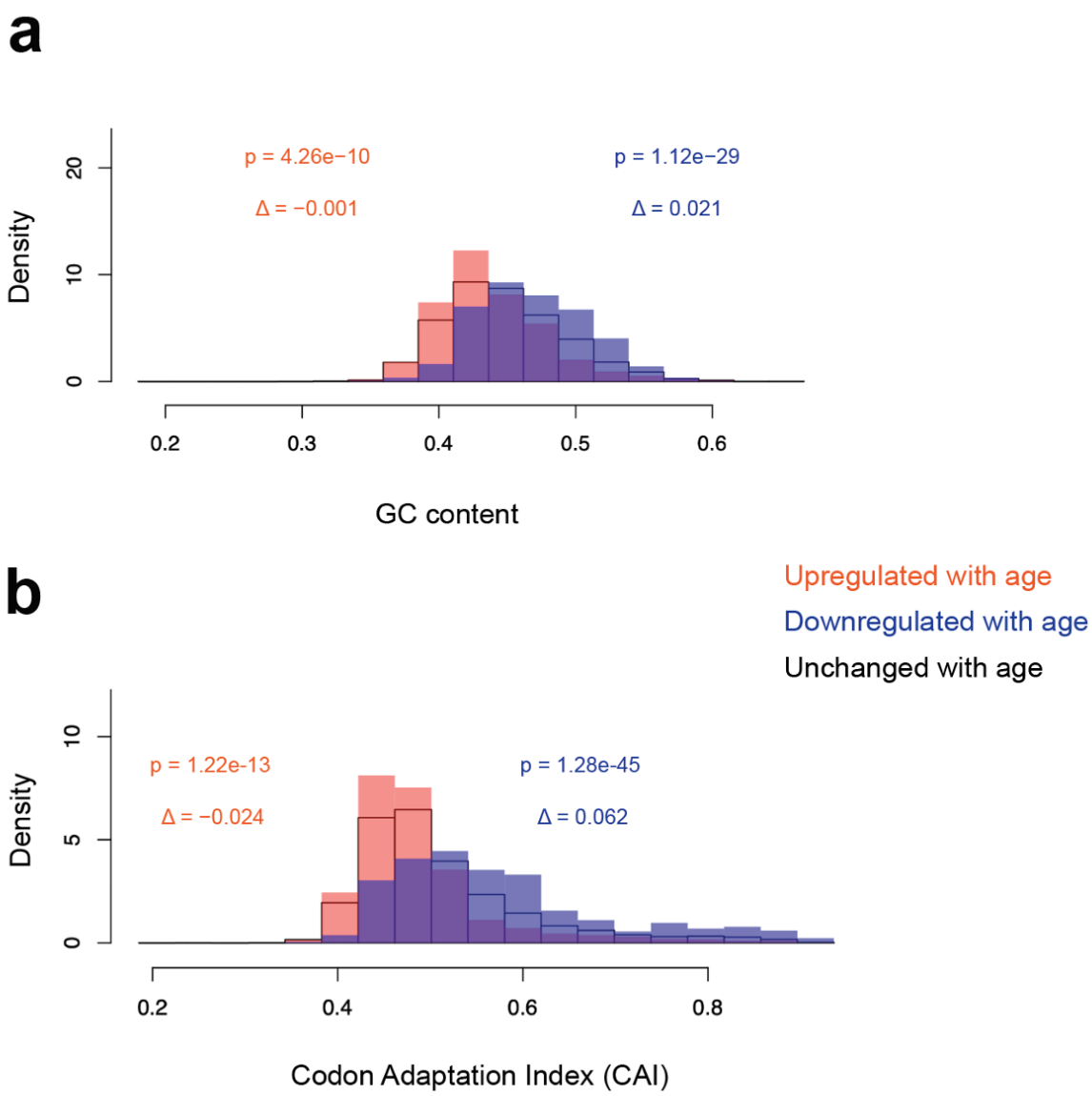


showing the distributions of GC content (**a**) and Codon Adaptation Index (CAI) (**b**) for transcripts translationally upregulated, downregulated, or unchanged from day 1 to day 12. Statistical significance between distributions was assessed using a two-sided Wilcoxon rank-sum test, with Δ representing the difference in means compared to the unchanged group. **a,** GC content distribution. Upregulated vs unchanged (p = 4.26e−10, Δ = −0.001), downregulated vs unchanged (p = 1.12e−29, Δ = 0.021). **b,** CAI

distribution. Upregulated vs unchanged (p = 1.22e-13, Δ = −0.024), downregulated vs unchanged (p = 1.28e-45, Δ = 0.062).

## 7.4 Minor ISR translational signature with ageing

Another aim of this project was to assess how the ISR contributes to the ageing translatome. I did this by comparing age-matched TE between WT and S51A eIF2α mutants. I was particularly searching for ISR translational targets, which would presumably be translationally downregulated in S51A mutants.

Surprisingly, I found minimal differences between these genotypes at the level of mRNA translation. On day 1 and on day 6, only two (**Fig. 28a**) and one transcript (**Fig. 28b**) respectively, were differentially translated to a significant level. At day 12 the differences started to increase, with 25 transcripts differentially translated (**Fig. 28c**). This number was still too small for a meaningful enrichment analysis and did not contain known translational targets of the ISR. Most transcripts (24 out of 25) differentially translated at day 12 were upregulated in WT (**Fig. 28d**). 11 of these (*fan-1, C41D11.3, H05C05.2, stam-1, ent-6, T25D3.4, T28F4.4, impt-1, tdp-1, phf-14, knl-2*) were also transcripts translationally upregulated with age.

Interestingly, the only well described ISR effector in *C. elegans*, ATF4, which should be translated upon ISR activation, was not expressed at any age in WT worms. Most Ribo-seq reads instead overlapped with the inhibitory uORF2 (**Fig. 28e**).

**a** **Day 1** differentially translated transcripts

| gene name | WT TE | S51A TE | p-value |
|---|---|---|---|
| *dhhc-6* | -2.43 | -4.78 | 0.047 |
| *dpm-1* | -0.18 | 0.89 | 0.047 |

**b** **Day 6** differentially translated transcripts

| gene name | WT TE | S51A TE | p-value |
|---|---|---|---|
| *zip-2* | -2.66 | -1.10 | 0.004 |

**c**

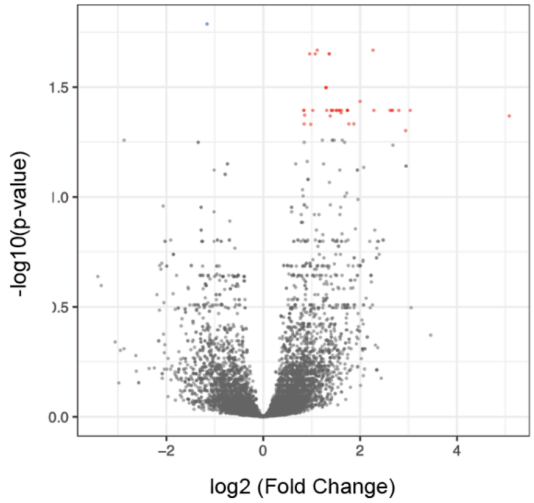


**d** **Day 12** differentially translated transcripts

| gene name | WT TE | S51A TE | p-value |
|---|---|---|---|
| *tag-153* | -0.89 | -0.01 | 0.016 |
| *fan-1* | -1.20 | -3.41 | 0.021 |
| *Y47G6A.18* | 1.25 | 0.08 | 0.021 |
| *C41D11.3* | -1.54 | -2.48 | 0.022 |
| *H05C05.2* | 1.51 | 0.58 | 0.022 |
| *ZK512.2* | -0.41 | -1.82 | 0.031 |
| *C17E4.20* | 0.49 | -1.66 | 0.036 |
| *stam-1* | 0.15 | -0.77 | 0.040 |
| *repo-1* | 0.72 | -0.18 | 0.040 |
| *ncbp-2* | -0.61 | -1.92 | 0.040 |
| *ent-6* | -1.07 | -2.16 | 0.040 |
| *mspn-1* | -0.03 | -2.90 | 0.040 |
| *his-18* | -3.07 | -4.26 | 0.040 |

| gene name | WT TE | S51A TE | p-value |
|---|---|---|---|
| *klp-12* | -0.62 | -2.62 | 0.040 |
| *T25D3.4* | -0.74 | -2.48 | 0.040 |
| *T28F4.4* | -0.83 | -3.71 | 0.040 |
| *dsbn-1* | 0.57 | -0.61 | 0.040 |
| *Y106G6D.1* | 1.54 | -1.81 | 0.040 |
| *impt-1* | -0.54 | -2.76 | 0.040 |
| *gpa-16* | -0.31 | -1.09 | 0.040 |
| *tdp-1* | -0.02 | -0.81 | 0.042 |
| *ltah-1.1* | 0.31 | -1.08 | 0.046 |
| *phf-14* | -0.35 | -2.16 | 0.046 |
| *knl-2* | -1.22 | -2.20 | 0.046 |
| *Y47G6A.9* | -0.25 | -3.30 | 0.049 |

**e**

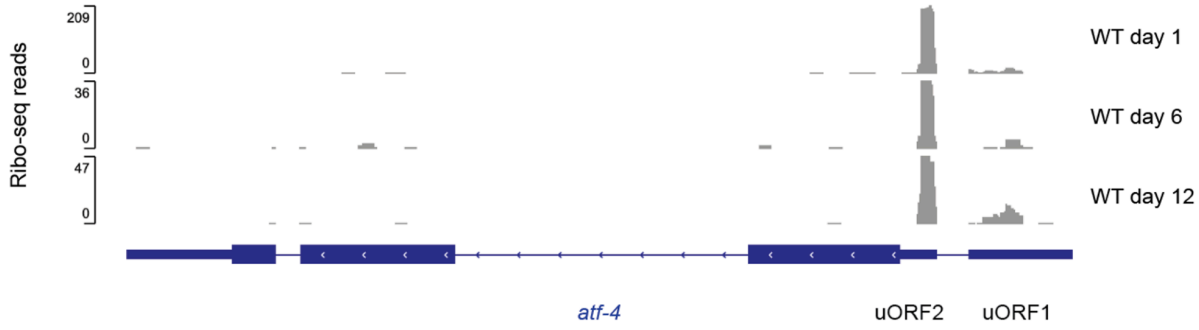


**Figure 28. TE differences between WT and S51A eIF2α mutants.** Transcripts differentially translated between WT and S51A eIF2α mutants at day 1 (**a**), 6 (**b**) and 12 (**c - d**). In red, transcripts downregulated in mutants compared to WT; in blue, transcripts upregulated in mutants. Significance calculated by Riborex, with $p < 0.05$. **e**, Integrative Genomics Viewer (IGV) visualisation of Ribo-seq read coverage at the *atf-4* locus. Tracks represent bigWig files showing the distribution of Ribo-seq reads in WT worms at days 1, 6, and 12. The gene model below highlights the positions of uORF1 and uORF2.

## 7.5 No evidence for improved olfactory memory in ISR mutants

Because of the established role of the ISR in mammalian memory formation (section 4.6), I also wanted to test if this may be conserved in *C. elegans*. To answer this question I focused on the long-lived *ppp-1*

eIF2B$\gamma$ mutants with inhibited ISR[194]. I tested the hypothesis that *ppp-1* mutants would show improved learning and/or memory formation, particularly in the context of long-term memory which requires protein synthesis.

I applied two different training protocols. First, a single training bout of butanone positive conditioning (paired with food) to increase chemotaxis towards butanone (against benzaldehyde as control odorant). With this I could produce a short term memory that lasted less than one hour, and as expected I did not observe any difference between the genotypes tested (**Fig. 29a**). The second training protocol consisted of repeated butanone aversive conditioning (paired with food deprivation) to decrease chemotaxis towards butanone (against ethanol as control odorant). With this I could produce a long term memory that lasted up to two hours, but again did not observe any difference between *ppp-1* mutants and WT worms (**Fig. 29b**).

Together, these results indicate that *C. elegans* models of ISR inhibition may not share salient features of the mammalian ISR: differential translation of stress-response mRNAs or improved memory function.

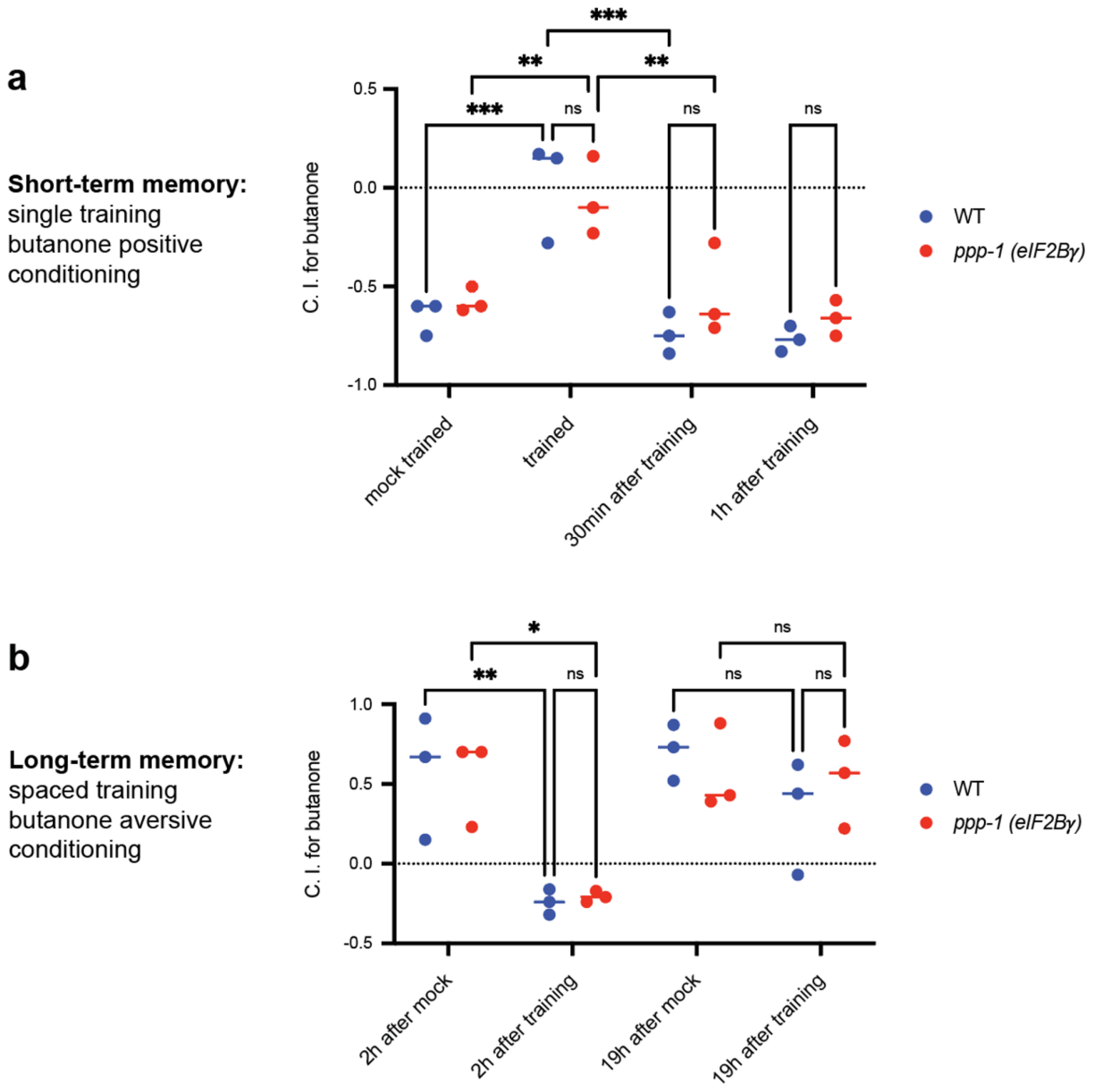


**Figure 29. No evidence for improved olfactory memory in eIF2B$\gamma$ ISR mutants. a,** Butanone positive conditioning, Benzaldehyde as control chemical. Short-term olfactory memory measured immediately, 30 minutes and 1 hour after training. Two-way ANOVA Sidak's post hoc test with ***P = 0.0005 (mock vs trained, WT), **P = 0.0052 (mock vs trained, eIF2B$\gamma$), ***P = 0.0001 (trained vs 30 min, WT), **P = 0.0086 (trained vs 30 min, eIF2B$\gamma$). **b,** Butanone aversive conditioning, Ethanol as control chemical. Long-term olfactory memory measured 2 hours and 19 hours after training. Two-way ANOVA Sidak's post hoc test with **P = 0.0086 (2h mock vs 2h after training, WT), *P = 0.017 (2h mock vs 2h after training, eIF2B$\gamma$).

.

# 8. Discussion

## 8.1 From a volatile food cue to gene expression: the DHAP shunt as an Anticipatory Food Response (AFR)

Through a high-resolution transcriptomic time-course, I set out to delineate acute responses to a volatile food signal (diacetyl) in *C. elegans*. This approach revealed a rapid and transient induction of gene expression beginning as early as 30 minutes following exposure, matching the speed of transcriptional AFRs observed in other organisms[101,102]. Only 12 genes were significantly altered by diacetyl, all of which were upregulated (**Fig. 7a**), suggesting a targeted transcriptional response. Among the induced genes, several are regulators of metabolic homeostasis. One example is *pqm-1*, a transcription factor regulating longevity of insulin signalling mutants[203] and lipid metabolism under hypoxia[204]. I also observed induction of *ogt-1* (O-GlcNAc transferase), a nutrient-sensing enzyme that mediates entry into adult reproductive diapause following starvation[205] as well as storage levels of glycogen and triglycerides[205,206]. OGT-1 has also been recently described as a regulator of the hyperosmotic stress response that enables sustained *gpdh-1* expression through a post-transcriptional mechanism that does not require its catalytic domain[195], directly linking this gene to my primary diacetyl transcriptional target.

The gene most induced by diacetyl exposure was in fact *gpdh-1*, upregulated alongside three other enzymes responsible for converting DHAP into Gro-3P, and Gro-3P into glycerol. Together, these enzymes form the DHAP shunt, a side pathway of glycolysis. Besides hyperosmotic stress, these genes are linked to glucotoxicity responses in *C. elegans* (section 3.2) and hyperglycemia/metabolic dysfunction in mice models and humans (section 2.4). Cytoplasmic GPDH has two molecular functions. First, it converts DHAP into Gro-3P, providing the essential building block for both glycerophospholipid and glycerol synthesis. Second, while converting DHAP into Gro-3P, cGPDH also oxidises NADH. Together with the mitochondrial isozyme GPD2, this powers the Gro-3P shuttle transferring electrons into mitochondria. NADH oxidation by cGPDH also serves as an important backup pathway to regenerate cytosolic NAD+ when mitochondrial oxidation is impaired, for instance during hypoxia[69] and glucotoxicity[207], thus maintaining redox balance.

I confirmed that *gpdh-1* was modulated by both osmotic stress and metabolic effects of glucose excess (**Fig. 10a**). For the first time, I also demonstrated that *gpdh-1* is modulated by food availability (**Fig. 10c**).

I speculate that under nutrient-rich conditions, *gpdh-1* is expressed at levels sufficient to shunt some DHAP toward phospholipid production while keeping levels of glycolytic intermediates low. Conversely, during food deprivation, *gpdh-1* is actively suppressed, likely to ensure all available DHAP is directed toward pyruvate production. Interestingly, food deprivation even blocked *gpdh-1* induction by hyperosmotic stress (**Fig. 11a**). GPDH-1 is thus seemingly positioned at an important juncture, balancing the conflicting needs of nutrient homeostasis and hyperosmotic stress protection. *gpdh-2* expression was not repressed by food deprivation (**Fig. 10c**) and may remain inducible under hyperosmotic stress conditions (to be tested). This regulatory mechanism may be evolutionary conserved; in yeast, the two GPDH orthologs are differentially regulated, with GPD1 being de-repressed by hyperosmotic stress, while GPD2 is inhibited by nutrient limitation[208]. Unlike hyperosmotic stress, diacetyl induced *gpdh-1* expression particularly when worms were food-deprived (**Fig. 11b**). This supports the hypothesis that diacetyl functions as a cue anticipating the arrival of food and nutrients.

In summary, these data provide the first evidence of a transcriptional AFR in *C. elegans*. This includes induction of genes related to metabolic homeostasis and glucotoxicity, particularly those part of the DHAP shunt. The gene most induced by diacetyl is *gpdh-1*, a key regulator of glycolytic flux, glycerol metabolism and redox balance

## 8.2 Coupling gene expression to a metabolic shift: glycerol and phosphatidylglycerol (PG) accumulation

I then sought to confirm whether the transcriptional induction of the DHAP shunt translated into metabolic effects. First, I observed that diacetyl exposure increased the levels of free glycerol (**Fig. 8b**). Then, using an unbiased metabolomics and lipidomics approach, I found that diacetyl exposure induced accumulation of phosphatidylglycerols (PGs), with three species being particularly highly increased (**Fig. 8c**). This metabolic shift suggests that the Gro-3P generated by GPDH-1 is being redirected to synthesise glycerol and PGs.

This response closely overlapped with the metabolic effects of hyperosmotic stress (**Fig. 8e**), adding support to the shared activation of DHAP shunt enzymes under both conditions. The open question here is whether PG accumulation actively protects the worms from hyperosmotic stress, or whether the protection is derived entirely from glycerol. Unlike free glycerol, PGs are not widely studied in the

context of hyperosmotic stress, although there is evidence that they accumulate in some plant species under hyperosmotic conditions[209] . Phosphatidylglycerols are generally understudied lipid species, particularly in *C. elegans*. While they constitute a major phospholipid component of lung surfactant in mammals, PGs account for less than 1% of total phospholipids in most other tissues. Their synthesis begins in the mitochondria, after which they are processed in the ER and transported back to the mitochondria[210]. Within the mitochondria, PGs serve as the primary precursor for the synthesis of cardiolipin. Cardiolipin is an essential component of the inner mitochondrial membrane, where it maintains structural integrity and supports ETC function[211].

However, the direct roles of PGs within the mitochondria are not entirely clear. A study in yeast has demonstrated that the accumulation of PGs can increase mitochondrial fragmentation and respiration rates[212]. Interestingly, PGs have also been described as a class of phospholipid particularly affected by excess adiposity: serum levels of PGs are strongly increased by a high fat diet in mice and in obese humans[213]. In line with this, my conservative hypothesis is that the PG accumulation observed with diacetyl exposure is a metabolic byproduct of increased *gpdh-1* expression and Gro-3P availability. While it is possible that these PGs are directly (or indirectly, through cardiolipin synthesis) contributing to mitochondrial respiration or to a specific metabolic stress response, there is currently too little information regarding their functions in *C. elegans* to make this claim.

## 8.3 Diacetyl boosts starvation response and *fmo-2* expression

At the 90-minute timepoint, I identified nine genes upregulated by diacetyl exposure (**Fig. 12a**). This represents a distinct transcriptional shift, as the profile is largely different from the earlier 30-minute response. The single exception is *F20G2.1*, an uncharacterised oxidoreductase that was strongly upregulated at both timepoints; the persistent expression of this enzyme makes it an interesting candidate for further study. The 90-minute response also featured the induction of other uncharacterised oxidoreductases, including *C06E4.3*, *F56D5.3*, and *D1054.8*. Interesting genes induced by diacetyl included *argk-1* and *cth-1*. *argk-1* encodes for a creatine kinase involved in maintaining ATP levels in invertebrates, and acts as a longevity effector downstream of S6K inhibition[214]. *cth-1* encodes for a cystathionine gamma-lyase associated with $H_2S$ production, NAD+ recycling, and longevity[215].

Given its strong upregulation and connection to dietary restriction longevity, I decided to focus further analyses on *fmo-2*. As outlined in section 3.2, FMO-2 (Flavin-containing Monooxygenase-2) is induced in

the intestine of *C. elegans* exposed to hypoxia and dietary restriction, and this enzyme has been shown to be necessary and sufficient to extend lifespan downstream of these interventions[112]. Additionally, *fmo-2* and its mammalian orthologs are induced by oxidative stress and mediate oxidative stress resistance[113, 216]. Using a transcriptional reporter, I confirmed that diacetyl exposure boosted *fmo-2* induction five-fold, an effect that plateaued within a few hours of exposure (**Fig. 12c**). Critically, this diacetyl-driven *fmo-2* induction was largely suppressed in the presence of food (**Fig. 12h**). This food dependency indicates that diacetyl is specifically altering the starvation response, rather than inducing *fmo-2* through independent mechanisms such as direct chemical oxidative stress or hypoxia mimicking.

At the metabolic level, I found that three hours of diacetyl exposure decreased the levels of ATP, CTP and UTP (**Fig. 13b** - **d**). CTP is the precursor used to produce CDP-diacylglycerol (**Fig. 8d**), and thus plays an essential role in phospholipid synthesis[217]. CTP is also the nucleotide with typically lowest cellular concentrations, and its levels are replenished by CTP synthase, using UTP as a substrate and consuming ATP in the reaction[218]. My interpretation of these results is that by inducing the DHAP shunt, worms exposed to diacetyl are actively redirecting glycolytic intermediates away from mitochondrial respiration and into anabolic PG synthesis, consuming high-energy phosphate donors in the process and potentially decreasing ATP regeneration. Consistently, pyruvic acid was decreased in diacetyl exposed worms (**Fig. 13e**). This observed energy deficit matches the transcriptomic data, providing a metabolic basis for the compensatory induction of *argk-1* (**Fig. 12b**). By suppressing the DHAP shunt in the absence of food, worms may prevent the wasteful diversion of metabolites that are required for ATP production during starvation.

To evaluate behavioural and physiological outcomes of diacetyl exposure, I examined appetite and stress resistance. Diacetyl boosted starvation-related appetite behaviour (**Fig. 14a**), which aligns with recent evidence demonstrating that FMO-2 modulates exploratory behaviour and satiety[115]. Additionally, I developed an assay to measure the short-term benefits of food deprivation and confirmed that a short period of adult fasting protected the worms from heat shock. Because *fmo-2* induction during control fasting is minimal within this early three-hour period, other fasting-induced responses must largely contribute to the baseline protective phenotype. However, concurrent diacetyl exposure improved the benefits of fasting (**Fig. 15a**). This enhancement is consistent with the established role of FMO-2 in heat shock protection[112].

In conclusion, I have shown that prolonged diacetyl exposure in the absence of food exposure induces transcriptional and metabolic signatures of energy depletion. Diacetyl particularly boosted the starvation-related expression of *fmo-2*, as well as starvation-related appetite and thermotolerance phenotypes.

## 8.4 The unknown diacetyl sensing mechanisms

I used *fmo-2* induction as a readout to dissect the mechanisms underlying diacetyl sensing. While I had previously focused on a 1% diacetyl concentration, diacetyl is known to be chemoattractive to *C. elegans* across a wide range of dilutions, from 0.0001% up to 10–100% depending on the specific study (section 3.5). I found that diacetyl induced *fmo-2* at concentrations between 0.1% and 1% (**Fig. 16a**), and did not test higher concentrations because they have been reported to trigger aversive behaviours in some studies[147, 149]. Notably, the ethanol solvent alone induced *fmo-2* to a low degree (**Fig. 16b**). Determining if ethanol induces the DHAP shunt at the earlier 30-minute timepoint is a critical next step. To determine whether *fmo-2* induction is a general reaction to volatile food cues, I tested two other chemoattractive volatiles: 2-butanone and isoamyl alcohol. Exposing fasting worms to 2-butanone has been reported to increase fat storage levels within four hours[137], suppress *fmo-2* induction by DR (but see discussion below), and abrogate DR-mediated lifespan extension[142]. Conversely, chronic exposure to isoamyl alcohol has been shown to promote longevity via a *daf-16*-dependent mechanism[143]. In my assays, neither odorant induced *fmo-2* expression (**Fig. 16c**). This indicates that the upregulation of *fmo-2* is not a universal response to all food cues. Curiously, this specificity aligns with literature linking *fmo-2* to both diacetyl chemotaxis[115] and ethanol-seeking behaviours [219].

I then tested whether known diacetyl receptors are required to mediate this response. The canonical diacetyl receptor, ODR-10, primarily mediates chemotaxis over the 1% to 0.1% dilution range[146], while SRI-14 mediates avoidance to undiluted diacetyl[148]. More recently, the LITE-1 receptor was shown to modulate avoidance to high concentrations (10–100%) of diacetyl[149]. I found that both *odr-10* and *sri-14* mutant strains remained fully responsive, successfully inducing *fmo-2* upon diacetyl exposure (**Fig. 16e**). I did not have a *lite-1* mutant available to test during this study. Having found no individual receptor mutant capable of suppressing the diacetyl effect, I shifted my focus to broader signalling pathways. Serotonin and dopamine signalling have been previously reported to induce *fmo-2* downstream of DR[142]. I therefore tested *tph-1* mutants, which are defective in serotonin synthesis, and *cat-2* mutants, which

are defective in dopamine production. Both mutant strains remained competent for *fmo-2* induction (**Fig. 16f**). Insulin signalling is another master regulator of food deprivation responses in *C. elegans*[107,197]. *daf-2* mutants exhibited an even stronger *fmo-2* upregulation in response to diacetyl treatment compared to wild-type controls (**Fig. 16g**). Because targeting specific neurotransmitter pathways did not abrogate the response, I tested whether the signal relied on more fundamental mechanisms of neuronal transmission. I used *unc-13* mutants to block systemic neurotransmitter release, and *unc-31* mutants to block dense-core vesicle neuropeptide release. I found that neither mutation could stop *fmo-2* induction (**Fig. 16h**).

Based on these results, I can draw some conclusions regarding how worms sense this volatile signal. First, diacetyl induces *fmo-2* over a range of concentrations that are well-established as chemoattractive rather than aversive. This supports the hypothesis that the metabolic and transcriptional effects described throughout my thesis are the result of a chemoattractive food stimulus, rather than a noxious stress response to an aversive chemical. Second, the literature indicates that diacetyl sensing involves multiple receptors, some of them still uncharacterised[148], suggesting that receptor redundancy may account for the persistent *fmo-2* induction observed in the single-receptor mutants tested here. If *fmo-2* induction were strictly controlled by sensory neurons, one would expect the response to be severely impaired when broad neuronal signalling mechanisms are blocked. The persistent responsiveness of *unc-13* and *unc-31* mutants challenges this assumption. It is important to note, however, that gap junctions are ubiquitous in *C. elegans* neuronal networks[220] and may account for neuronal signalling independent of neurotransmitters or neuropeptides. To definitively confirm the requirement of the sensory nervous system, future experiments should incorporate the targeted ablation of specific olfactory neurons. All mutant strains tested exhibited either a wild-type level of response or higher *fmo-2* induction (*daf-2*, *tph-1*, and *unc-31*). Notably, these mutants also had lower baseline levels of *fmo-2* in the starvation control conditions. Underlying differences in the baseline starvation response in these mutants may explain the differential magnitudes of *fmo-2* induction upon diacetyl exposure.

In conclusion, given the inability of established sensory and synaptic mutants to abrogate this transcriptional response, I propose two potential mechanisms for diacetyl sensing:

1. A non-neuronal, cell-autonomous mechanism: Diacetyl may exert a direct, cell-autonomous effect within the responding tissues. This mechanism would be largely unprecedented in the

current *C. elegans* literature, where volatile odorants are assumed to operate strictly through sensory neuronal pathways.

2. A non-canonical neuronal sensory pathway: The organism may utilise a neuronal sensory network independent of the canonical diacetyl receptors and major signalling pathways evaluated in this thesis.

## 8.5 DHAP shunt enhances starvation response in the absence of food

The transcriptomic and metabolomic analyses established a distinct chronological sequence following diacetyl exposure: activation of DHAP shunt gene expression (30 to 90 minutes), followed by the accumulation of phosphatidylglycerols (PGs) (from 1 hour), and finally the induction of *fmo-2* (from 90 minutes onward). To determine whether this chronological correlation represented a causal relationship, I investigated whether the DHAP shunt is necessary and sufficient for *fmo-2* induction.

First, I demonstrated that RNAi-mediated knockdown of PGPH enzymes significantly reduced *fmo-2* induction by diacetyl (**Fig. 17a**). This provided the initial evidence that shunt activation is necessary for the downstream *fmo-2* response. I then tested whether shunt induction would be sufficient to trigger *fmo-2* expression (**Fig. 17 c**). Hyperosmotic stress in the presence of food resulted in a small but significant induction of *fmo-2*, resembling the muted effect of diacetyl exposure in fed worms. Combining starvation with hyperosmotic stress did not further enhance *fmo-2* expression. This result is entirely consistent with my previous finding that *gpdh-1* transcription is actively suppressed during food deprivation (**Fig. 11a**). To bypass this nutritional block, I designed a pre-treatment paradigm: worms were exposed to hyperosmotic shock while on food (to permit *gpdh-1* induction), and then immediately transferred to food deprivation under normal osmolarity. This sequential treatment was sufficient to robustly induce *fmo-2*, phenocopying the effects of diacetyl exposure. Critically, the *fmo-2* induction generated by this pre-treatment was strongly suppressed by the knockdown of GPDH or PGPH enzymes (**Fig. 17e**). Together, these data demonstrate that expression of the DHAP shunt genes is both necessary and, when paired with food deprivation, sufficient to activate *fmo-2*.

The mechanism by which the DHAP shunt causes *fmo-2* induction remains an open question. I first evaluated DHAP itself as a potential molecular mechanism. Previous studies have shown that mTORC1 senses glucose availability through intracellular levels of DHAP[26], and that glycolytic intermediates downstream of phosphofructokinase and upstream of GAPDH can upregulate mTORC1 during

hyperglycemia[27]. I partially replicated these findings in an *in vitro* model, showing that overexpression of DHAP shunt genes reduced S6 phosphorylation (**Fig. 20c**), suggesting mTORC1 inhibition (though additional markers are required to confirm this). However, in the *C. elegans* model, I found that diacetyl exposure did not decrease whole-body levels of DHAP at any measured time point. This excludes DHAP depletion as the mechanism triggering *fmo-2* in my model.

To identify alternative shared metabolic signatures, I compared the metabolomic profiles of three conditions: control food deprivation, food deprivation during diacetyl exposure and hyperosmotic stress (on food). All three treatments resulted in the upregulation of some PGs (including the three species most highly induced by diacetyl) and the downregulation of some PAs (**Fig. 18a**). While the exact mechanism by which these PGs accumulate during food deprivation, a condition that suppresses the DHAP shunt, remains to be elucidated, these lipids represent a potential candidate as the molecular trigger driving the starvation response.

FMO-2 is not particularly induced in the first few hours of food deprivation (**Fig. 12c**). Therefore, the control starvation included in my metabolomics (four hours) likely does not reflect a metabolic state associated with high *fmo-2* expression. Other metabolic consequences of shunt induction, such as the low GSH/GSSG (**Fig. 18b**) or ATP/ADP (**Fig. 18c**) ratios observed during prolonged diacetyl exposure, may be triggers for *fmo-2* expression. Low ATP levels, sensed through AMPK, activate TFEB-dependent starvation responses. In line with this, I showed that HLH-30 is required for *fmo-2* induction by diacetyl (**Fig. 19a**), and positioned it downstream or in parallel to the DHP shunt (**Fig. 19b**).

As mentioned above, the DHAP shunt may be depleting the cellular energy levels by both redirecting glycolytic intermediates away from mitochondrial respiration and forcing the synthesis of PGs, consuming high-energy phosphate donors in the process. By consuming NADH, GPDH-1 may also drive an oxidative shift in cellular redox state. While I could not directly calculate the NADH/NAD+ ratio from my current metabolomics platform, a decreased ratio would serve as an excellent candidate signal for *fmo-2* induction. In support of this, caloric restriction extends lifespan in yeast specifically by decreasing NADH levels[221]. Furthermore, fasting and starvation are known to decrease GSH levels in the liver[222] and various cell lines[223], and decrease the GSH/GSSG ratio in specific *C. elegans* tissues[116]. Given that *fmo-2* is induced by both starvation and hypoxia, oxidative stress could be a common trigger, also supported by the diacetyl-induced upregulation of various oxidoreductases, *pqm-1*, and *gpdh-1/2*.

I conclude that inducing DHAP shunt gene expression is sufficient to trigger *fmo-2* strictly when paired with food deprivation. I propose that a direct metabolic consequence of GPDH or PGPH activity is responsible for this trigger. Potential metabolic triggers are: specific phospholipid changes (**Fig. 18a**), decreased ATP levels (**Fig. 18c**) or an oxidative shift (**Fig. 18b**). The suppressive effect of food ingestion on *fmo-2* induction may act via an independent regulatory axis (e.g., HLH-30 regulation) or by directly neutralising the metabolic trigger, such as by replenishing NADH levels and preventing the GPDH-1-induced oxidative shift. Such multiple checkpoints would ensure that *fmo-2* expression is not inappropriately activated by a transient absence of food or hyperosmotic stress.

My findings are entirely consistent with the observation that a moderate hyperosmotic stress extends *C. elegans* lifespan through a mechanism overlapping with the DR response, and requiring *gpdh-1* and *gpdh-2*[126]. My results also add novel support to the emerging importance of DHAP shunt enzymes in metabolic homeostasis and resilience. A recent study[224] demonstrated that an algae-derived bifunctional enzyme (containing both cGPDH and G3PP functions, functionally analogous to my *in vitro* vector) supported proliferation in cancer cells under pharmacological ETC dysfunction or hypoxia, as well as in patient-derived cells with mitochondrial dysfunction. *In vivo*, this enzyme could reverse some ethanol induced metabolic changes. Further underscoring the protective role of this pathway, ergothioneine has been shown to extend *C. elegans* lifespan by stimulating cystathionine gamma-lyase activity, H2S production, and NAD+ regeneration via increased cGPDH activity; crucially, ergothioneine longevity effects were dependent on functional *gpdh-1/2* and *cth-1*[225]. Finally, as an enzyme catalysing the inverse reaction of mGPDH, GPD1 expression has been shown to enhance metformin anti-cancer effects[226]. A recent genetic study also implicated GPD1 in mediating the beneficial effects of metformin on ageing biomarkers[227].

## 8.6 *gpdh-1* induction depends on MDT-15

Finally, I sought to identify upstream regulatory mechanisms controlling the DHAP shunt. I found MDT-15 and NHR-49 (**Fig. 21a**) by screening RNAi clones previously shown to modulate the *C. elegans* response to high glucose[68]. NHR-49 and MDT-15 are well-described co-factors that regulate metabolic responses to fasting[111], and previous studies have highlighted their importance in maintaining lipid homeostasis and directing fatty acid catabolism[228]. I found that the knockdown of *nhr-49* and *mdt-15* suppressed *fmo-2* induction by diacetyl, an outcome similar to the effects observed with *hlh-30* RNAi. However, unlike

*hlh-30*, these genes appear to act upstream of shunt induction. I demonstrated that their knockdown also suppressed diacetyl-induced *gpdh-1* expression (**Fig. 22a**) as well as the associated hyperosmotic stress resistance (**Fig. 22b**). I subsequently focused on *mdt-15* RNAi, as it exhibited a stronger suppressive effect. I found that *mdt-15* knockdown completely suppressed the metabolic consequences of diacetyl exposure (**Fig. 22d**), most notably preventing the accumulation of PGs. This result is consistent with the conclusion that the metabolic effects of diacetyl are dependent on the induction of *gpdh-1*. I next asked if NHR-49 and MDT-15 could regulate shunt induction independently of nutritional stressors. I found that *nhr-49* RNAi significantly reduced *gpdh-1* induction by hyperosmotic stress, while *mdt-15* RNAi completely suppressed it (**Fig. 23a**). Accordingly, *mdt-15* RNAi also increased sensitivity to hyperosmotic stress, tested both through developmental (**Fig. 23c**) and survival (**Fig. 23e**) assays.

Through these data, I describe a new function for NHR-49 and particularly MDT-15 in regulating the DHAP shunt. This novel link to the hyperosmotic stress response expands upon their established roles in regulating starvation and glucotoxicity responses. It is also noteworthy that MDT-15 is required for oxidative stress survival[229], an observation that aligns with the oxidative stress signatures and metabolic shifts discussed in the previous section. Interestingly, some of the *gpdh-1* regulatory mechanisms described here may be conserved in mammals. PPAR receptors, which are the mammalian orthologs to *nhr-49*, are also involved in metabolic responses to fasting and high-fat diets[230]. PPAR receptors have been previously shown to mediate the expression of glycerol metabolism genes, particularly *GPD1*[231]. Specifically, PPARα controls glycerol metabolism in the liver, while PPARγ regulates glycerol metabolism in adipose tissue. PPARα activation has also been reported to induce cardiolipin synthesis in the heart[232].

## 8.7 Model for acute effects of diacetyl exposure

Based on the results provided in this thesis, I propose a model for the acute physiological response to diacetyl (**Fig. 30**).

1. Food deprived worms exposed to volatile diacetyl activate MDT-15 to induce expression of *gpdh-1* and other enzymes in the DHAP shunt, in preparation of food arrival.
2. This leads to accumulation of glycerol, PGs, and protection from acute hyperosmotic stress.
3. The metabolic shift induced by the DHAP shunt, in combination with food deprivation, triggers a state of enhanced starvation characterised by an oxidative shift, low ATP levels and upregulation of *fmo-2* expression.

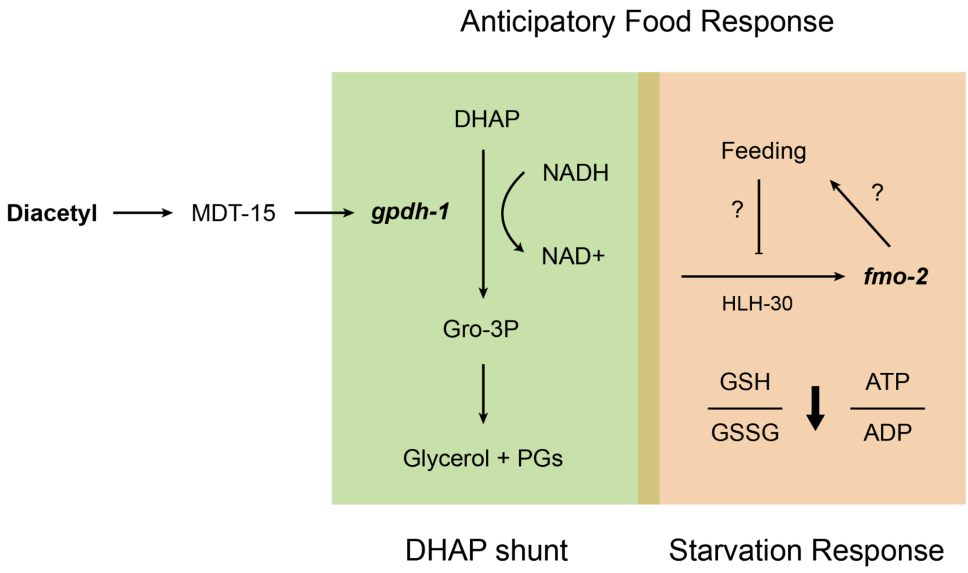


**Figure 30. Model for acute effects of diacetyl exposure on gene expression and metabolism.** Food deprived worms exposed to volatile diacetyl activate MDT-15 to induce expression of *gpdh-1* and other enzymes in the DHAP shunt, in preparation of food arrival. This leads to accumulation of glycerol, PGs and protection from acute hyperosmotic stress. The metabolic shift induced by the DHAP shunt, in combination with food deprivation (possibly sensed through HLH-30), then triggers a state of enhanced starvation characterised by an oxidative shift, low ATP levels and upregulation of *fmo-2* expression.

The induction of *gpdh-1* may serve to maintain nutrient homeostasis upon impending refeeding. *C. elegans* likely recognises diacetyl as an indicator of abundant bacterial growth, signalling the presence of food in the environment. In lactic acid bacteria, diacetyl is produced as a byproduct of pyruvate excess when the bacteria are growing on substrates containing glucose and citrate[145]. Therefore, the worm may use diacetyl as an environmental cue for excess pyruvate and an impending carbohydrate influx. Consistent with this hypothesis, *C. elegans* may also have the capacity to sense pyruvate directly, and pyruvate has been identified as an *in vitro* ligand for the canonical diacetyl receptor ODR-10[233].

A counterintuitive finding from this model is the induction of a starvation response by a food cue. I propose that this may also serve an ecological purpose, namely to stimulate foraging. Recent evidence indicates that *fmo-2* possesses a behavioural function, as *fmo-2* modulates chemotaxis towards diacetyl and other volatiles[115]. My interpretation of the literature, supported by my own data demonstrating that

diacetyl exposure increased feeding rates, is that *fmo-2* induction during starvation may drive food-seeking behaviours. In this framework, exposure to diacetyl (or other food cues like ethanol) in fasting worms would induce *fmo-2* to increase chemotaxis towards the source of the cue. Once the worm located the food, the act of feeding would rapidly repress further *fmo-2* expression. This model is supported by the observation that both *fmo-2* KO and overexpression strains have impaired diacetyl chemotaxis, likely because of a broken feedback loop between odor sensing, FMO-2 induction and a satiety response[115].

Therefore, the biological purpose of triggering this "starvation response" via a food cue may be to hyper-activate food-seeking behaviours precisely when worms sense that a food source is nearby. Under natural conditions, a food cue would not normally induce such a sustained, massive transcriptional response because worms would quickly commence feeding, thereby suppressing the pathway. The extreme *fmo-2* induction observed in my experimental setup is likely an artifact of the artificial combination of a strong food cue with persistent food deprivation.

## 8.8 Conflicting reports of diacetyl effect on *fmo-2* expression and DR lifespan

The acute effect of diacetyl on *fmo-2* induction was particularly unexpected, because the consensus in the field is that the olfactory perception of food represses the longevity effects of DR (section 3.4). Continuous exposure to volatiles produced by live bacteria reduces effects of DR on lifespan extension[141]. Diacetyl in particular has been shown to reduce DR lifespan independently of ODR-10 and SRI-14[150].
The main study contradicting my results was published in 2022[142], and included a comprehensive screen of volatile compounds exposed to worms either in fed or DR conditions and tested for their effect on *fmo-2* induction. The authors exposed worms expressing an *fmo-2p::mCherry* reporter to 100 µL of odorant solutions (I used 50 µL) and imaged after 20 hours. They reported that attractants were more likely to suppress DR-mediated induction of *fmo-2*, while some neutral and repellant compounds could induce *fmo-2* even under fed conditions. In their Figure 1 they focused particularly on 2-butanone, which they also reported could suppress DR lifespan.

Looking deeper into their supplementary data, I found that most volatiles they tested, including diacetyl, benzaldehyde and isoamyl alcohol, seemed to slightly induce *fmo-2* in fed conditions (**Fig. 31a**). This was

also true for odors secreted from live HB101 bacteria. Regarding the DR suppression, most attractive volatiles did not have a stronger effect than the ethanol solvent control, which slightly reduced *fmo-2* induction (**Fig. 31b**). While this figure only reported odorant concentration for benzaldehyde (200 mM), in their supplementary Table 3 the authors listed "optimal concentrations" for all odorants used, including 50 mM for 2-butanone and 100 mM (0.88 %) for diacetyl. They claimed to have established these optimal concentrations through titration experiments, but I found that these did not match the reported values.

The titration/dose finding experiments (without ethanol controls) are reported in Supplementary Fig. 2. In this figure, 2-butanone did not repress DR *fmo-2*, but instead increased it at every concentration, including the 50 mM "optimal concentration"(**Fig. 31c**). In the same figure, diacetyl decreased DR *fmo-2* induction at the concentrations of 0.1 mM (0.00087 %) and 200 mM (1.7 %), but not at 50 mM (0.44 %) (**Fig. 31d**). It is also not clear what concentration of odorants the worms actually experienced during the experiments. In their methods, the authors stated that "A small pad of NGM agar (2 mL) was poured on the lid of each plate and allowed to solidify before 100 µL of each smell concentration was added to the agar pads. Plates were prepared the day prior to use to allow the ethanol solutions to dry". I believe that both the ethanol solvent and any diluted volatile would largely evaporate over a day of drying. Accordingly, volatile dilutions for odor treatments are typically prepared fresh and directly exposed to worms[137, 139, 150].

In summary, the claims regarding the suppressive effects of volatiles on *fmo-2* induction are challenged by internal inconsistencies within the study's own data. The results vary across different panels and contradict the optimal concentrations reported. Given these discrepancies, and potential methodological issues like evaporation, the broader claims remain unsupported. The most conservative and consistent interpretation of their data is that many volatiles, including diacetyl, seem to slightly increase *fmo-2* expression in fed worms. Similarly, the conclusion that attractants are more likely to suppress DR longevity is difficult to align with their survival assays. The authors reported that 5-nonanone, a volatile repellant, shortened both fed and DR lifespans; however, the data show that this lifespan-shortening effect is considerably stronger in DR worms (**Fig. 31e**). This disproportionate sensitivity suggests that DR animals might generally be more vulnerable to volatile compounds, regardless of whether these are attractants or repellants.

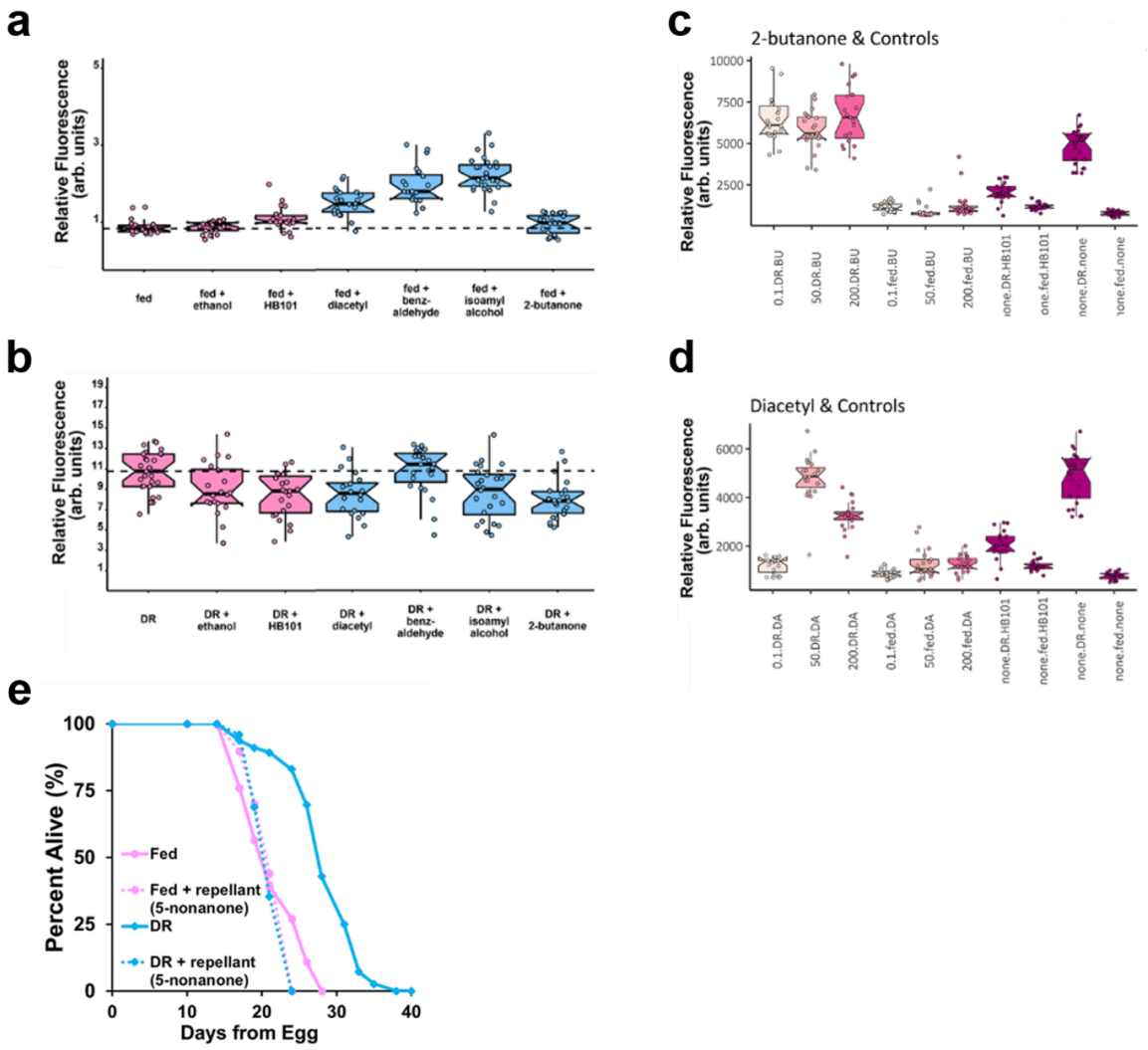


**Figure 31. Adapted from Miller et al. (2022)[142]. a** - **d,** Induction of *fmo-2*p::mCherry reporter by volatiles. (**a**) is cropped from Supplementary Fig. 1g, (**b**) is cropped from Supplementary Fig. 1h, (**c**) is Supplementary Fig. 2i, (**d**) is Supplementary Fig. 2g, (**e**) is Supplementary Fig. 1j. **a** - **b**, *fmo-2* induction by exposure to ethanol, HB101 bacteria and volatiles in ethanol dilutions: benzaldehyde, isoamyl alcohol and 2-butanone. Experiments performed on fed (**a**) and DR (**b**) conditions. **c** - **d**, Dose finding experiments for *fmo-2* induction by dilutions of 2-butanone (**c**) and diacetyl (**d**) in ethanol. Tested dilutions from 0.1 to 200 mM, both in fed and DR conditions. Comparing to unexposed fed worms (none.fed.none), unexposed DR worms (none.DR.none), fed worms exposed to HB101 bacteria (none.fed.HB101) and DR worms exposed to HB101 bacteria (none.DR.HB101). **e**, Survival of worms exposed to 5-nonanone in fed and DR conditions.

This is consistent with recent findings on the effects of DR and ageing on olfaction. Suryawinata et al. have discovered that the worm's ability to sense and move towards volatiles, including diacetyl, declines when worms are aged on OP50. Chemotaxis could be maintained by feeding worms LAB or by food deprivation, and the effect was dependent on *daf-16*$^{234}$. These results demonstrate that olfaction declines with ageing, which I believe complicates the interpretation of studies using chronic exposure to bacterial volatiles. In particular, the fact that dietary restriction suppresses this effect might explain why DR lifespan has been more frequently reported as sensitive to olfactory stimulation.

Additionally, the results in this field have often been contradictory. Zhang et al. reported that exposing worms to volatiles produced by live OP50 could reduce by 50% DR-induced longevity, while having no effect on the lifespan of ad libitum fed worms[141]. Park et al. found that OP50 odor shortened the lifespan of worms in either fed or DR conditions[150], while diacetyl producing LAB did not have any effect on lifespan. However, these authors claimed that chronic diacetyl exposure could specifically shorten DR longevity. They also tested chronic exposure to 2-butanone and isoamyl alcohol, and found no lifespan effects. In contrast, Miller et al. claimed that 2-butanone specifically decreased DR lifespan[142], and Kurino et al. claimed that isoamyl alcohol could extend lifespan[143]. The variable outcomes from these may be explained by inconsistent odor exposure protocols ("sandwich plates" for live bacteria odors; quantity, concentration, duration and frequency of exposure for selected volatiles) and DR conditions.

In this thesis, I showed that a single exposure to volatile diacetyl (across physiological concentrations) consistently induced *fmo-2* expression in food-deprived worms (**Fig. 12h**), regardless of specific worm age (**Fig. 12g**) or food deprivation length (**Fig. 12e** -**f**). I validated this observation by RNA-seq (**Fig. 12a**), a transcriptional reporter (**Fig. 12c**), qPCR (**Fig. 16**), metabolic (**Fig. 13**) and behavioural (**Fig. 14**) signatures of starvation. While I have characterised a model of acute responses to a volatile food cue, a chronic or repeated treatment of this kind may have a different impact on worm physiology and lifespan. I speculate that a major, yet largely unaddressed, confounding variable in repeated odor treatments is the role played by olfactory learning and memory. While *C. elegans* innately perceives specific volatile compounds (such as diacetyl) as food cues, this positive association is likely reversed by the repeated pairing of the odor with food deprivation. In support of this hypothesis, previous studies have demonstrated that worms pre-exposed to diacetyl in the absence of food lose their attraction to diacetyl-producing lactic acid bacteria[145]. Therefore, repeated odor exposure without a corresponding nutritional reward likely extinguishes its efficacy as an anticipatory food cue, and may even condition an aversive response.

## 8.9 Volatile food cue responses across temporal and biological scales: open questions

I designed this project with the goal of creating a simple, tractable model of organismal responses to a volatile food cue. I found instead a complex, interconnected cascade of dynamic responses that bridged transcription, metabolism, stress adaptation, and behaviour. By breaking down these responses across distinct temporal and biological scales, several interesting mechanisms and unanswered questions emerge.

A first limitation in this work is the missing mechanism of diacetyl sensing (section 8.4). More in-depth analyses of tissue and cell specific diacetyl responses will be required to tackle this problem. Direct diacetyl effects are likely occurring in a timescale of seconds, while the first transcriptional response I detected (DHAP shunt induction) occurred between 15 and 30 minutes. Future investigations should focus on the 0 to 15-minute time window to search for changes in neuronal signalling, rapid post-translational modifications (such as phosphorylation), shifts in transcription factor localisation, and metabolic fluctuations. Additionally, further study is required to understand the DHAP shunt role in maintaining nutrient homeostasis during rapid fasting and refeeding cycles, outside the context of diacetyl exposure.

The first diacetyl transcriptional wave at thirty minutes also included upregulation of the histone demethylase *jmjd-3.3*. This suggests that chromatin reorganisation may be another layer of early gene expression regulation in the AFR. Early transcriptional DHAP induction leads to a metabolic shift (glycerol and PG accumulation), which then leads to another transcriptional response (*fmo-2*). The biological function of PGs represents a fascinating and underexplored area of research where diacetyl exposure could prove as a useful model. PG accumulation likely affects mitochondrial membrane organisation and function to some extent. Concurrently, the diversion of glycolytic intermediates through the DHAP shunt should also affect mitochondrial respiration.

The second transcriptional wave at ninety minutes included the upregulation of the translation elongation factor *eef-1A.2*, and *fmo-2* upregulation was dependent on HLH-30. Together, these data strongly imply that modulation of mRNA translation constitutes another layer of gene expression control during the AFR. The second major unanswered question of this project is the precise mechanistic link

between DHAP shunt induction and the following DR-like response. I propose that one or more specific metabolic consequences of DHAP shunt (section 8.5) acts as the trigger for this DR response. In this sense, it will be interesting to test if the benefits associated with DHAP shunt induction in other organisms[224] share features in common with my *C. elegans* model.

Finally, FMO-2 induction does not only enable benefits related to food deprivation, but also regulates satiety signals and chemotaxis[115]. A key future step in this project should be to test how the AFR induced by acute diacetyl exposure acutely modulates foraging behaviours. Understanding exactly how the specific gene expression and metabolic responses identified in this thesis integrate to drive behavioural decisions will provide a comprehensive picture of how *C. elegans* anticipates, seeks, and adapts to food availability.

## 8.10 Ageing translatome: open questions

My primary aim in the second project was to characterise translatome changes during *C. elegans* ageing, specifically focusing on the translational efficiency (TE) of individual genes. I identified hundreds of genes that significantly altered their TE from the youngest (day 1) to the oldest (day 12) age (**Fig. 25b**). Furthermore, a number of genes exhibited linear changes across all three collected ages (**Fig. 25d**), supporting a real ageing phenotype. The use of a linear model was arbitrary, as there is no evidence indicating that ageing-related translational shifts should occur at a constant rate. Ideally, more samples would have been collected to determine the kinetic rate of ageing changes.

Interestingly, I found more transcripts increasing rather than decreasing in TE with age. This contrasts with observations in yeast replicative ageing[188], where no transcripts exhibited age-related increases in TE. Despite this divergence, my data aligns with that study in finding that the age-related decrease in TE is most pronounced for genes that are highly expressed in young age. These data suggest that global translational decline particularly impacts heavily translated transcripts, potentially allowing lowly translated transcripts to "escape" and increase in relative proportion within the ageing translatome. I also observed a moderate anticorrelation between transcriptional and translational ageing changes (**Fig. 25c**), which I interpret as a form of gene expression buffering. My results cannot resolve the directionality of this process. The translational machinery may possess intrinsic resilience, compensating for an age-related transcriptional drift by actively altering the TE of specific genes. Vice versa, ageing may alter TE of particular transcripts, and worms may compensate for this by altering their transcription.

To determine the biological implications of these TE shifts, I utilised GO-term enrichment analyses. Genes translationally upregulated with age were enriched in terms related to chromatin organisation, DNA repair and transcription (**Fig. 26a**). Conversely, the top terms enriched among translationally downregulated genes were translation, protein folding and ribosome biogenesis (**Fig. 26b** and **d**). The age-related translational repression of the protein synthesis machinery is in line with published studies across diverse model organisms. For example, the greatest reduction in TE during yeast replicative ageing occurs in transcripts encoding ribosomal subunits and core translation machinery[188], while ageing mice exhibit a targeted downregulation of translation-related transcripts enriched in 5' TOP motifs[172]. Furthermore, ribosomal pausing has recently been identified as a shared feature of ageing gene expression[173,165]. This pausing disproportionately affects transcripts related to proteostasis and translation, particularly those encoding tRNA synthetases[173]. Similarly, my data revealed that tRNA synthetases were particularly affected by ageing, with six tRNA synthetases showing a linear ageing decline in TE (**Fig. 26e**). This may be another factor contributing to the decrease in tRNA charging observed with age[165].

To uncover the mechanistic basis for these translational shifts, I evaluated differences in intrinsic mRNA properties. Transcripts downregulated with age possessed higher GC content and codon adaptation metrics, whereas transcripts upregulated with age exhibited the opposite trends (**Fig. 27**).
While higher GC content has previously been linked to increased baseline gene expression, either via enhanced transcription[235] or greater mRNA stability[236], my results suggest it may also influence translation levels. Because general translational elongation capacity declines with age (as discussed above), the ageing ribosome likely suffers a decreased capacity to unfold highly stable, GC-rich mRNA secondary structures. This limitation would confer a translational advantage to mRNAs with lower GC content, supporting a model of translational ageing decline.

On the other hand, the association with metrics of codon adaptation may point to the existence of an ageing-related "translational program". Synonymous codons are not utilised with equal frequencies (section 1.4): highly expressed genes (including the translation machinery itself) are heavily enriched in "optimal" codons that match the most abundant tRNA isoacceptors, supporting their highly efficient translation[11]. The first study that looked at ageing translatome changes in yeast found that transcripts highly expressed in young cells were more likely to be translationally downregulated with age[188], and my data matched this pattern. Because baseline expression levels correlate strongly with codon adaptation,

this could partially explain the observed TE shifts. However, the correlation between codon adaptation and ageing TE remained significant even after statistical correction for baseline expression differences, indicating that this phenomenon cannot be fully explained by simple transcriptional effects.

This shift in codon usage efficiency could be driven by an underlying change in the pool of available isoacceptor tRNAs. Ageing related alterations in tRNA levels, modifications and charging are just beginning to be characterised[165, 237]. A compelling precedent for this hypothesis exists in yeast, where various acute stress types rapidly alter the total tRNA pool, directly leading to the preferential translation of specific stress-response transcripts[44]. If an adaptive "aging translational program" was driving the effects seen in my data, I could expect to find downregulation of growth functions coupled with a compensatory upregulation of maintenance functions. While my data provided strong evidence for the former (repression of protein synthesis), evidence for the latter was limited (modest enrichment in DNA repair related genes). Alternatively, rather than representing a coordinated adaptive program, the ageing translational decline in protein synthesis and folding machinery could be driving a vicious cycle of maladaptive protein synthesis and proteostatic decline.

In conclusion, the next steps for this project should focus on the experimental validation of these correlative findings. Specifically, translational reporters with varying GC content and codon adaptation could be used to confirm if these intrinsic mRNA properties directly alter protein synthesis during ageing. In parallel, this should be supported by studying ageing-related changes in mRNA accessibility (linked to GC content) and the tRNA pool (linked to codon adaptation). Because these ageing effects on translation might vary across different tissue types, future studies should also explore this complexity level. Most importantly, we will need new data on ageing TE changes in other animals to test the evolutionary conservation of these findings.

## 8.11 Limited ISR translational signatures

Another aim of this project was to assess how the ISR contributes to the ageing translatome. The ISR is understood to become excessively activated during ageing, potentially causing translational deregulation and disease[166]. My expectation was to identify ISR translational targets as genes translationally downregulated in S51A mutants with inactive ISR. Surprisingly, I found few translational differences between genotypes. Only one gene was translationally downregulated in S51A mutants on day 1 (**Fig. 28a**), and this had no obvious connection to the ISR.

Clear translational differences only appeared on day 12 (**Fig. 28c**). Most genes (24 out of 25) differentially translated at day 12 were downregulated in S51A mutants, but again none of them had an obvious link to the ISR. 11 of these genes (*fan-1, C41D11.3, H05C05.2, stam-1, ent-6, T25D3.4, T28F4.4, impt-1, tdp-1, phf-14, knl-2*) were also translationally upregulated with age, suggesting that they might be translationally upregulated simply because of faster ageing in WT worms. It would be interesting to check if these genes are differentially regulated in S51A mutants under a different type of ISR-inducing stress. ATF4, a canonical ISR target, was also not differentially translated between the genotypes, nor was it translationally upregulated with age (**Fig. 28e**). This matches the results from replicative ageing in yeast, where the ATF4 ortholog was also not increasingly expressed with age[188]. In this study however, ISR inhibition seemed to restore the ageing-related translation decline. I also tested olfactory learning and memory in long-lived eIF2B$\gamma$ mutants but could not find any improvement in these functions (**Fig. 29**). This is in contrast with findings of improved memory function in mice from pharmacological or genetic ISR inhibition[190]. Taken all together, these findings could suggest that in *C. elegans* the ISR functions in ways that we do not yet understand and that are quite different from other model organisms. I found no evidence suggesting that complete genetic inhibition of the ISR broadly altered TE of specific mRNAs in ageing.

*C. elegans* gene expression is different from other organisms (such as yeast or mammals) in two notable ways: 1- many genes are organised in operons, 2- trans-splicing is pervasive. About 15% of *C. elegans* genes are co-transcribed in operons that contain between 2 and 8 genes. This is believed to facilitate coordinated expression of proteins with related functions[238]. When a pre-mRNA encoding multiple transcripts is spliced, a short splice-leader RNA (SL) is added before the start codon to facilitate translation of each coding sequence. This trans-splicing phenomenon is pervasive and affects also genes that are not part of operons: it is estimated that most *C. elegans* genes are trans-spliced to some level, and at least 70% of genes are highly efficiently trans-spliced[239]. Because trans-splicing replaces most of the original 5' UTR of a gene (**Fig. 32**), I speculate that both uORFs and the ISR play a minor role in translational regulation of most mRNAs in *C. elegans*.

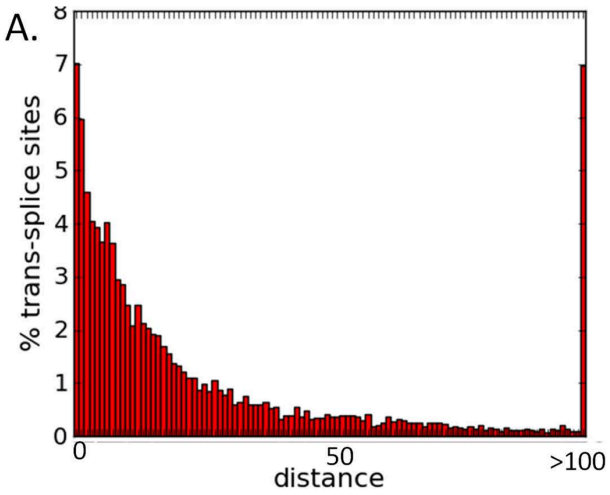


**Figure 32. Adapted from Allen et al. (2011)[240].** Distance (in base pairs) between splice leader and start codon across all *C. elegans* trans-splice sites. Percentage of the gene trans-splice sites in that category on the Y axis. Cropped from Supplementary Fig. 2.

# 9. Materials and Methods

## *C. elegans* strains and culture

*C. elegans* strains were maintained at 20 °C on nematode growth medium (NGM) agar plates[103] seeded with the *Escherichia coli* (E. coli) strain OP50, unless indicated otherwise.

| Strain | Genotype | Source |
|---|---|---|
| Bristol N2 | wild-type | CGC |
| VP198 | *kbIs5 [gpdh-1p::GFP + rol-6(su1006)]* | CGC |
| KAE28 | *unc-119(ed3) III; seaEx13 [fmo-2p::GFP + unc-119(+)]* | CGC |
| VC1668 | *fmo-2(ok2147) IV* | CGC |
| CX3410 | *odr-10(ky225) X* | CGC |
| VC2123 | *sri-14(ok2865) I* | CGC |
| CB450 | *unc-13(e450) I* | CGC |
| CB928 | *unc-31(e928) IV* | CGC |
| MT15434 | *tph-1(mg280) II* | CGC |
| MT15620 | *cat-2(n4547) II* | CGC |
| CB1370 | *daf-2(e1370) III* | CGC |
| MSD310 | *ppp-1(wrm15) II* | Derisbourg et al. (2021)[194] |
| SYB1385 | *eIF2α(syb1385) I* | Derisbourg et al. (2021)[194] |

Glucose and sorbitol plates were prepared by adding filter-sterilised glucose and sorbitol solutions to NGM agar after autoclaving, to reach a final concentration of 111 mM. Plates were seeded with live OP50, and worms were maintained at 25 °C to measure *gpdh-1* induction. Food deprivation was performed by keeping worms on unseeded NGM plates.

Hyperosmotic stress plates for metabolomics and for induction of transcriptional reporters were prepared by increasing NaCl concentration in agar to 200 mM (regular NaCl concentration in NGM is 51 mM).

For collection of aged worm samples, WT and S51A mutants were grown from eggs on regular NGM plates and transferred to plates supplemented with FUDR (10 µM) at the L4 stage to stop egg development. Samples were collected at day 1, 6 and 12 of adulthood. Worms were regularly transferred to FUDR plates with fresh food to avoid starvation.

# Exposure to diacetyl and other volatiles

Unless specified otherwise, day 1 adult worms were washed for 1 hour with M9 in rotating falcon tubes to remove bacteria, then transferred to unseeded 10 cm NGM agar plates and allowed to air dry for a few minutes. Worms were split into control (no volatile) and diacetyl-exposed plates. A 1% solution of diacetyl (2,3-Butanedione, SB85307, Sigma-Aldrich) in 100% ethanol was prepared immediately before experiments. 50 µL of this solution was pipetted on a 90 mm square of blue roll placed on the centre of the lid, then immediately closed, sealed with tape and kept lid-side down throughout the exposure.

Exposure to 2-butanone (360473, Sigma-Aldrich), isoamyl alcohol (W205702, Sigma-Aldrich) and MGO (M0252, Sigma-Aldrich) followed the same protocol. These compounds were also diluted to a 1% concentration in ethanol.

# RNA-seq and Ribo-seq for Translation Efficiency

## Sample collection and generation of RPFs

Sample collection and processing was performed on ice and with cold buffers. Worms were first collected in M9, washed once in M9 with 1mM cycloheximide, then washed in Lysis buffer (20 mM Tris Base, 140 mM KCl, 1.5 mM MgCl2, 0.5% NP-40, 1 mM DTT, 1mM cycloheximide). Worms were then resuspended in Lysis buffer supplemented with 1% sodium deoxycholate, lysed using a tissue grinder (Wheaton Dounce Dura-Grind) on ice, incubated for thirty minutes and cleared by centrifugation (12000 g, 10 min). After measuring RNA concentration, part of each sample was saved as total mRNA,which was extracted using the Direct-zol RNA MicroPrep Kit (Zymo Research) to analyse through RNA-seq.

The rest of the sample was digested with RNase I (5 U RNase per µg RNA) for one hour at room temperature to generate RPFs. These were isolated by ultracentrifugation (SW41T rotor, 39000 RPM for 3h at 4°C), running the sample through a linear sucrose gradient (15-60%) and collecting the monosome fraction. RPFs were extracted from the sucrose gradient by a sequence of extraction steps. First, the monosome fraction in sucrose was resuspended in an extraction buffer with final concentrations of 50 mM NaCl, 10 mM Tris, 5 mM EDTA, 120 µg/mL glycoblue, 0.8% SDS and 160 µg/mL of Proteinase K. This was incubated at 65 °C for 1h, then one volume of acid phenol chloroform was added and the sample was centrifuged (12000 g 10 min 4°C). The upper liquid phase was collected and added to one volume of chloroform, then centrifuged again (12000 g 10 min 4°C). The upper liquid phase was collected and added to 10% volume of 3M sodium acetate and 3 volumes of ice-cold EtOH. RNA was left to precipitate overnight at -80 °C and centrifuged (12000 g 30 min 4°C). The supernatant was removed and the pellet washed with 500 µL of ice-cold EtOH. The last centrifugation step was repeated. After removing the supernatant, the RNA pellet was left to dry on ice. Finally, an RNA Clean & Concentrator Kit (Zymo) was used for the last cleanup step before Ribo-seq.

## Sequencing and data analysis

cDNA libraries were generated with ribosomal RNA depletion at the Cologne Center for Genomics and sequenced on the Illumina HiSeq2000 platform. Raw sequencing reads were subjected to quality trimming and adapter removal using Flexbar[241]. Comprehensive quality control reports summarising all initial and post-alignment metrics (e.g., read distribution, coverage, duplication rates) were generated using MultiQC[242]. Reads were mapped to the reference genome and transcriptome using STAR[243]. RiboWaltz[244] was used to determine P-site offset and 3-nucleotide periodicity. RiboCode[245] was used to identify translated ORFs. Riborex[246] was used to integrate RNA-seq and Ribo-seq data to calculate TE and identify differentially translated genes. Locus-specific visualisation of Ribo-seq read distribution was performed using the Integrative Genomics Viewer (IGV). Track displays were generated from bigWig files and mapped against the *C. elegans* ce11 reference genome.

To determine age-related changes in translational efficiency across all timepoints, linear models were fitted to the TE values of individual genes across the three ages. The significance of the age-dependent linear trends was determined using Student's t-tests on the regression coefficients, and p-values were adjusted for multiple testing using the False Discovery Rate (FDR). DAVID analyses[247] were performed to

identify significantly enriched biological processes. Adjustment for multiple comparisons was completed using the Benjamini & Hochberg approach. Codon adaptation and GC content analyses were performed using CodonW[248]. To determine significant differences in CAI and GC content, the distributions of the regulated transcripts were compared to the unchanged background using a two-sided Wilcoxon rank-sum test, with effect sizes calculated as the difference in means (Δ).

## Transcriptomics of diacetyl exposure

Worms were washed in M9 and exposed to diacetyl on unseeded plates as described above. Worms were exposed to diacetyl for 5 to 90 minutes, then snap-frozen. The pellet was resuspended in TRI Reagent (Zymo) and RNA extraction was performed using the Direct-zol RNA MicroPrep Kit (Zymo Research). Poly-A selected cDNA libraries were produced using the NEBNext Ultra II Directional RNA Library Kit and sequenced on the Illumina NextSeq2000 platform. Raw sequencing data (FASTQ files) were processed using the nf-core/rnaseq pipeline (version 3.12.0) executed via Nextflow[249] (version 23.04.2). Raw sequencing reads were subjected to quality trimming and adapter removal using Trim Galore[250] (version 0.6.7) with Cutadapt[251] (version 3.4). Comprehensive quality control reports summarising all initial and post-alignment metrics (e.g., read distribution, coverage, duplication rates) were generated using MultiQC[242]. Reads were mapped to the reference genome and transcriptome using STAR[243]. Transcript-level quantification was performed using Salmon[252] (version 1.10.1) via a quasi-mapping approach. Separately, gene-level counts were generated using featureCounts (Subread package version 2.0.1). Reads aligned to the genome by STAR were further visualised and quantitated using SeqMonk[253] (v1.48.0). Limma and intensity difference filters were combined to define differentially expressed genes ($P < 0.05$).

## Glycerol measurements

For glycerol measurements in worms, frozen pellets were resuspended in RIPA buffer (150 mM NaCl, 1% NP40, 0.5% sodium deoxycholate, 0.1% sodium dodecyl sulfate (SDS), 50 mM Tris-HCl, pH 8.0, completed with protease inhibitors), sonicated and spun down. Protein quantification was done by bicinchoninic acid assay (Pierce BCA Protein Assay Kit, Thermo Fisher). Glycerol concentration was measured with a glycerol assay kit (MAK117, Sigma-Aldrich) following manufacturer´s protocol. Samples were pre-diluted

to fall in the detection range of the colorimetric detection. Glycerol concentration was normalised by the protein concentration in each sample. Experiments were carried out with four biological replicates.

For measurements of glycerol secreted from *in vitro* DHAP shunt induction, culture media was collected and cleared by centrifugation before measuring glycerol concentration as described above.

# Metabolomics and lipidomics

## Sample collection

Worms were washed in M9 and exposed to diacetyl on unseeded plates as described above. Worms were exposed to diacetyl for one or three hours, then snap-frozen. For the fed condition, worms were directly snap-frozen before M9 starvation. For hyperosmotic stress, worms were transferred to 200 mM NaCl seeded plates for three hours before snap-freezing. Experiments were carried out with ten biological replicates.

## Sample processing and LC-MS

Frozen worm pellets were extracted overnight using ice‑cold LC–MS grade solvent consisting of 800 µL 80% methanol / 20% water and 700 µL 53:33:12:1 (MeOH:$CHCl_3$:$H_2O$:acetic acid, v/v/v/v). Isotopically labeled internal standards prepared in 80% methanol / 20% water were spiked into each sample proportional to the average number of worms per condition. Samples were sonicated in a water bath to dissociate worms, vortexed, and incubated overnight at −80 °C. The extracts were then centrifuged at 30,000 × g for 20 min at 4 °C, and the supernatant was collected and dried in a speed vacuum concentrator at 4 °C overnight. Dried samples were resuspended in ACN:MeOH:$H_2O$ (40:40:20, v/v/v) at volumes normalised to worm number, followed by centrifugation at 30,000 × g for 20 min at 4 °C. The clarified supernatants were transferred to glass vials arranged in a 96‑well autosampler plate. Throughout processing, samples were handled on dry ice, and during LC–MS analysis they were maintained at 4 °C in the autosampler.

Metabolites were measured using an Exploris 240 mass spectrometer (Thermo Fisher Scientific) connected to a Vanquish Duo UHPLC system (Thermo Fisher Scientific) operated in both positive and negative ion modes. Anionic metabolites (negative ion mode) were separated on an Acquity Premier GLY BEH 130 Å, 1.7 µm, 2.1 × 150 mm column (Waters, #186009524) at a flow rate of 0.40 mL/min using a

binary gradient consisting of Mobile Phase A (10 mM ammonium acetate in 90:10 $H_2O$:acetonitrile with 5 µM medronic acid) and Mobile Phase B (10 mM ammonium acetate in 80:10 acetonitrile:$H_2O$ with 5 µM medronic acid). The gradient started at 0% Mobile Phase A and was increased to 30% A over 8 minutes, followed by 1 minute at 50% A. At 9.5 minutes, the gradient was returned to 0% A for 50 seconds and then held at 0% A for an additional 3 minutes. The column temperature was maintained at 40 °C. Cationic metabolites (positive ion mode) were separated on an InfinityLab Poroshell 120 HILIC‑Z column, 2.1 × 150 mm, 2.7 µm (Agilent Technologies, #683775‑924) at a flow rate of 0.40 mL/min with Mobile Phase A (10 mM ammonium formate in water with 0.1% formic acid) and Mobile Phase B (acetonitrile with 0.1% formic acid). The gradient started at 5% A and was held for 1 minute, then increased linearly to 50% A over 6 minutes. The mobile phase was held at 50% A for 3 minutes before being returned to 5% A and held for 2 minutes. The column temperature was maintained at 40 °C. Full‑scan MS data were acquired under the following conditions: m/z range 70–900; resolving power 120,000 (at m/z 200); automatic gain control target set to Standard; and maximum ion injection time set to Auto. Ion source parameters were: spray voltage, static; ion transfer tube temperature, 275 °C; RF lens level, 75; heater temperature, 320 °C; sheath gas, 50 (arbitrary units); and auxiliary gas, 10 (arbitrary units). Raw LC–MS data were imported into Skyline, and chromatographic peaks were manually inspected and curated for peak picking and integration to generate peak area values for downstream quantitative analysis.

Lipids were measured using a SCIEX Triple Quad 7500 mass spectrometer (SCIEX) operated in LC–MS/MS mode and connected to a Vanquish Duo UHPLC system (Thermo Fisher Scientific) operated in both positive and negative ion modes. Lipids in negative ion mode were separated on an ACQUITY UPLC BEH C18 column, 130 Å, 1.7 µm, 2.1 × 100 mm (Waters Technologies Corporation, #186002352) at a flow rate of 0.25 mL/min using a binary gradient consisting of Mobile Phase A (10 mM ammonium acetate in 60:40 acetonitrile:water) and Mobile Phase B (10 mM ammonium acetate in 90:10 isopropanol:acetonitrile). The gradient started at 45% Mobile Phase B and was increased to 99% B over 8 minutes and held at 99% B for 1 minute. At 9 minutes, the gradient was returned to 55% B for 1 minute and then held at 55% B for an additional 2 minutes. The column temperature was maintained at 55 °C. Lipids in positive ion mode were separated on the same ACQUITY UPLC BEH C18 column (130 Å, 1.7 µm, 2.1 × 100 mm; Waters Technologies Corporation, #186002352) at a flow rate of 0.25 mL/min using a binary gradient consisting of Mobile Phase A (10 mM ammonium formate in 60:40 acetonitrile:water with 0.1% formic acid) and Mobile Phase B (10 mM ammonium formate in 90:10 isopropanol:acetonitrile

with 0.1% formic acid). The gradient started at 45% Mobile Phase B and was increased to 99% B over 8 minutes and held at 99% B for 1 minute. At 9 minutes, the gradient was returned to 55% B for 1 minute and then held at 55% B for an additional 2 minutes. The column temperature was maintained at 55 °C. Data acquisition was performed in scheduled multiple reaction monitoring (MRM) mode using an optimised MS/MS transition and retention time table. Source and gas parameters were as follows: ion source gas 1, 45 psi; ion source gas 2, 60 psi; curtain gas, 50 psi; collision gas (CAD), 9 (arbitrary units); source temperature, 500 °C; and ion spray voltage, 4200 V. Raw LC–MS/MS data were imported into Skyline, and chromatographic peaks were manually inspected and curated for peak picking and integration to generate peak area values for downstream quantitative analysis.

## Data analysis

Chromatographic peak integration and extraction from raw data were performed in a targeted manner using Skyline[254]. Metabolites with poor peak shapes were excluded. Analyte measures were normalised using probabilistic quotient normalisation[255]. Briefly, analytes (excluding spiked internal standards) were median-scaled across samples. The median of these median-scaled analyte values across all analytes was used for each sample as the normalisation factor. Each analyte measurement value was divided by this normalisation factor to compute the final normalised value. Quality-control replicates from pooled samples were interspersed with study samples. Analytes with coefficient of variation (CV) values across these replicates that exceeded 25% after normalisation were removed. In cases where an analyte was measured across multiple LC-MS methods, measurements from the LC-MS method that produced the lower CV value for that analyte were used in downstream analyses.

Differential abundance testing was performed on normalised and log transformed measurements using Welch's T-Test. Adjustment for multiple comparisons was completed using the Benjamini & Hochberg approach. Analyte ratios for GSH/GSSG and ATP/ADP were computed using the unnormalised LC-MS peak areas. Analyte ratio comparisons were performed using Brown-Forsythe and Welch ANOVA tests, corrected for multiple comparisons with Dunnett's T3 tests.

## Worm imaging

Worms were arranged in stacks on unseeded NGM plates and kept on ice. Images were taken on a Leica M205 FCA fluorescence stereo microscope. Images were acquired with the Leica Application Suite X. Images were quantified with ImageJ (version 2.9.0). Scale bar is indicated in the figure legends.

For imaging of *fmo-2p::GFP* reporter activation, worms were washed off unseeded exposure plates and transferred to seeded NGM plates for 2 hours before imaging to stop reporter induction and allow GFP maturation. A minimum of 15 worms were imaged per replicate. For screening of *far-3p::GFP* suppressors blocking *fmo-2p::GFP* reporter activation by diacetyl, RNAi clones were screened in batches, each normalised to a luciferase nontargeting control.

## qPCR

Worm pellets were resuspended in TRI Reagent (Zymo) and RNA extraction was performed using the Direct-zol RNA MicroPrep Kit (Zymo Research). Gene expression levels were quantified using a 1-step RT-qPCR kit (A6020, Promega) on a QuantStudio 7 Pro System (Applied Biosystems). Expression levels of the genes *act-1* and *tba-1* were used as internal controls for normalisation.

| **Target** | **Forward primer** | **Reverse primer** |
|---|---|---|
| *act-1* | GCTCTTGCCCCATCAACCAT | TGCAAGTTGACGAAGTTGTGC |
| *tba-1* | TCTCGCAGGTTGTGTCTTCC | AGCCTCATGGTAAGCCTTGT |
| *gpdh-1* | AAGTTCTGCGAGGCGACAAT | CGCAGGCGACAATGTTCTTT |
| *gpdh-2* | AGTGAATGCTGAGTCGTCTTAGTT | CCACATACGGACGGTTGGAT |
| *pgph-2* | ACAATGATGATTGGAGACAGAACT | TGGAACAAGAGCTCCAAGGC |
| *pgph-3* | CACTTCCAACCCCAGTCGAA | GCCAAAGTACACCATCAGCG |
| *fmo-2* | CTCACGAAACGAATGAGTCGTCA | GTGACGGAGCTTGATATGCTTCA |

## Ivermectin treatment

For ivermectin treatment of the *fmo-2p::GFP* reporter strain, worms were treated as described above but 100 nM of Ivermectin (I8898, Sigma-Aldrich) was added to the M9 during the one hour wash preceding diacetyl exposure.

## Feeding rate measurements

Worms were exposed to diacetyl for three hours as described above, then immediately washed onto plates seeded with GFP-expressing OP50 (CGC) and allowed to feed for five minutes. Worms were then washed onto unseeded NGM plates kept on ice for imaging. A minimum of 15 worms were imaged per replicate.

## Thermotolerance assays

Day 1 adult worms were starved by transferring to unseeded NGM plates for three hours. For combination with diacetyl exposure worms were treated as described above. For combination with hyperosmotic stress, worms were pre-treated for three hours on seeded NGM plates with 200 mM NaCl. Worms were maintained on seeded plates after day 1 treatments. On day 2, worms were placed at 36 °C for three hours and then recovered at 20 °C overnight. Survival was scored on day 3 for (touch-provoked) movement. A minimum of 100 worms were scored per replicate.

## RNAi experiments

For RNAi-mediated knockdown of specific genes, HT115 bacteria carrying vectors for dsRNA of the target gene under a promoter inducible by isopropyl β-d-1-thiogalactopyranoside (IPTG) and ampicillin resistance were used. Bacteria were seeded on NGM plates containing 100 µg/µL ampicillin (Merck Millipore) and 1 mM IPTG (Roth). Eggs were transferred to RNAi plates. RNAi against luciferase was used as nontargeting control. All RNAi clones were obtained from the Ahringer and Vidal RNAi libraries[256, 257]. Clones were validated by plasmid purification (Zyppy Plasmid Miniprep Kit, Zymo research) and whole plasmid sequencing was performed by Plasmidsaurus using Oxford Nanopore Technology with custom analysis and annotation.

For combined RNAi treatments targeting *gpdh* and *pgph* paralogs in Figure 17, RNAi cultures were mixed in equal volumes before seeding on RNAi plates.

## Acute hyperosmotic stress resistance assay

Worms were exposed to diacetyl for one hour as described above. Worms were washed off the exposure plates in M9 and spun down. 30 µL of worm pellets were pipetted on unseeded high salt plates containing 500 mM NaCl. Control and diacetyl exposed worms were placed in droplets side to side to record under the same field of view. Starting three minutes after pipetting, one minute videos were recorded on a Leica S9i stereo microscope. For quantification of hyperosmotic stress resistance, body bends of each worm were manually recorded from the last 30 seconds of each video. A minimum of 15 worms were scored per replicate.

## Hyperosmotic stress developmental assay

Eggs were placed on either control RNAi plates or RNAi plates supplemented with 200 mM NaCl. Development was assessed after three days and worm area was quantified with ImageJ (version 2.9.0). A minimum of 15 worms were quantified per replicate.

## Hyperosmotic stress survival

Worms were grown on RNAi plates as described above and transferred on day 1 of adulthood to RNAi plates supplemented with 400 mM NaCl. Survival was assessed two and four days after the start of hyperosmotic stress by monitoring (touch-provoked) movement and pharyngeal pumping. A minimum of 100 worms were scored per replicate. Worms that had undergone internal hatching, vulval bursting, or worms crawling off the plates were censored.

## Cell culture

Two doxycycline-inducible C2C12 cell lines were generated to express either a stuffer control sequence or the DHAP shunt construct. The DHAP shunt Tet-inducible gene expression lentiviral vector, consisting of the mouse *Gpd1* (cGPDH) and *Pgp* (G3PP) genes fused by a P2A linker under the control of a tetracycline response element (TRE) promoter, was synthesised by VectorBuilder (VB240305-1170adq).

Lentiviral particles were packaged in HEK293 cells using the Lenti-X Packaging Single Shots protocol according to the manufacturer's instructions. C2C12 cells already stably expressing the reverse tetracycline transactivator (rtTA) were then transduced with the packaged lentivirus and selected with puromycin to establish stable construct integration. Cells were cultured in DMEM high-glucose media (11965092, Gibco) supplemented with 10% FBS and 1% Penicillin. To induce construct expression, subconfluent cells were cultured for 24 hours with 2 ug/mL doxycycline.

### Western blots

Proteins were extracted by lysing cells in RIPA buffer supplemented with Phosphatase Inhibitor Cocktail 3 (P0044, Sigma-Alrdich) and cOmplete™ Protease Inhibitor Cocktail (05892791001, Roche). Protein quantification was done by bicinchoninic acid assay (Pierce BCA Protein Assay Kit, Thermo Fisher). Protein samples were suspended in Laemmli SDS sample buffer and ran on Mini-PROTEAN TGX Stain-Free Precast Gels (Bio-Rad). Proteins were transferred to a nitrocellulose membrane using a Trans-Blot Turbo Midi Transfer Pack (#1704159, Bio-Rad). Total S6 was detected with acS6 (54D2) antibody (#38889, Cell Signalling), while phosphorylated S6 was detected with a phospho-S6 (S235/236) antibody (#2211, Cell Signalling). Total S6 and pS6 were blotted separately, and each band was normalised to the corresponding actin (β-Actin monoclonal antibody 8H10D10) loading control band, before calculating the pS6/S6 ratios. Band intensities were quantified using the Qualitative Western Blot analysis workflow in Empiria Studio software (LI-COR Biosciences).

## Olfactory memory

Olfactory learning and memory tests were performed on day 1 adult worms. For short-term memory, a single training bout of butanone positive conditioning (paired with food) was performed to increase chemotaxis towards butanone (against benzaldehyde as control odorant). This was done following an established protocol[258]. In brief, worms were pre-starved for 1h in M9 and then exposed for 1h to 2-butanone (10% solution in ethanol) on plates with food. Chemotaxis was measured with the test chemical 2-butanone (10% solution) paired with 10% benzaldehyde as control odorant.

For long-term memory, a spaced training protocol was performed to reduce chemotaxis towards 2-butanone (against ethanol as control odorant). Worms were starved for 80 minutes in a 0.01% solution of 2-butanone in S-basal, repeated three times with thirty minute intervals on food between training

sessions. Chemotaxis was measured with the test chemical 2-butanone (10% solution) paired with ethanol as control odorant.

Chemotaxis was measured on unseeded 10 cm plates. 1 µL of 1 M $NaN_3$ was added to the odorant and control spots (equidistant from the spot where worms were deposited at the start of the experiment) to immobilise worms. After this dried, 1 µL of the odorants was added. Worms were allowed to crawl for an hour at room temperature, after which plates were moved to ice to stop further movement before scoring. The chemotaxis index (C. I.) was measured by the percentage of worms preferring the test chemical over the control. A minimum of 200 worms was scored per replicate.

## Statistics

Unless stated otherwise, results are presented as means ± SD. Depending on the experimental design and data distribution, statistical significance was assessed using Welch's t-test, Wilcoxon rank-sum (Mann-Whitney) test, one-way ANOVA (followed by Tukey's, Sidak's, or Dunnett's post hoc tests), Brown-Forsythe and Welch ANOVA, two-way ANOVA (with Sidak's or Fisher's LSD post hoc tests), and hypergeometric test. Specific tests are indicated in figure legends, where significance levels are indicated as *$p<0.05$, **$p<0.01$, ***$p<0.001$ and ****$P < 0.0001$. Experiments were carried out with at least three biological replicates unless noted otherwise.

# 10. Bibliography


1. Telser, A. Molecular Biology of the Cell, 4th Edition. *Shock* **18**, 289 (2002).
2. Weisser, M. & Ban, N. Extensions, Extra Factors, and Extreme Complexity: Ribosomal Structures Provide Insights into Eukaryotic Translation. *Cold Spring Harb. Perspect. Biol.* **11**, a032367 (2019).
3. Sonenberg, N. & Hinnebusch, A. G. Regulation of Translation Initiation in Eukaryotes: Mechanisms and Biological Targets. *Cell* **136**, 731–745 (2009).
4. Dever, T. E., Dinman, J. D. & Green, R. Translation Elongation and Recoding in Eukaryotes. *Cold Spring Harb. Perspect. Biol.* **10**, a032649 (2018).
5. Hellen, C. U. T. Translation Termination and Ribosome Recycling in Eukaryotes. *Cold Spring Harb. Perspect. Biol.* **10**, a032656 (2018).
6. Gebauer, F. & Hentze, M. W. Molecular mechanisms of translational control. *Nat. Rev. Mol. Cell Biol.* **5**, 827–835 (2004).
7. Fernandes, L. D., Moura, A. P. S. de & Ciandrini, L. Gene length as a regulator for ribosome recruitment and protein synthesis: theoretical insights. *arXiv* **7**, 17409 (2017).
8. Thompson, M. K. & Gilbert, W. V. mRNA length-sensing in eukaryotic translation: reconsidering the "closed loop" and its implications for translational control. *Curr. Genet.* **63**, 613–620 (2017).
9. Babendure, J. R., Babendure, J. L., Ding, J.-H. & Tsien, R. Y. Control of mammalian translation by m*RNA* structure near caps. RNA **12**, 851–861 (2006).
10. Courel, M. *et al.* GC content shapes mRNA decay and storage in human cells. *bioRxiv* 373498 (2019) doi:10.1101/373498.
11. Wu, X., Xu, M., Yang, J.-R. & Lu, J. Genome-wide impact of codon usage bias on translation optimization in Drosophila melanogaster. *Nat. Commun.* **15**, 8329 (2024).
12. Rocha, E. P. C. Codon usage bias from tRNA's point of view: Redundancy, specialization, and efficient decoding for translation optimization. *Genome Res.* **14**, 2279–2286 (2004).
13. Barrington, C. L. *et al.* Synonymous codon usage regulates translation initiation. *Cell Rep.* **42**, 113413 (2023).
14. Liu, Y. A code within the genetic code: codon usage regulates co-translational protein folding. *Cell Commun Signal* (2020) doi:10.21203/rs.3.rs-106674/v1.
15. Thomson, A. M., Rogers, J. T. & Leedman, P. J. Iron-regulatory proteins, iron-responsive elements and ferritin mRNA translation. *Int. J. Biochem. Cell Biol.* **31**, 1139–1152 (1999).
16. Georgakopoulos-Soares, I., Parada, G. E. & Hemberg, M. Secondary structures in RNA synthesis, splicing and translation. *Comput. Struct. Biotechnol. J.* **20**, 2871–2884 (2022).
17. Barbosa, C., Peixeiro, I. & Romão, L. Gene Expression Regulation by Upstream Open Reading Frames and Human Disease. *PLoS Genet.* **9**, e1003529 (2013).
18. Wu, Q. *et al.* Translation of small downstream ORFs enhances translation of canonical main open reading frames. *EMBO J.* **39**, e104763 (2020).
19. Babaylova, E. S., Gopanenko, A. V., Tupikin, A. E., Kabilov, M. R. & Malygin, A. A. The intrinsic properties of mRNAs define their translation efficiency at ribosome shortage. *Nucleic Acids Res.* **53**, gkaf1013 (2025).
20. Mayr, C. What Are 3′ UTRs Doing? *Cold Spring Harb. Perspect. Biol.* **11**, a034728 (2019).

21. Peer, E., Moshitch-Moshkovitz, S., Rechavi, G. & Dominissini, D. The Epitranscriptome in Translation Regulation. *Cold Spring Harb. Perspect. Biol.* **11**, a032623 (2018).
22. Shore, D. & Albert, B. Ribosome biogenesis and the cellular energy economy. *Curr. Biol.* **32**, R611–R617 (2022).
23. Buttgereit, F. & Brand, M. D. A hierarchy of ATP-consuming processes in mammalian cells. *Biochem. J.* **312 ( Pt 1)**, 163–7 (1995).
24. Spriggs, K. A., Bushell, M. & Willis, A. E. Translational Regulation of Gene Expression during Conditions of Cell Stress. *Mol. Cell* **40**, 228–237 (2010).
25. Roux, P. P. & Topisirovic, I. Signaling Pathways Involved in the Regulation of mRNA Translation. *Mol. Cell. Biol.* **38**, e00070-18 (2018).
26. Orozco, J. M. *et al.* Dihydroxyacetone phosphate signals glucose availability to mTORC1. *Nat. Metab.* **2**, 893–901 (2020).
27. Haythorne, E. *et al.* Altered glycolysis triggers impaired mitochondrial metabolism and mTORC1 activation in diabetic β-cells. *Nat. Commun.* **13**, 6754 (2022).
28. Hochstoeger, T., Papasaikas, P., Piskadlo, E. & Chao, J. A. Distinct roles of LARP1 and 4EBP1/2 in regulating translation and stability of 5′TOP mRNAs. *Sci. Adv.* **10**, eadi7830 (2024).
29. Cockman, E., Anderson, P. & Ivanov, P. TOP mRNPs: Molecular Mechanisms and Principles of Regulation. *Biomolecules* **10**, 969 (2020).
30. Costa-Mattioli, M. & Walter, P. The integrated stress response: From mechanism to disease. *Science* **368**, (2020).
31. Pakos-Zebrucka, K. *et al.* The integrated stress response. *EMBO Rep.* **17**, 1374–1395 (2016).
32. Harding, H. P. *et al.* Regulated Translation Initiation Controls Stress-Induced Gene Expression in Mammalian Cells. *Mol. Cell* **6**, 1099–1108 (2000).
33. Somers, J., Pöyry, T. & Willis, A. E. A perspective on mammalian upstream open reading frame function. *Int. J. Biochem. Cell Biol.* **45**, 1690–1700 (2013).
34. Vattem, K. M. & Wek, R. C. Reinitiation involving upstream ORFs regulates ATF4 mRNA translation in mammalian cells. *Proc. Natl. Acad. Sci.* **101**, 11269–11274 (2004).
35. Neill, G. & Masson, G. R. A stay of execution: ATF4 regulation and potential outcomes for the integrated stress response. *Front. Mol. Neurosci.* **16**, 1112253 (2023).
36. Vihervaara, A., Duarte, F. M. & Lis, J. T. Molecular mechanisms driving transcriptional stress responses. *Nat. Rev. Genet.* **19**, 385–397 (2018).
37. Suzuki, N. *et al.* Ultra-fast alterations in mRNA levels uncover multiple players in light stress acclimation in plants. *Plant J.* **84**, 760–772 (2015).
38. D'Urso, A. & Brickner, J. H. Epigenetic transcriptional memory. *Curr. Genet.* **63**, 435–439 (2017).
39. Sonawane, A. R. *et al.* Understanding Tissue-Specific Gene Regulation. *Cell Rep.* **21**, 1077–1088 (2017).
40. Zinani, O. Q. H., Keseroğlu, K. & Özbudak, E. M. Regulatory mechanisms ensuring coordinated expression of functionally related genes. *Trends Genet.* **38**, 73–81 (2022).
41. Bexley, K. *et al.* Rapid remodeling of NTP levels enables immediate translational adaptation to energy stress in yeast. *Mol. Cell* **85**, 3623-3639.e7 (2025).
42. Anisimova, A. S. *et al.* Human Tissues Exhibit Diverse Composition of Translation Machinery. *Int. J.*

*Mol. Sci.* **24**, 8361 (2023).
43. Waldman, Y. Y., Tuller, T., Shlomi, T., Sharan, R. & Ruppin, E. Translation efficiency in humans: tissue specificity, global optimization and differences between developmental stages. *Nucleic Acids Res.* **38**, 2964–2974 (2010).
44. Torrent, M., Chalancon, G., Groot, N. S. de, Wuster, A. & Babu, M. M. Cells alter their tRNA abundance to selectively regulate protein synthesis during stress conditions. *Sci. Signal.* **11**, eaat6409 (2018).
45. Zedan, M. *et al.* Timing of transcription controls the selective translation of newly synthesized mRNAs during acute environmental stress. *Mol. Cell* **85**, 4379-4392.e5 (2025).
46. Hino, S., Nagaoka, K. & Nakao, M. Metabolism–epigenome crosstalk in physiology and diseases. *J. Hum. Genet.* **58**, 410–415 (2013).
47. Biffo, S., Ruggero, D. & Santoro, M. M. The crosstalk between metabolism and translation. *Cell Metab.* **36**, 1945–1962 (2024).
48. Serefidou, M., Venkatasubramani, A. V. & Imhof, A. The Impact of One Carbon Metabolism on Histone Methylation. *Front. Genet.* **10**, 764 (2019).
49. Alam, M. *et al.* mTORC1-independent translation control in mammalian cells by methionine adenosyltransferase 2A and S-adenosylmethionine. *J. Biol. Chem.* **298**, 102084 (2022).
50. Liu, H. *et al.* Energy metabolism in health and diseases. *Signal Transduct. Target. Ther.* **10**, 69 (2025).
51. Grüning, N. *et al.* The return of metabolism: biochemistry and physiology of glycolysis. *Biol. Rev.* (2025) doi:10.1111/brv.70104.
52. Peralta, D. *et al.* A proton relay enhances H2O2 sensitivity of GAPDH to facilitate metabolic adaptation. *Nat. Chem. Biol.* **11**, 156–163 (2015).
53. Borst, P. The malate–aspartate shuttle (Borst cycle): How it started and developed into a major metabolic pathway. *IUBMB Life* **72**, 2241–2259 (2020).
54. Oh, S. *et al.* Glycerol 3-phosphate dehydrogenases (1 and 2) in cancer and other diseases. *Exp. Mol. Med.* **56**, 1066–1079 (2024).
55. Robertson, R. P. Chronic Oxidative Stress as a Central Mechanism for Glucose Toxicity in Pancreatic Islet Beta Cells in Diabetes*. *J. Biol. Chem.* **279**, 42351–42354 (2004).
56. Luo, X., Wu, J., Jing, S. & Yan, L.-J. Hyperglycemic Stress and Carbon Stress in Diabetic Glucotoxicity. *Aging Dis.* **7**, 90 (2016).
57. Yan, L. Redox imbalance stress in diabetes mellitus: Role of the polyol pathway. *Anim. Model. Exp. Med.* **1**, 7–13 (2018).
58. Buse, M. G. Hexosamines, insulin resistance, and the complications of diabetes: current status. *Am. J. Physiol.-Endocrinol. Metab.* **290**, E1–E8 (2006).
59. Pan, D., Xu, L. & Guo, M. The role of protein kinase C in diabetic microvascular complications. *Front. Endocrinol.* **13**, 973058 (2022).
60. Allaman, I., Bélanger, M. & Magistretti, P. J. Methylglyoxal, the dark side of glycolysis. *Front. Neurosci.* **9**, 23 (2015).
61. Lai, S. W. T., Gonzalez, E. D. J. L., Zoukari, T., Ki, P. & Shuck, S. C. Methylglyoxal and Its Adducts: Induction, Repair, and Association with Disease. *Chem. Res. Toxicol.* **35**, 1720–1746 (2022).
62. He, Y. *et al.* Glyoxalase system: A systematic review of its biological activity, related-diseases,

screening methods and small molecule regulators. *Biomed. Pharmacother.* **131**, 110663 (2020).
63. Morgenstern, J., Campos, M. C., Nawroth, P. & Fleming, T. The Glyoxalase System—New Insights into an Ancient Metabolism. *Antioxidants* **9**, 939 (2020).
64. Qin, B., Wang, Y. & Ding, J. The role of mitochondrial function in the pathogenesis of diabetes. *Front. Endocrinol.* **16**, 1607641 (2025).
65. Yan, L.-J. Pathogenesis of Chronic Hyperglycemia: From Reductive Stress to Oxidative Stress. *J. Diabetes Res.* **2014**, 137919 (2014).
66. Du, X. *et al.* Inhibition of GAPDH activity by poly(ADP-ribose) polymerase activates three major pathways of hyperglycemic damage in endothelial cells. *J. Clin. Investig.* **112**, 1049–1057 (2003).
67. Zhang, Z. *et al.* Dihydroxyacetone phosphate accumulation leads to podocyte pyroptosis in diabetic kidney disease. *J. Cell. Mol. Med.* **28**, e18073 (2024).
68. Lee, D. *et al.* SREBP and MDT-15 protect C. elegans from glucose-induced accelerated aging by preventing accumulation of saturated fat. *Genes Dev.* **29**, 2490–2503 (2015).
69. Liu, S. *et al.* Glycerol-3-phosphate biosynthesis regenerates cytosolic NAD+ to alleviate mitochondrial disease. *Cell Metab.* **33**, 1974-1987.e9 (2021).
70. Li, H. *et al.* Lactate dehydrogenase and glycerol-3-phosphate dehydrogenase cooperatively regulate growth and carbohydrate metabolism during Drosophila melanogaster larval development. *Development* **146**, dev175315 (2019).
71. Mo, J. *et al.* Intestinal GPDH-1 regulates high glucose diet induced lifespan extension in aged worms. *PeerJ* **11**, e15845 (2023).
72. Swierczynski, J. *et al.* Enhanced glycerol 3-phosphate dehydrogenase activity in adipose tissue of obese humans. *Mol. Cell. Biochem.* **254**, 55–59 (2003).
73. Sledzinski, T. *et al.* Association Between Cytosolic Glycerol 3-Phosphate Dehydrogenase Gene Expression in Human Subcutaneous Adipose Tissue and BMI. *Cell. Physiol. Biochem.* **32**, 300–309 (2013).
74. Joshi, M. *et al.* A compound heterozygous mutation in GPD1 causes hepatomegaly, steatohepatitis, and hypertriglyceridemia. *Eur. J. Hum. Genet.* **22**, 1229–1232 (2014).
75. Basel-Vanagaite, L. *et al.* Transient Infantile Hypertriglyceridemia, Fatty Liver, and Hepatic Fibrosis Caused by Mutated GPD1, Encoding Glycerol-3-Phosphate Dehydrogenase 1. *Am. J. Hum. Genet.* **90**, 49–60 (2012).
76. Lin, H. *et al.* Case Report: Identification of a Novel Homozygous Mutation in GPD1 Gene of a Chinese Child With Transient Infantile Hypertriglyceridemia. *Front. Genet.* **12**, 726116 (2021).
77. Mugabo, Y. *et al.* Identification of a mammalian glycerol-3-phosphate phosphatase: Role in metabolism and signaling in pancreatic β-cells and hepatocytes. *Proc. Natl. Acad. Sci.* **113**, E430–E439 (2016).
78. Possik, E. *et al.* Phosphoglycolate phosphatase homologs act as glycerol-3-phosphate phosphatase to control stress and healthspan in C. elegans. *Nat. Commun.* **13**, 177 (2022).
79. Al-Mass, A. *et al.* Glycerol-3-phosphate phosphatase operates a glycerol shunt in pancreatic β-cells that controls insulin secretion and metabolic stress. *Mol. Metab.* **60**, 101471 (2022).
80. Al-Mass, A. *et al.* Hepatic glycerol shunt and glycerol-3-phosphate phosphatase control liver metabolism and glucodetoxification under hyperglycemia. *Mol. Metab.* **66**, 101609 (2022).
81. Collard, F. *et al.* A conserved phosphatase destroys toxic glycolytic side products in mammals and

yeast. *Nat. Chem. Biol.* **12**, 601–607 (2016).
82. Jeanclos, E. *et al.* Glycolytic flux control by drugging phosphoglycolate phosphatase. *Nat. Commun.* **13**, 6845 (2022).
83. Wu, J., Zhang, N., Hayes, A., Panoutsopoulou, K. & Oliver, S. G. Global analysis of nutrient control of gene expression in Saccharomyces cerevisiae during growth and starvation. *Proc. Natl. Acad. Sci.* **101**, 3148–3153 (2004).
84. Harvald, E. B. *et al.* Multi-omics Analyses of Starvation Responses Reveal a Central Role for Lipoprotein Metabolism in Acute Starvation Survival in C. elegans. *Cell Syst.* **5**, 38-52.e4 (2017).
85. Michenthaler, H. *et al.* Systemic and transcriptional response to intermittent fasting and fasting-mimicking diet in mice. *BMC Biol.* **22**, 268 (2024).
86. Régnier, M. *et al.* Insights into the role of hepatocyte PPARα activity in response to fasting. *Mol. Cell. Endocrinol.* **471**, 75–88 (2018).
87. Rakhshandehroo, M., Knoch, B., Müller, M. & Kersten, S. Peroxisome Proliferator-Activated Receptor Alpha Target Genes. *PPAR Res.* **2010**, 612089 (2010).
88. Iavazzo, M. *et al.* TFEB coordinates autophagosome biogenesis and ribophagy during starvation via SQSTM1. *Sci. Adv.* **12**, eaea9302 (2026).
89. Settembre, C. *et al.* TFEB controls cellular lipid metabolism through a starvation-induced autoregulatory loop. *Nat. Cell Biol.* **15**, 647–658 (2013).
90. Zhang, F., Xu, X., Zhou, B., He, Z. & Zhai, Q. Gene Expression Profile Change and Associated Physiological and Pathological Effects in Mouse Liver Induced by Fasting and Refeeding. *PLoS ONE* **6**, e27553 (2011).
91. Chi, Y. *et al.* Regulation of gene expression during the fasting-feeding cycle of the liver displays mouse strain specificity. *J. Biol. Chem.* **295**, 4809–4821 (2020).
92. Fu, J. *et al.* Optimal fasting duration for mice as assessed by metabolic status. *Sci. Rep.* **14**, 21509 (2024).
93. Woerle, H. J. *et al.* Pathways for glucose disposal after meal ingestion in humans. *Am. J. Physiol.-Endocrinol. Metab.* **284**, E716–E725 (2003).
94. Lee, C.-H. *et al.* PPARδ regulates glucose metabolism and insulin sensitivity. *Proc. Natl. Acad. Sci.* **103**, 3444–3449 (2006).
95. Leonardini, A., Laviola, L., Perrini, S., Natalicchio, A. & Giorgino, F. Cross-Talk between PPARγ and Insulin Signaling and Modulation of Insulin Sensitivity. *PPAR Res.* **2009**, 818945 (2009).
96. Sterling, P. Allostasis: A model of predictive regulation. *Physiol. Behav.* **106**, 5–15 (2012).
97. Mora-García, S., Leone, M. J. de & Yanovsky, M. Time to grow: circadian regulation of growth and metabolism in photosynthetic organisms. *Curr. Opin. Plant Biol.* **35**, 84–90 (2017).
98. Pavlov, I. *The Work of the Digestive Glands*. (Charles Griffin & Company Ltd., London, 1902).
99. Skvortsova, A., Veldhuijzen, D. S., Kloosterman, I. E. M., Pacheco-López, G. & Evers, A. W. M. Food anticipatory hormonal responses: A systematic review of animal and human studies. *Neurosci. Biobehav. Rev.* **126**, 447–464 (2021).
100. Pullicin, A. J., Glendinning, J. I. & Lim, J. Cephalic phase insulin release: A review of its mechanistic basis and variability in humans. *Physiol. Behav.* **239**, 113514 (2021).
101. Lushchak, O. V., Carlsson, M. A. & Nässel, D. R. Food odors trigger an endocrine response that

affects food ingestion and metabolism. *Cell. Mol. Life Sci.* **72**, 3143–3155 (2015).
102. Brandt, C. *et al.* Food Perception Primes Hepatic ER Homeostasis via Melanocortin-Dependent Control of mTOR Activation. *Cell* **175**, 1321-1335.e20 (2018).
103. Brenner, S. THE GENETICS OF CAENORHABDITIS ELEGANS. *Genetics* **77**, 71–94 (1974).
104. Schulenburg, H. & Félix, M.-A. The Natural Biotic Environment of Caenorhabditis elegans. *Genetics* **206**, 55–86 (2017).
105. Frézal, L. & Félix, M.-A. C. elegans outside the Petri dish. *eLife* **4**, e05849 (2015).
106. Rashid, S., Wong, C. & Roy, R. Developmental plasticity and the response to nutrient stress in Caenorhabditis elegans. *Dev. Biol.* **475**, 265–276 (2021).
107. You, Y., Kim, J., Raizen, D. M. & Avery, L. Insulin, cGMP, and TGF-β Signals Regulate Food Intake and Quiescence in C. elegans: A Model for Satiety. *Cell Metab.* **7**, 249–257 (2008).
108. Lee, G. D. *et al.* Dietary deprivation extends lifespan in Caenorhabditis elegans. *Aging Cell* **5**, 515–524 (2006).
109. Lapierre, L. R. *et al.* The TFEB orthologue HLH-30 regulates autophagy and modulates longevity in Caenorhabditis elegans. *Nat. Commun.* **4**, 2267 (2013).
110. Gilst, M. R. V., Hadjivassiliou, H. & Yamamoto, K. R. A Caenorhabditis elegans nutrient response system partially dependent on nuclear receptor NHR-49. *Proc. Natl. Acad. Sci.* **102**, 13496–13501 (2005).
111. Taubert, S., Gilst, M. R. V., Hansen, M. & Yamamoto, K. R. A Mediator subunit, MDT-15, integrates regulation of fatty acid metabolism by NHR-49-dependent and -independent pathways in C. elegans. *Genes Dev.* **20**, 1137–1149 (2006).
112. Leiser, S. F. *et al.* Cell nonautonomous activation of flavin-containing monooxygenase promotes longevity and health span. *Science* **350**, 1375–1378 (2015).
113. Goh, G. Y. S. *et al.* NHR-49/HNF4 integrates regulation of fatty acid metabolism with a protective transcriptional response to oxidative stress and fasting. *Aging Cell* **17**, e12743 (2018).
114. Choi, H. S. *et al.* FMO rewires metabolism to promote longevity through tryptophan and one carbon metabolism in C. elegans. *Nat. Commun.* **14**, 562 (2023).
115. Kitto, E. S. *et al.* Metabolic regulation of behavior by the intestinal enzyme FMO-2. *Sci. Adv.* **11**, eadx3018 (2025).
116. Qiao, X. *et al.* Exploring the precision redox map during fasting-refeeding and satiation in C. elegans. *Stress Biol.* **3**, 17 (2023).
117. Gerisch, B. *et al.* HLH-30/TFEB Is a Master Regulator of Reproductive Quiescence. *Dev. Cell* **53**, 316-329.e5 (2020).
118. Schlotterer, A. *et al.* C. elegans as Model for the Study of High Glucose– Mediated Life Span Reduction. *Diabetes* **58**, 2450–2456 (2009).
119. Kingsley, S. F. *et al.* Bacterial processing of glucose modulates C. elegans lifespan and healthspan. *Sci. Rep.* **11**, 5931 (2021).
120. Lee, S.-J., Murphy, C. T. & Kenyon, C. Glucose Shortens the Life Span of C. elegans by Downregulating DAF-16/FOXO Activity and Aquaporin Gene Expression. *Cell Metab.* **10**, 379–391 (2009).
121. Garcia, A. M. *et al.* Glucose Induces Sensitivity to Oxygen Deprivation and Modulates Insulin/IGF-1 Signaling and Lipid Biosynthesis in Caenorhabditis elegans. *Genetics* **200**, 167–184 (2015).
122. Urso, S. J. & Lamitina, T. The C. elegans Hypertonic Stress Response: Big Insights from Shrinking

Worms. *Cell. Physiol. Biochem.* **55**, 89–105 (2021).
123. Lamitina, T., Huang, C. G. & Strange, K. Genome-wide RNAi screening identifies protein damage as a regulator of osmoprotective gene expression. *Proc. Natl. Acad. Sci.* **103**, 12173–12178 (2006).
124. Beaudoin-Chabot, C. *et al.* The unfolded protein response reverses the effects of glucose on lifespan in chemically-sterilized C. elegans. *Nat. Commun.* **13**, 5889 (2022).
125. Possik, E. *et al.* Glycerol 3-phosphate phosphatase/PGPH-2 counters metabolic stress and promotes healthy aging via a glycogen sensing-AMPK-HLH-30-autophagy axis in C. elegans. *Nat. Commun.* **14**, 5214 (2023).
126. Chandler-Brown, D. *et al.* Sorbitol treatment extends lifespan and induces the osmotic stress response in Caenorhabditis elegans. *Front. Genet.* **6**, 316 (2015).
127. Altun, Z. F. & Hall, D. H. *WormAtlas* Hermaphrodite Handbook - Nervous System - General Description. WormAtlas (2005) doi:10.3908/wormatlas.1.18.
128. Robertson, H. M. & Thomas, J. H. The putative chemoreceptor families of C. elegans. *WormBook* 1–12 (2006) doi:10.1895/wormbook.1.66.1.
129. Bargmann, C. I., Hartwieg, E. & Horvitz, H. R. Odorant-selective genes and neurons mediate olfaction in C. elegans. *Cell* **74**, 515–527 (1993).
130. Bargmann, C. Chemosensation in C. elegans. *WormBook* 1–29 (2006) doi:10.1895/wormbook.1.123.1.
131. Brissette, B. *et al.* Chemosensory detection of polyamine metabolites guides C. elegans to nutritive microbes. *Sci. Adv.* **10**, eadj4387 (2024).
132. Liu, Z. *et al.* Predator-secreted sulfolipids induce defensive responses in C. elegans. *Nat. Commun.* **9**, 1128 (2018).
133. Li, X. *et al.* Serotonin-Mediated Avoidance and Immune Suppression in Caenorhabditis elegans Exposed to Sodium Arsenite. *Biochem. Res. Int.* **2025**, 8485137 (2025).
134. Wan, X. *et al.* Efficient pheromone navigation via antagonistic detectors in Caenorhabditis elegans male. *Nat. Commun.* (2026) doi:10.1038/s41467-026-69392-2.
135. Zhang, M. G. *et al.* Sensory integration of food and population density during the diapause exit decision involves insulin-like signaling in Caenorhabditis elegans. *Proc. Natl. Acad. Sci.* **121**, e2405391121 (2024).
136. Fujiwara, M., Sengupta, P. & McIntire, S. L. Regulation of Body Size and Behavioral State of C. elegans by Sensory Perception and the EGL-4 cGMP-Dependent Protein Kinase. *Neuron* **36**, 1091–1102 (2002).
137. Mutlu, A. S., Gao, S. M., Zhang, H. & Wang, M. C. Olfactory specificity regulates lipid metabolism through neuroendocrine signaling in Caenorhabditis elegans. *Nat. Commun.* **11**, 1450 (2020).
138. Finger, F. *et al.* Olfaction regulates organismal proteostasis and longevity via microRNA-dependent signalling. *Nat. Metab.* **1**, 350–359 (2019).
139. Dishart, J. G. *et al.* Olfaction regulates peripheral mitophagy and mitochondrial function. *Sci. Adv.* **10**, eadn0014 (2024).
140. Alcedo, J. & Kenyon, C. Regulation of C. elegans Longevity by Specific Gustatory and Olfactory *Neuron*s. Neuron **41**, 45–55 (2004).
141. Zhang, B., Jun, H., Wu, J., Liu, J. & Xu, X. Z. S. Olfactory perception of food abundance regulates

dietary restriction-mediated longevity via a brain-to-gut signal. *Nat. Aging* **1**, 255–268 (2021).
142. Miller, H. A. *et al.* Serotonin and dopamine modulate aging in response to food odor and availability. *Nat. Commun.* **13**, 3271 (2022).
143. Kurino, C., Furuhashi, T., Sudoh, K. & Sakamoto, K. Isoamyl alcohol odor promotes longevity and stress tolerance via DAF-16 in Caenorhabditis elegans. *Biochem. Biophys. Res. Commun.* **485**, 395–399 (2017).
144. Brass, D. M. & Palmer, S. M. Models of toxicity of diacetyl and alternative diones. *Toxicology* **388**, 15–20 (2017).
145. Choi, J. I., Yoon, K., Kalichamy, S. S., Yoon, S.-S. & Lee, J. I. A natural odor attraction between lactic acid bacteria and the nematode Caenorhabditis elegans. *ISME J.* **10**, 558–567 (2016).
146. Sengupta, P., Chou, J. H. & Bargmann, C. I. odr-10 Encodes a Seven Transmembrane Domain Olfactory Receptor Required for Responses to the Odorant Diacetyl. *Cell* **84**, 899–909 (1996).
147. Yoshida, K. *et al.* Odour concentration-dependent olfactory preference change in C. elegans. *Nat. Commun.* **3**, 739 (2012).
148. Taniguchi, G., Uozumi, T., Kiriyama, K., Kamizaki, T. & Hirotsu, T. Screening of Odor-Receptor Pairs in Caenorhabditis elegans Reveals Different Receptors for High and Low Odor Concentrations. *Sci. Signal.* **7**, ra39 (2014).
149. Portman, D. eLife Assessment: The C. elegans gustatory receptor homolog LITE-1 is a chemoreceptor required for diacetyl avoidance. (2025) doi:10.7554/elife.107442.1.sa3.
150. Park, S. *et al.* Diacetyl odor shortens longevity conferred by food deprivation in C. elegans via downregulation of DAF-16/FOXO. *Aging Cell* **20**, e13300 (2021).
151. Ooi, F. K. & Prahlad, V. Olfactory experience primes the heat shock transcription factor HSF-1 to enhance the expression of molecular chaperones in C. elegans. *Sci. Signal.* **10**, (2017).
152. Prakash, D. *et al.* 1-Undecene from Pseudomonas aeruginosa is an olfactory signal for flight-or-fight response in Caenorhabditis elegans. *EMBO J.* **40**, EMBJ2020106938 (2021).
153. De-Souza, E. A., Thompson, M. A. & Taylor, R. C. Olfactory chemosensation extends lifespan through TGF-β signaling and UPR activation. *Nat. Aging* **3**, 938–947 (2023).
154. Brandel-Ankrapp, K. L. & Arey, R. N. Uncovering novel regulators of memory using C. elegans genetic and genomic analysis. *Biochem. Soc. Trans.* **51**, 161–171 (2023).
155. Stein, G. M. & Murphy, C. T. C. elegans positive olfactory associative memory is a molecularly conserved behavioral paradigm. *Neurobiol. Learn. Mem.* **115**, 86–94 (2014).
156. Hrachovec, J. P. Age Changes in Amino Acid Incorporation by Rat Liver Microsomes. *Gerontology* **15**, 52–63 (1969).
157. Motizuki, M. & Tsurugi, K. The effect of aging on protein synthesis in the yeast Saccharomyces cerevisiae. *Mech. Ageing Dev.* **64**, 235–245 (1992).
158. Vincow, E. S., Thomas, R. E., Merrihew, G. E., MacCoss, M. J. & Pallanck, L. J. Slowed Protein Turnover in Aging Drosophila Reflects a Shift in Cellular Priorities. *J. Gerontol.: Ser. A* **76**, 1734–1739 (2021).
159. Blazejowski, C. A. & Webster, G. C. Decreased rates of protein synthesis by cell-free preparations from different organs of aging mice. *Mech. Ageing Dev.* **21**, 345–356 (1983).
160. YOUNG, V. R., STEFFEE, W. P., PENCHARZ, P. B., WINTERER, J. C. & SCRIMSHAW, N. S. Total human

body protein synthesis in relation to protein requirements at various ages. *Nature* **253**, 192–194 (1975).
161. Rattan, S. I. S. Protein synthesis and the components of protein synthetic machinery during cellular ageing. *Mutat. Res.DNAging* **256**, 115–125 (1991).
162. Walther, D. M. *et al.* Widespread Proteome Remodeling and Aggregation in Aging C. elegans. *Cell* **161**, 919–932 (2015).
163. Keele, G. R. *et al.* Global and tissue-specific aging effects on murine proteomes. *Cell Rep.* **42**, 112715 (2023).
164. Sacramento, E. K. *et al.* Reduced proteasome activity in the aging brain results in ribosome stoichiometry loss and aggregation. *Mol. Syst. Biol.* **16**, MSB209596 (2020).
165. Fraia, D. D. *et al.* Altered translation elongation contributes to key hallmarks of aging in the killifish brain. *Science* **389**, eadk3079 (2025).
166. Solyga, M., Majumdar, A. & Besse, F. Regulating translation in aging: from global to gene-specific mechanisms. *EMBO Rep.* **25**, 5265–5276 (2024).
167. Luchessi, A. D. *et al.* Insights on eukaryotic translation initiation factor 5A (eIF5A) in the brain and aging. *Brain Res.* **1228**, 6–13 (2008).
168. Vargas, R. & Castañeda, M. Age-dependent decrease in the activity of protein-synthesis initiation factors in rat brain. *Mech. Ageing Dev.* **21**, 183–191 (1983).
169. Webster, G. C. & Webster, S. L. Specific disappearance of translatable messenger RNA for elongation factor one in aging Drosophila melanogaster. *Mech. Ageing Dev.* **24**, 335–342 (1984).
170. Gerashchenko, M. V., Peterfi, Z., Yim, S. H. & Gladyshev, V. N. Translation elongation rate varies among organs and decreases with age. *Nucleic Acids Res.* **49**, e9–e9 (2020).
171. Jung, M. *et al.* Longitudinal epigenetic and gene expression profiles analyzed by three-component analysis reveal down-regulation of genes involved in protein translation in human aging. *Nucleic Acids Res.* **43**, e100–e100 (2015).
172. Anisimova, A. S. *et al.* Multifaceted deregulation of gene expression and protein synthesis with age. *Proc. Natl. Acad. Sci.* **117**, 15581–15590 (2020).
173. Stein, K. C., Morales-Polanco, F., Lienden, J. van der, Rainbolt, T. K. & Frydman, J. Ageing exacerbates ribosome pausing to disrupt cotranslational proteostasis. *Nature* **601**, 637–642 (2022).
174. Lu, J. & Deutsch, C. Electrostatics in the Ribosomal Tunnel Modulate Chain Elongation Rates. *J. Mol. Biol.* **384**, 73–86 (2008).
175. Kim, H. S. & Pickering, A. M. Protein translation paradox: Implications in translational regulation of aging. *Front. Cell Dev. Biol.* **11**, 1129281 (2023).
176. Steffen, K. K. *et al.* Yeast Life Span Extension by Depletion of 60S Ribosomal Subunits Is Mediated by Gcn4. *Cell* **133**, 292–302 (2008).
177. Pan, K. Z. *et al.* Inhibition of mRNA translation extends lifespan in Caenorhabditis elegans. *Aging Cell* **6**, 111–119 (2007).
178. Selman, C. *et al.* Ribosomal Protein S6 Kinase 1 Signaling Regulates Mammalian Life Span. *Science* **326**, 140–144 (2009).
179. Xu, B. *et al.* Loss of Pol III repressor Maf1 in neurons promotes longevity by preventing the age-related decline in 5S rRNA and translation. *PLOS Biol.* **23**, e3003250 (2025).
180. Hansen, M. *et al.* Lifespan extension by conditions that inhibit translation in Caenorhabditis elegans.

*Aging Cell* **6**, 95–110 (2007).
181. Wang, J. *et al.* RNAi Screening Implicates a SKN-1–Dependent Transcriptional Response in Stress Resistance and Longevity Deriving from Translation Inhibition. *PLoS Genet.* **6**, e1001048 (2010).
182. Malik, Y. *et al.* Disruption of tRNA biogenesis enhances proteostatic resilience, improves later-life health, and promotes longevity. *PLOS Biol.* **22**, e3002853 (2024).
183. Kim, H. S. *et al.* Early-adulthood spike in protein translation drives aging via juvenile hormone/germline signaling. *Nat. Commun.* **14**, 5021 (2023).
184. Solis, G. M. *et al.* Translation attenuation by minocycline enhances longevity and proteostasis in old post-stress-responsive organisms. *eLife* **7**, e40314 (2018).
185. Iwasaki, S. & Ingolia, N. T. The Growing Toolbox for Protein Synthesis Studies. *Trends Biochem. Sci.* **42**, 612–624 (2017).
186. Ingolia, N. T., Ghaemmaghami, S., Newman, J. R. S. & Weissman, J. S. Genome-Wide Analysis in Vivo of Translation with Nucleotide Resolution Using Ribosome Profiling. *Science* **324**, 218–223 (2009).
187. Brar, G. A. & Weissman, J. S. Ribosome profiling reveals the what, when, where and how of protein synthesis. *Nat. Rev. Mol. Cell Biol.* **16**, 651–664 (2015).
188. Hu, Z. *et al.* Ssd1 and Gcn2 suppress global translation efficiency in replicatively aged yeast while their activation extends lifespan. *eLife* **7**, e35551 (2018).
189. Ladiges, W., Morton, J., Blakely, C. & Gale, M. Tissue specific expression of PKR protein kinase in aging B6D2F1 mice. *Mech. Ageing Dev.* **114**, 123–132 (2000).
190. Costa-Mattioli, M. *et al.* eIF2α Phosphorylation Bidirectionally Regulates the Switch from Short- to Long-Term Synaptic Plasticity and Memory. *Cell* **129**, 195–206 (2007).
191. Zhu, P. J. *et al.* Activation of the ISR mediates the behavioral and neurophysiological abnormalities in Down syndrome. *Science* **366**, 843–849 (2019).
192. Devi, L. & Ohno, M. PERK mediates eIF2α phosphorylation responsible for BACE1 elevation, CREB dysfunction and neurodegeneration in a mouse model of Alzheimer's disease. *Neurobiol. Aging* **35**, 2272–2281 (2014).
193. Halliday, M. *et al.* Partial restoration of protein synthesis rates by the small molecule ISRIB prevents neurodegeneration without pancreatic toxicity. *Cell Death Dis.* **6**, e1672–e1672 (2015).
194. Derisbourg, M. J., Wester, L. E., Baddi, R. & Denzel, M. S. Mutagenesis screen uncovers lifespan extension through integrated stress response inhibition without reduced mRNA translation. *Nat. Commun.* **12**, 1678 (2021).
195. Urso, S. J., Comly, M., Hanover, J. A. & Lamitina, T. The O-GlcNAc transferase OGT is a conserved and essential regulator of the cellular and organismal response to hypertonic stress. *PLoS Genet.* **16**, e1008821 (2020).
196. Tataridas-Pallas, N. *et al.* Mitochondrial clearance and increased HSF-1 activity are coupled to promote longevity in fasted Caenorhabditis elegans. *iScience* **27**, 109834 (2024).
197. Dillon, J., Holden-Dye, L., O'Connor, V. & Hopper, N. A. Context-dependent regulation of feeding behaviour by the insulin receptor, DAF-2, in Caenorhabditis elegans. *Invertebr. Neurosci.* **16**, 4 (2016).
198. Richmond, J. E., Davis, W. S. & Jorgensen, E. M. UNC-13 is required for synaptic vesicle fusion in C. elegans. *Nat. Neurosci.* **2**, 959–964 (1999).
199. Speese, S. *et al.* UNC-31 (CAPS) Is Required for Dense-Core Vesicle But Not Synaptic Vesicle

Exocytosis in Caenorhabditis elegans. *J. Neurosci.* **27**, 6150–6162 (2007).
200. Paquette, M. *et al.* AMPK-dependent phosphorylation is required for transcriptional activation of TFEB and TFE3. *Autophagy* **17**, 3957–3975 (2021).
201. Meyer, D. H. & Schumacher, B. BiT age: A transcriptome-based aging clock near the theoretical limit of accuracy. *Aging Cell* **20**, e13320 (2021).
202. Janssens, G. E. *et al.* Transcriptomics-Based Screening Identifies Pharmacological Inhibition of Hsp90 as a Means to Defer Aging. *Cell Rep.* **27**, 467-480.e6 (2019).
203. Tepper, R. G. *et al.* PQM-1 Complements DAF-16 as a Key Transcriptional Regulator of DAF-2-Mediated Development and Longevity. *Cell* **154**, 676–690 (2013).
204. Heimbucher, T., Hog, J., Gupta, P. & Murphy, C. T. PQM-1 controls hypoxic survival via regulation of lipid metabolism. *Nat. Commun.* **11**, 4627 (2020).
205. Eustice, M. *et al.* Nutrient sensing pathways regulating adult reproductive diapause in C. elegans. *PLoS ONE* **17**, e0274076 (2022).
206. Hanover, J. A. *et al.* A Caenorhabditis elegans model of insulin resistance: Altered macronutrient storage and dauer formation in an OGT-1 knockout. *Proc. Natl. Acad. Sci.* **102**, 11266–11271 (2005).
207. Zhang, S. *et al.* Reductive stress: The key pathway in metabolic disorders induced by overnutrition. *J. Adv. Res.* **77**, 569–584 (2025).
208. Lee, Y. J., Jeschke, G. R., Roelants, F. M., Thorner, J. & Turk, B. E. Reciprocal Phosphorylation of Yeast Glycerol-3-Phosphate Dehydrogenases in Adaptation to Distinct Types of Stress. *Mol. Cell. Biol.* **32**, 4705–4717 (2012).
209. Bavaro, L. *et al.* Lipid content in higher plants under osmotic stress. *Bioelectrochemistry* **70**, 12–17 (2007).
210. Sun, H. *et al.* LPGAT1 controls MEGDEL syndrome by coupling phosphatidylglycerol remodeling with mitochondrial transport. *Cell Rep.* **42**, 113214 (2023).
211. Paradies, G., Paradies, V., Ruggiero, F. M. & Petrosillo, G. Role of Cardiolipin in Mitochondrial Function and Dynamics in Health and Disease: Molecular and Pharmacological Aspects. *Cells* **8**, 728 (2019).
212. Pokorná, L. *et al.* Specific degradation of phosphatidylglycerol is necessary for proper mitochondrial morphology and function. *Biochim. Biophys. Acta (BBA) - Bioenerg.* **1857**, 34–45 (2016).
213. Kayser, B. D. *et al.* Phosphatidylglycerols are induced by gut dysbiosis and inflammation, and favorably modulate adipose tissue remodeling in obesity. *FASEB J.* **33**, 4741–4754 (2019).
214. McQuary, P. R. *et al.* C. elegans S6K Mutants Require a Creatine-Kinase-like Effector for Lifespan Extension. *Cell Rep.* **14**, 2059–2067 (2016).
215. Wu, N. *et al.* The metabolite alpha-ketobutyrate extends lifespan by promoting peroxisomal function in C. elegans. *Nat. Commun.* **14**, 240 (2023).
216. Huang, S., Howington, M. B., Dobry, C. J., Evans, C. R. & Leiser, S. F. Flavin-Containing Monooxygenases Are Conserved Regulators of Stress Resistance and Metabolism. *Front. Cell Dev. Biol.* **9**, 630188 (2021).
217. Chang, Y.-F. & Carman, G. M. CTP synthetase and its role in phospholipid synthesis in the yeast Saccharomyces cerevisiae. *Prog. Lipid Res.* **47**, 333–339 (2008).
218. Thangadurai, S., Bajgiran, M., Manickam, S., Mohana-Kumaran, N. & Azzam, G. CTP synthase: the

hissing of the cellular serpent. *Histochem. Cell Biol.* **158**, 517–534 (2022).
219. Jee, C., Batsaikhan, E. & Salim, C. Neurobiological Basis of Aversion-Resistant Ethanol Seeking in C. elegans. *Metabolites* **13**, 62 (2022).
220. Hall, D. H. Gap junctions in C. elegans: Their roles in behavior and development. *Dev. Neurobiol.* **77**, 587–596 (2017).
221. Lin, S.-J., Ford, E., Haigis, M., Liszt, G. & Guarente, L. Calorie restriction extends yeast life span by lowering the level of NADH. *Genes Dev.* **18**, 12–16 (2004).
222. Siegers, C.-P., Bartels, L. & Riemann, D. Effects of Fasting and Glutathione Depletors on the GSH-Dependent Enzyme System in the Gastrointestinal Mucosa of the Rat. *Pharmacology* **38**, 121–128 (1989).
223. Desideri, E., Filomeni, G. & Ciriolo, M. R. Glutathione participates in the modulation of starvation-induced autophagy in carcinoma cells. *Autophagy* **8**, 1769–1781 (2012).
224. Pan, X. *et al.* A genetically encoded bifunctional enzyme mitigates redox imbalance and lipotoxicity. *Nat. Metab.* 1–21 (2026) doi:10.1038/s42255-025-01450-3.
225. Petrovic, D. *et al.* Ergothioneine improves healthspan of aged animals by enhancing cGPDH activity through CSE-dependent persulfidation. *Cell Metab.* **37**, 542-556.e14 (2025).
226. Xie, J. *et al.* GPD1 Enhances the Anticancer Effects of Metformin by Synergistically Increasing Total Cellular Glycerol-3-Phosphate. *Cancer Res.* **80**, 2150–2162 (2020).
227. Luo, S. *et al.* Effects of putative metformin targets on phenotypic age and leukocyte telomere length: a mendelian randomisation study using data from the UK Biobank. *Lancet Heal. Longev.* **4**, e337–e344 (2023).
228. Sala, A. J. *et al.* Nuclear receptor signaling via NHR-49/MDT-15 regulates stress resilience and proteostasis in response to reproductive and metabolic cues. *Genes Dev.* **38**, 380–392 (2024).
229. Goh, G. Y. S. *et al.* The conserved Mediator subunit MDT-15 is required for oxidative stress responses in Caenorhabditis elegans. *Aging Cell* **13**, 70–79 (2014).
230. Kersten, S. *et al.* Peroxisome proliferator–activated receptor α mediates the adaptive response to fasting. *J. Clin. Investig.* **103**, 1489–1498 (1999).
231. Patsouris, D. *et al.* PPARα governs glycerol metabolism. *J. Clin. Investig.* **114**, 94–103 (2004).
232. Jiang, Y. J. *et al.* Stimulation of cardiac cardiolipin biosynthesis by PPARα activation. *J. Lipid Res.* **45**, 244–252 (2004).
233. Zhang, Y., Chou, J. H., Bradley, J., Bargmann, C. I. & Zinn, K. The Caenorhabditis elegans seven-transmembrane protein ODR-10 functions as an odorant receptor in mammalian cells. *Proc. Natl. Acad. Sci.* **94**, 12162–12167 (1997).
234. Suryawinata, N. *et al.* Dietary E. coli promotes age-dependent chemotaxis decline in C. elegans. *Sci. Rep.* **14**, 5529 (2024).
235. Kudla, G., Lipinski, L., Caffin, F., Helwak, A. & Zylicz, M. High Guanine and Cytosine Content Increases mRNA Levels in Mammalian Cells. *PLoS Biol.* **4**, e180 (2006).
236. Courel, M. *et al.* GC content shapes mRNA storage and decay in human cells. *eLife* **8**, e49708 (2019).
237. Zhou, Z., Sun, B., Yu, D. & Bian, M. Roles of tRNA metabolism in aging and lifespan. *Cell Death Dis.* **12**, 548 (2021).
238. Blumenthal, T. & Gleason, K. S. Caenorhabditis elegans operons: form and function. *Nat. Rev. Genet.*

**4**, 110–118 (2003).
239. Bernard, F., Dargère, D., Rechavi, O. & Dupuy, D. Quantitative analysis of C. elegans transcripts by Nanopore direct-cDNA sequencing reveals terminal hairpins in non trans-spliced mRNAs. *Nat. Commun.* **14**, 1229 (2023).
240. Allen, M. A., Hillier, L. W., Waterston, R. H. & Blumenthal, T. A global analysis of C. elegans trans-splicing. *Genome Res.* **21**, 255–264 (2011).
241. Dodt, M., Roehr, J. T., Ahmed, R. & Dieterich, C. FLEXBAR—Flexible Barcode and Adapter Processing for Next-Generation Sequencing Platforms. *Biology* **1**, 895–905 (2012).
242. Ewels, P., Magnusson, M., Lundin, S. & Käller, M. MultiQC: summarize analysis results for multiple tools and samples in a single report. *Bioinformatics* **32**, 3047–3048 (2016).
243. Dobin, A. *et al.* STAR: ultrafast universal RNA-seq aligner. *Bioinformatics* **29**, 15–21 (2012).
244. Lauria, F. *et al.* riboWaltz: Optimization of ribosome P-site positioning in ribosome profiling data. *PLoS Comput. Biol.* **14**, e1006169 (2018).
245. Xiao, Z. *et al.* De novo annotation and characterization of the translatome with ribosome profiling data. *Nucleic Acids Res.* **46**, gky179- (2018).
246. Li, W., Wang, W., Uren, P. J., Penalva, L. O. F. & Smith, A. D. Riborex: fast and flexible identification of differential translation from Ribo-seq data. *Bioinformatics* **33**, 1735–1737 (2017).
247. Fresno, C. & Fernández, E. A. RDAVIDWebService: a versatile R interface to DAVID. *Bioinformatics* **29**, 2810–2811 (2013).
248. Peden, J. *CodonW*.
249. Tommaso, P. D. *et al.* Nextflow enables reproducible computational workflows. *Nat. Biotechnol.* **35**, 316–319 (2017).
250. Krueger, F. *Trim Galore!*
251. Martin, M. Cutadapt removes adapter sequences from high-throughput sequencing reads. *EMBnetJ.* **17**, 10–12 (2011).
252. Patro, R., Duggal, G., Love, M. I., Irizarry, R. A. & Kingsford, C. Salmon provides fast and bias-aware quantification of transcript expression. *Nat. Methods* **14**, 417–419 (2017).
253. Andrews, S. *SeqMonk*.
254. Pino, L. K. *et al.* The Skyline ecosystem: Informatics for quantitative mass spectrometry proteomics. *Mass Spectrom. Rev.* **39**, 229–244 (2020).
255. Dieterle, F., Ross, A., Schlotterbeck, G. & Senn, H. Probabilistic Quotient Normalization as Robust Method to Account for Dilution of Complex Biological Mixtures. Application in 1H NMR Metabonomics. *Anal. Chem.* **78**, 4281–4290 (2006).
256. Kamath, R. S. *et al.* Systematic functional analysis of the Caenorhabditis elegans genome using RNAi. *Nature* **421**, 231–237 (2003).
257. Rual, J.-F. *et al.* Toward Improving Caenorhabditis elegans Phenome Mapping With an ORFeome-Based RNAi Library. *Genome Res.* **14**, 2162–2168 (2004).
258. Kauffman, A. *et al.* C. elegans Positive Butanone Learning, Short-term, and Long-term Associative Memory Assays. *J. Vis. Exp. : JoVE* 2490 (2011) doi:10.3791/2490.